

**NUMERICAL AND EXPERIMENTAL INVESTIGATION
OF
FATIGUE LIFE IN DEEP DRAWN PARTS**

**A THESIS SUBMITTED TO
THE GRADUATE SCHOOL OF NATURAL AND APPLIED SCIENCES
OF
MIDDLE EAST TECHNICAL UNIVERSITY**

BY

OĞUZ AYTEKİN

**IN PARTIAL FULFILLMENT OF THE REQUIREMENTS FOR THE
DEGREE OF MASTER OF SCIENCE
IN
MECHANICAL ENGINEERING**

MAY 2005

Approval of the Graduate School of Natural and Applied Sciences.

Prof.Dr. Canan Özgen
Director

I certify that this thesis satisfies all the requirements as a thesis for the degree of Master of Science.

Prof.Dr. S. Kemal İder
Head of Department

This is to certify that we have read this thesis and that in our opinion it is fully adequate, in scope and quality, as a thesis for the degree of Master of Science.

Prof.Dr. Metin Ersoy
Co-Supervisor

Prof.Dr. Eres Söylemez
Supervisor

Examining Committee Members

Prof.Dr. Levend Parnas (METU, ME)

Prof.Dr. Eres Söylemez (METU, ME)

Assoc.Dr. Suat Kadiođlu (METU, ME)

Prof.Dr. Őakir Bor (METU, METE)

Asst.Prof. Serkan Dađ (METU, ME)

I hereby declare that all information in this document has been obtained and presented in accordance with academic rules and ethical conduct. I also declare that, as required by these rules and conduct, I have fully cited and referenced all material and results that are not original to this work.

Oğuz Aytekin

ABSTRACT

NUMERICAL AND EXPERIMENTAL INVESTIGATION OF FATIGUE LIFE IN DEEP DRAWN PARTS

Aytekin, Oğuz

M.S., Department of Mechanical Engineering

Supervisor: Prof. Dr. Eres Söylemez

Co-Supervisor: Prof. Dr. Metin Ersoy

May 2005, 110 pages

Sheet metal forming has an important place among metal forming processes. As the usage of sheet metal increases, the fatigue simulation and optimization of these parts become more important. This thesis study examines the change of the fatigue life of a sheet metal part after forming. A sphere-like shape is deep drawn and change in thickness and residual stresses are analyzed. To understand the effect of residual stresses, deep drawn parts with and without residual stress tested against the fatigue failure. In parallel, the forming process is simulated with an implicit finite element method (FEM). The success of forming simulation is discussed in the study. Thickness changes and residual stresses calculated with FEM are included in computer aided fatigue analysis. The effect of thickness changes is examined with the results of FEM analysis. The effectiveness of the whole simulation process is discussed by comparing the outputs of experiments and computational analysis.

Keywords: Sheet Metal Forming, Finite Element Method, Fatigue Life Prediction, Residual Stress, Thickness Change

ÖZ

DERİN ÇEKME PARÇA ÖMÜRLERİNİN NUMERİK VE DENEYSEL OLARAK İNCELENMESİ

Aytekin, Oğuz

Y.Lisans, Makina Mühendisliği Bölümü

Tez Yöneticisi: Prof. Dr. Eres Söylemez

Ortak Tez Yöneticisi: Prof. Dr. Metin Ersoy

Mayıs 2005, 110 sayfa

Sac metal şekillendirme, metal şekillendirme işlemleri arasında önemli bir yere sahiptir. Sac metal kullanımının artmasıyla, sac metalden üretilmiş parçaların tasarım aşamasında ömürlerinin hesaplanması ve optimizasyonu önem kazanmıştır. Bu tez çalışması sac metalden üretilmiş bir parçanın ömürünün, şekillendirme işlemi sonrasında ne şekilde değiştiğini inceler. Çalışmada derin çekme ile üretilmiş küresel bir parça şekillendirilmiş, şekillendirme sonrası değişen kalınlıklar ve oluşan kalıntı gerilmeler incelenmiştir. Kalıntı gerilmelerin etkisini anlamak için, derin çekilmiş parçaların bir kısmı gerilme alma tavına sokulmuş ve kalıntı gerilmeler testleri uygulanmıştır. Kalıntı gerilmeli ve kalıntı gerilmemiş parçaların ömürleri kıyaslanmıştır. Paralel olarak şekillendirme işleminin implisit sonlu elemanlar yöntemiyle benzeşim çalışması yapılmıştır. Bu benzeşim çalışmasının başarısı çalışma içinde incelenmiştir. Analiz sonucu bulunan kalınlık değişiklikleri ve kalıntı gerilmeler bilgisayar destekli ömür tahmini yönteminde kullanılmıştır. Kalınlık değişiminin sonuçlara etkisi analiz sonuçlarıyla incelenmiştir. Tüm benzeşim yönteminin yetkinliği test ve analiz sonuçlarının karşılaştırılmasıyla tartışılmıştır.

Anahtar Kelimeler: Sac Metal Şekillendirme, Sonlu Eleman Yöntemi, Ömür Tahmini, Kalıntı Gerilme, Kalınlık Değişimi

ACKNOWLEDGEMENTS

I would like to thank my supervisor Prof. Dr. Eres Söylemez for his trust and support throughout the study. He encouraged me at every stage of the study in spite of many interruptions. I thank Prof. Dr. Metin Ersoy for his support and arrangements for me to conduct the studies in Germany.

I would like to express my gratitude to my colleagues at ZF Lemförder for their understanding and help. My fellow Mr. Onur Kırılı encouraged me several times when I was to give up. I thank him especially for his gentleness. The fatigue tests would not be completed without efforts of Mr. Mustafa Hacıođlu for finding the required number of test specimens. I thank him for his sincere helps.

ZF Lemförder A.Ş. gave an important amount of financial support for all expensive tests and analyses. Their contribution is priceless.

Finally, I thank my wife Janis for her unbelievable patience, support, tenderness... and everything I can not name.

TABLE OF CONTENTS

ABSTRACT.....	iv
ÖZ.....	v
ACKNOWLEDGEMENT.....	vi
TABLE OF CONTENTS.....	vii
LIST OF TABLES.....	x
LIST OF FIGURES.....	xii

CHAPTERS

1	INTRODUCTION.....	1
	1.1 Drawing Process and Material.....	1
	1.2 Fatigue Life Test.....	2
2	BASIC CONCEPTS IN METAL FORMING SIMULATION AND FATIGUE LIFE EXPECTANCY.....	6
	2.1 Plastic Behavior of Metals.....	6
	2.1.1 Criteria for Initial Yield.....	6
	2.1.2 Elastic-Plastic Flow Rule.....	12
	2.1.3 Hardening Rules.....	13
	2.1.3.1 Isotropic Hardening.....	14
	2.1.3.2 Kinematic Hardening.....	15
	2.1.3.3 Mixed Hardening.....	15
	2.2 Sheet Metal Forming Methods.....	16
	2.2.1 Press Machines.....	19
	2.2.2 Related Material Properties.....	20
	2.2.3 Standard Tensile Test for Sheet Metals.....	21

2.3	Fatigue Behavior of Metals.....	28
2.3.1	Fatigue Failure	29
2.3.2	Crack Nucleation and Propagation	30
2.3.3	Wöhler Diagram.....	32
2.3.4	High Cycle Fatigue and Low Cycle Fatigue.....	32
2.3.5	Factors Effecting Fatigue Life	34
2.3.5.1	Technological Size Effects.....	34
2.3.5.2	Nominal Stresses and Real Stresses (Effect of Notches).....	36
2.3.5.3	Surface Effects	37
2.3.5.4	Mean Stress Effects.....	39
2.3.6	Fatigue Analysis Approaches.....	42
2.3.6.1	The Stress-Life Approach	42
2.3.6.2	The Strain-Life Approach	48
2.3.6.3	The LEFM Approach	53
2.3.6.4	Variable Amplitude Loading, Cumulative Damage Hypothesis, Cycle Counting Methods	53
2.4	Residual Stress Determination with X-Ray Diffraction Method.....	56
3	DRAWING OF SHEET METAL	58
3.1	Process Description.....	58
3.2	Finite Element Modeling	60
3.2.1	Geometry and Mesh Structure	60
3.2.2	Boundary Conditions	61
3.2.3	Material Modeling.....	62
3.2.4	Program Parameters	63
3.3	Measurements, Tests and Evaluations of Results	65
3.3.1	Thickness Measurements	65
3.3.2	Residual Stress Measurements with X-Ray Diffraction Method.....	66
3.3.3	Evaluation of Results	68
4	FATIGUE BEHAVIOR OF THE COMPONENT	71

4.1	Fatigue Test Procedure.....	71
4.2	Finite Element Modeling	73
4.2.1	Geometry and Mesh Structure	74
4.2.2	Boundary Conditions	75
4.2.3	Material Modeling.....	77
4.2.4	Program Parameters	79
4.3	Evaluation of Result.....	80
4.3.1	Fatigue Analysis Results	80
4.3.2	Fatigue Test Results	82
5	CONCLUSIONS AND FURTHER RECOMMENDATIONS	85
6	APPENDIX A. FATIGUE LOAD PRINCIPAL STRESS RESULTS.....	95
7	APPENDIX B. FATIGUE LOAD PRINCIPAL STRESS	101

LIST OF TABLES

Table 1.1	Chemical composition of the material, weight percentages	2
Table 1.2	Quality numbers of the material.....	2
Table 1.3	Fatigue load amplitudes	4
Table 2.1	Hill's and Barlat-Karafilis criteria [2]	9
Table 2.2	Representation of common sheet metal forming methods.....	17
Table 2.3	Suggested size factors of Shigley and Mitschke.....	35
Table 2.4	Surface process effects on fatigue limit [8]	37
Table 2.5	Surface process effect on fatigue limit [5].....	38
Table 2.6	Decarburization effect on fatigue limit [20]	38
Table 2.7	Mean stress correction methods.....	40
Table 2.8	Empirical fatigue limits for steel, related with ultimate strength.....	46
Table 2.9	Empirical fatigue limits for steel, related with Brinell hardness number	46
Table 2.10	Empirical coefficients to generate synthetic S-N curves	46
Table 2.11	Modified uniform material law, Baumel-Seeger	50
Table 3.1	Calculated values for K , n and r different angles to the rolling direction	63
Table 3.2	Residual stresses measured with Psi XRD equipment.....	67
Table 4.1	Fatigue test loads.....	71
Table 4.2	Models prepared for analysis	74
Table 4.3	Fatigue load maximum principal results of constant and variable thickness models	80
Table 4.4	Fatigue simulation models, Case 1, 7 bars, 5498N-5154N cyclic load	80

Table 4.5	Fatigue simulation models, Case 2, 6 bars, 4712N-4418N cyclic load	81
Table 4.6	Fatigue test results.....	82
Table 5.1	Fatigue life cycle differences in percentage between	88
Table 5.2	Percentage error residue in strain-life methods, comparison with test results with and without residual stresses	89
Table 5.3	Percentage error residue in strain-life methods with residual stresses, comparison with test results with residual stresses.....	90

LIST OF FIGURES

Figure 1.1	Blank after trimming and the final part.....	2
Figure 1.2	Fatigue test setup.....	3
Figure 1.3	Fatigue test boundary conditions	3
Figure 1.4	Pneumatic cylinder for fatigue loading.....	4
Figure 2.1	Von Mises yield surface in principal stress space [26].....	7
Figure 2.2	Von Mises and Tresca criteria on π plane [1].....	8
Figure 2.3	Tensile test directions for Hill criteria parameter determination for sheet metals	12
Figure 2.4	Expansion of von Mises yield surface with isotropic hardening	13
Figure 2.5	Schematic representation of loading/unloading corresponding to (a) isotropic (b) and kinematic hardening rules for tensile response [2]..	14
Figure 2.6	Isotropic hardening in 2D principal stress (π plane representation) space associated with (a) von Mises surface (b) Tresca yield surface [2].....	14
Figure 2.7	Sheet metal products from Erdemir A.Ş., (a) plates (b) coils (c) galvanized coils.....	21
Figure 2.8	Tensile test specimen (a) circular cross section [DIN 50125:2004-01] (b) rectangular cross section and (c) grips and fixtures [Instron 2716-0003]	22
Figure 2.9	Mechanical extensometer.....	23
Figure 2.10	Tensile test realized in Ege University Laboratories, engineering stress-engineering strain data of a St-37 steel.....	23
Figure 2.11	Formation of wave like shapes caused by anisotropy [27]	27
Figure 2.12	Typical fatigue failure stages [6]	29

Figure 2.13 Slip formation on the metal surface and slip directions in case of uniaxial loading [6]	30
Figure 2.14 Propagation of a crack starting from the surface of the metal [4].....	31
Figure 2.15 Fatigue process developments [7].....	31
Figure 2.16 Zones of fatigue behaviors	32
Figure 2.17 Crack initiation and propagation periods [8]	33
Figure 2.18 Area under critical stress [13]	36
Figure 2.19 Nominal stresses to real stresses	37
Figure 2.20 (a) Effect of chrome plating on SN curve for 4140 steel (b) Effect of nickel plating on SN curve of steel ($S_u=63\text{ksi}$) [23]	39
Figure 2.21 a. Soderberg b. Goodman c. Gerber d. Morrow.....	40
Figure 2.22 Mean stress effect on strain life curve [20].....	41
Figure 2.23 Schematic representation of fatigue test machines [7].....	42
Figure 2.24 Fatigue test machines [7]	43
Figure 2.25 Stress gradient of rotating bending and axial loading tests [7]	43
Figure 2.26 Common fatigue test specimens [6].....	44
Figure 2.27 Logarithmic P-S-N Curve (Wöhler diagram) [3].....	44
Figure 2.28 Statistical method used for determination of fatigue limit [3].....	45
Figure 2.29 Material laws for static and cyclic loading, Langrad [19]	48
Figure 2.30 A typical Strain-Life (ϵ -N) curve [3]	50
Figure 2.31 Cyclic to monotonic stress-strain diagram of a strain hardened material [4]	51
Figure 2.32 Schematic presentation of Neuber's rule [31]	52
Figure 2.33 Palmgren-Miner's rule [3]	54
Figure 2.34 Stresses under fatigue limit [31]	54
Figure 2.35 Linear/Non-linear damage rules [2].....	55
Figure 2.36 X-Ray beam diffraction in accordance with Bragg's law [28].....	56
Figure 2.37 X-Ray beam angles [28].....	57
Figure 3.1 Double action hydraulic press.....	58
Figure 3.2 2D drawing of the part	59

Figure 3.3	Photographs of the final part.....	59
Figure 3.4	FEM analysis bodies	60
Figure 3.5	A portion of blank mesh.....	61
Figure 3.6	Load of the female pattern and blank holder	62
Figure 3.7	Engineering stress-engineering strain data	63
Figure 3.8	Measured thickness of the formed sheet metal and the FE analysis results	66
Figure 3.9	Residual stress measurement sample locations.....	67
Figure 3.10	Thickness distribution after forming.....	68
Figure 3.11	Total equivalent plastic strain distribution before release of contact bodies	68
Figure 3.12	Principal residual stresses in cylindrical coordinates, σ_r	69
Figure 3.13	Principal residual stresses in cylindrical coordinates, σ_θ	69
Figure 3.14	Measured and calculated residual stresses.....	70
Figure 4.1	Fatigue test setup.....	72
Figure 4.2	Fatigue test fixtures.....	72
Figure 4.3	FE model with measured thickness distribution after sheet metal forming (a) measured (b) FE results	73
Figure 4.4	Mesh structure used for fatigue analysis, totally 12.672 quad4 elements	75
Figure 4.5	Boundary conditions used for fatigue analysis; RBE2 elements are used to create nodal degree of freedom tying	76
Figure 4.6	Fatigue analysis load graph.....	77
Figure 4.7	Synthetic S-N curve, stresses are in range	78
Figure 4.8	Synthetic strain-N curve.....	78
Figure 4.9	Cyclic stress strain curve and Ludwik's fit of P245NB	79
Figure 4.10	Fatigue test results, load cycles vs. cylinder pressure.....	83
Figure 4.11	First visible fatigue cracks, part with (a) stress relieve (b) residual stresses (c) advanced fatigue crack	83
Figure 4.12	First visible fatigue cracks with zoom factor (a) 500 (b) 1000.....	84

Figure 5.1	Calculated thickness effect on fatigue life for two load cases	86
Figure 5.2	Residual stress effect on fatigue life, driven from test results	87
Figure 5.3	Residual stress effect on fatigue life, driven from fatigue simulation results of model 2 and model 4	88
Figure 5.4	Comparison of strain life Morrow method with fatigue test results with and without residual stresses.....	91
Figure A. 1	Model 1, maximum principal stress results for 7 bars (a) 5498N forward, (b) 5154N backward load	95
Figure A. 2	Model 1, maximum principal stress results for 6 bars (a) 4712N forward, (b) 4418N backward load	96
Figure A. 3	Model 2, maximum principal stress results for 7 bars (a) 5498N forward, (b) 5154N backward load	97
Figure A. 4	Model 2, maximum principal stress results for 6 bars (a) 4712N forward, (b) 4418N backward load	98
Figure A. 5	Model 3, maximum principal stress results for 7 bars (a) 5498N forward, (b) 5154N backward load	99
Figure A. 6	Model 3, maximum principal stress results for 6 bars (a) 4712N forward, (b) 4418N backward load	100
Figure B. 1	Case 1 (7 bars) Model 1 Stress-Life.....	101
Figure B. 2	Case 1 (7 bars) Model 1 Strain-Life.....	102
Figure B. 3	Case 1 (7 bars) Model 2 Stress-Life.....	103
Figure B. 4	Case 1 (7 bars) Model 2 Strain-Life.....	104
Figure B. 5	Case 1 (7 bars) Model 3 Stress-Life.....	105
Figure B. 6	Case 1 (7 bars) Model 3 Strain-Life.....	106
Figure B. 7	Case 1 (7 bars) Model 4 Stress-Life.....	107
Figure B. 8	Case 1 (7 bars) Model 4 Strain-Life.....	108
Figure B. 9	Case 1 (7 bars) Model 5 Stress-Life.....	109
Figure B. 10	Case 1 (7 bars) Model 5 Strain-Life.....	110

CHAPTER 1

INTRODUCTION

There is a number of sheet metal forming methods that are frequently used. Bending, roll forming, stretch forming, shearing, drawing, rubber forming, spinning, super plastic forming, hydro forming are some common sheet metal forming methods. It is known that mechanical property changes occur on the sheet metal part while forming. These changes are effective on the strength and the fatigue life of the part. Nevertheless, it is hard to predict the effect of forming on the part. In this study, two main effects of sheet metal forming are studied for a deep drawn sheet metal component. These effects are;

- Local thickness changes
- Formation of residual stresses

1.1 Drawing Process and Material

A double action hydraulic press with 2000 kN capacity is used for the drawing process. Edge trimming of the blank is done before forming process. The blank after trimming and the final product are shown in Figure 1.1. The schematic view of the press can be seen in Figure 3.1.

The chemical composition of the material is given in Table 1.1. The material is provided by Erdemir Çelik San. ve Tic. A.Ş. Material is hot rolled as strips,

normalized and no special surface processes are applied to the material. These materials are deep drawable and non-ageing. Standards and quality numbers of the material are given in Table 1.2.



Figure 1.1 Blank after trimming and the final part

Table 1.1 Chemical composition of the material, weight percentages

Material	C	Si	Mn	P	S	Al	N	Ti
Gas cylinder steel	max.	max.	min.	max.	max.	min.	max.	max.
	0.15	0.10	0.40	0.015	0.010	0.020	0.009	0.03

Table 1.2 Quality numbers of the material

Material	Standard	Grade	Erdemir Quality No
Gas cylinder steel	EN 10 120-97	P245NB	6837

1.2 Fatigue Life Test

Fatigue tests are conducted by a uniaxial alternating load with non-zero mean at different amplitudes. A special testing apparatus is designed and produced for fatigue life measurements. The designed system is powered with pressurized air and is able to complete a load cycle (front-back loading of max. 6000 N) in 2 seconds. A load controlled test is done with two digital pressure sensors, a solenoid

pneumatic valve, electronic cycle counter and an electronic control circuit. This apparatus is shown in Figure 1.2.



Figure 1.2 Fatigue test setup

Figure 1.3 shows the fixing and loading of the part and gives the amplitudes used in fatigue tests. Load is applied in one direction and in both negative and positive senses with different amplitudes and non-zero mean.

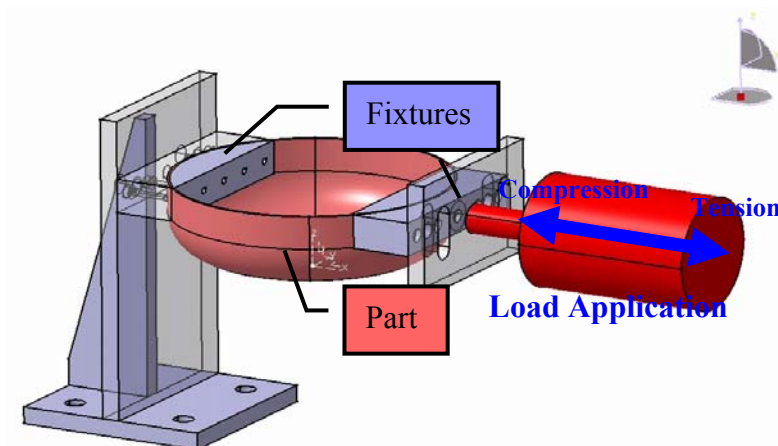


Figure 1.3 Fatigue test boundary conditions

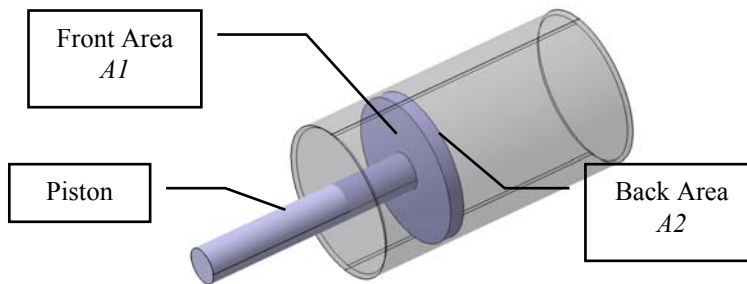


Figure 1.4 Pneumatic cylinder for fatigue loading

The front and back areas of pneumatic cylinder are different. This causes a difference in the front and back forces generated at the piston. The ratio of the forces is equal to the ratio of the areas $A1$ and $A2$, which is 0,94.

Table 1.3 Fatigue load amplitudes

Loadcase No	Cylinder Pressure	Forward Load (N)	Backward Load (N)
1	7 bar	5498	5154
2	6 bar	4713	4418

Throughout the study, finite element analysis tools are used and a method to include forming effects in fatigue life analysis is developed. The effectiveness of the method is discussed in the study. A finite element analysis (FEA) program, MSC.Marc, is utilized for the forming process simulation. In order to understand the effect of each factor alone and also together, different models with one or several of these mentioned affects are analyzed with MSC.Fatigue, which utilizes FEA for fatigue analysis. The results obtained are compared with each other and with the results of measurements and tests.

Two measurements and one test are conducted. Measurements are;

- Local thickness control after sheet metal forming
- Residual stress measurement with X-Ray diffraction

Finally, two sets of fatigue tests are performed to find out the fatigue life of the part. One set of tests are done with deep drawn parts as drawn and the other set with deep drawn parts that are heat treated for residual stress relieve.

The part to be analyzed is the half of a pressure tube, which has a half sphere-like geometry. The sheet metal forming process is drawing realized with a hydraulic press. Implicit non linear algorithm is used for the sheet metal forming process simulation and both stress and strain based approach of fatigue life prediction finite element method are utilized with different mean stress correction algorithms.

CHAPTER 2

BASIC CONCEPTS IN METAL FORMING SIMULATION AND FATIGUE LIFE EXPECTANCY

2.1 Plastic Behavior of Metals

Plastic behavior of metals at relatively low temperatures, where the relation between stress and strain does not depend on strain rate and the onset of plastic deformation occurs at a well defined stress level, can be predicted by utilization of yield surface plasticity.

Yield surface plasticity models consist of a yield criterion, a plastic flow equation and a hardening rule. The yield criterion defines the limit of elastic behavior throughout the loading history for a general state of stress. The flow equation relates the plastic strain increment to the stress state and loading increment. The hardening rule is used to predict changes in the yield criterion and flow equation as a result of straining. [1]

2.1.1 Criteria for Initial Yield

Yielding, transition from elastic to plastic state, occurs when the stress reaches to a value for which some prescribed value of plastic strain is produced. For uniaxial stress state, this stress is defined by σ_y , which is calculated as;

$$\sigma_y = \left| \frac{F}{A} \right| \quad 2.1$$

where F is the axial load and A is the cross-sectional area of the specimen.

For a general three dimensional stress state, yield criterion or yield function is used to determine the limit for the elastic state. The yield function is frequently referred as yield surface since it forms a surface in stress space and can be written as;

$$f(\sigma_{ij}) = k \quad 2.2$$

Yielding is assumed to occur if the yield function value is greater than a prescribed value, k . For polycrystalline metals it is reasonable to assume that the initial yield behavior of the material is isotropic. Von Mises and Tresca (or maximum shear) criteria are the most common criteria among isotropic criteria.

The mathematical representation of von Mises criterion is as follows;

$$\sigma_y = \sqrt{\frac{1}{2} [(\sigma_1 - \sigma_2)^2 + (\sigma_2 - \sigma_3)^2 + (\sigma_3 - \sigma_1)^2]} \quad 2.3$$

Physically, von Mises value is proportional to the distortion energy, which is stored in the elastically deformed material before yielding. Figure 2.1 is a representation of the von Mises criteria in principal stress space.

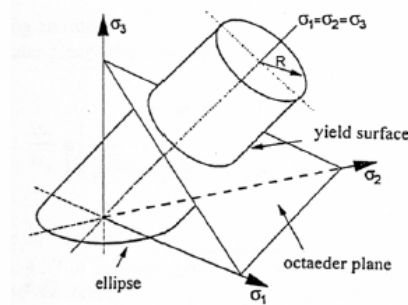


Figure 2.1 Von Mises yield surface in principal stress space [26]

Tresca criterion is identical to von Mises for uniaxial loading but it is more conservative for any other stress state. Mathematical representation for Tresca is as below;

$$\sigma_y = \max(|\sigma_1 - \sigma_3|, |\sigma_2 - \sigma_3|, |\sigma_1 - \sigma_2|) \quad 2.4$$

Figure 2.2 shows both von Mises and Tresca criterion on π plane. π plane is obtained by viewing the principal stress space through hydrostatic line (line on which $\sigma_1 = \sigma_2 = \sigma_3$) direction. As can be seen, Tresca criterion forms a hexagon into von Mises yield cylinder.

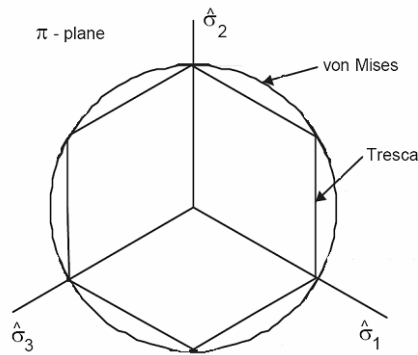


Figure 2.2 Von Mises and Tresca criteria on π plane [1]

There are several criteria for anisotropic materials like Hill, Barlat and Karafilles. Descriptive tables are prepared by Anne-Marie Habraken [2] for these criteria. Table 2.1 summarizes Hill's and Barlat-Karafillis models.

Table 2.1 Hill's and Barlat-Karafilis criteria [2]

Law	Description	Characteristics	Parameters & Experiments	References
Hill 1948	$2f(\sigma_{ij}) \equiv F(\sigma_y - \sigma_z)^2 + G(\sigma_z - \sigma_x)^2 + H(\sigma_x - \sigma_y)^2 + 2L\tau_{yz}^2 + 2M\tau_{zx}^2 + 2N\tau_{xy}^2 = 1$	General quadratic equation with 6 parameters, 3D state	6 parameters, 3 uniaxial tests; 0, 45, 90°	Hill 1948, Vial 1997, Barlat <i>et al.</i> 1991, Vial & Hosford 1983,...
Hill 1979	$F \sigma_y - \sigma_z ^a + G \sigma_z - \sigma_x ^a + H \sigma_x - \sigma_y ^a + A 2\sigma_x - \sigma_y - \sigma_z ^a + B 2\sigma_y - \sigma_z - \sigma_x ^a + C 2\sigma_z - \sigma_x - \sigma_y ^a = \sigma_F^a$	Hill with variable exponent (non integer) and no shear stress term so that orthotropic material axes and principal stress axes must be superimposed. 3D state	7 parameters, 3 uniaxial tests + plane strain test	Vial 1997, Barlat <i>et al.</i> 1991, Suh <i>et al.</i> 1996, Vial & Hosford 1983.
Hill 1990	$ \sigma_1 + \sigma_2 ^a + \frac{\sigma_b^a}{\tau^a} \sigma_1 - \sigma_2 ^a + \left \sigma_1^2 - \sigma_2^2 \right ^{\frac{a}{2}+1} \left[-2A(\sigma_1^2 - \sigma_2^2) + B(\sigma_1 - \sigma_2)^2 \cos 2\beta \right] = 2\sigma_b^{a2}$	Extension of Hill 79 that suppresses its limitation in loading directions but is only defined for plane stress case. Plane Stress State	5 parameters, 3 uniaxial tests + equibiaxial tensile test	Hill 1990 Barlat <i>et al.</i> 1991, Vegter <i>et al.</i> 1999, Kuwabare & van Bael 1999.
Hill 1993	$\frac{\sigma_x^2}{\sigma_0^2} - C \frac{\sigma_x \sigma_y}{\sigma_0 \sigma_{90}} + \frac{\sigma_y^2}{\sigma_{90}^2} + \left[(A + B) - \frac{A\sigma_x + B\sigma_y}{\sigma_b} \right] \frac{\sigma_x \sigma_y}{\sigma_0 \sigma_{90}} = 1$	Expression enabling to model different r_0 and r_{90} values, when uniaxial stresses in rolling σ_0 and transversal σ_{90} direction are almost equal. Loads applied along orthotropic axes. Plane Stress State	5 parameters, 2 uniaxial tests 0;90° + equibiaxial tensile test	Hill 1993, Banabic 1996, Banabic, <i>et al.</i> 1999, Vegter <i>et al.</i> 1999.
Barlat 1989	$A K_1 + K_2 ^a + A K_1 - K_2 ^a + (2 - A) 2K_2 ^a = 2\sigma_F^a$ $K_1 = \frac{(\sigma_x + \sigma_y)}{2}$ $K_2 = \sqrt{\left[\frac{(\sigma_x - \sigma_y)}{2} \right]^2 + (p\sigma_{xy})^2}$	Generalization of isotropic Hosford's (1972) equation with a shear term, defined by 4 parameters, a, h, p, A plane stress case, plane stress	4 parameters, 2 uniaxial tests + pure shear test	Vial 1997, Barlat & Lian 1989, Berg <i>et al.</i> 1998, Moshfegh <i>et al.</i> 1998, Andersson <i>et al.</i> 1999.

table continued...				
Barlat 1991	$ S_1 + S_2 ^a + S_s - S_3 ^a + S_3 - S_1 ^a = 2\sigma_{F1}^2$ with $\underline{S} = \underline{L}\underline{\sigma}$ $L = \begin{bmatrix} (c_2 + c_3)/3 & -c_3/3 & -c_2/3 & 0 & 0 & 0 \\ -c_3/3 & (c_3 + c_1)/3 & -c_1/3 & 0 & 0 & 0 \\ -c_2/3 & -c_1/3 & (c_1 + c_3)/3 & 0 & 0 & 0 \\ 0 & 0 & 0 & c_4 & 0 & 0 \\ 0 & 0 & 0 & 0 & c_5 & 0 \\ 0 & 0 & 0 & 0 & 0 & c_6 \end{bmatrix}$	Generalization of isotropic Hosford's (1972) equation with a shear term, defined by 6 anisotropy coefficients $c1$ to $c6$ + exponent m adapted for general stress state and orthotropic symmetric material. (RD, TD, ND). 3D state	6+1 parameters, 3 uniaxial tests	Barlat <i>et al.</i> 1991, Hayashida <i>et al.</i> 1995, Suh <i>et al.</i> 1996, Vegter <i>et al.</i> 1999.
Karafillis 1993	$\Phi_1 = S_1 - S_2 ^{2a} + S_2 - S_3 ^{2a} + S_3 - S_1 ^{2a} = 2\sigma_{F1}^{2a}$ $\Phi_2 = S_1^{2a} + S_2^{2a} + S_3^{2a} = \frac{2^{2a} + 2}{3^{2a}} \sigma_{F1}^{2a}$ $\Phi = (1 - C)\Phi_1 + C \frac{3^{2a}}{2^{2a} + 1} \Phi_2 = 2\sigma_{F1}^{2a}$ $\underline{S} = \underline{L}\underline{\sigma}$ with \underline{L} tensor 4 th order	Generalization of Barlat's 91 work to nonorthotropic material, 3D state	6+2 parameters, 3 uniaxial tests	Karafillis & Boyce 1993, Andersson <i>et al.</i> 1999 Barlat <i>et al.</i> 1997.
Barlat 1997	$\Phi = A S_1 + S_2 ^a + B S_s - S_3 ^a + C S_3 - S_1 ^a = 2\sigma_{F1}^a$ with \underline{S} and \underline{L} defined in Barlat 1991	Extension of Barlat 1991 to model high pure shear yield stress and to better fit r_0 and r_{90} , plane stress	6+1 parameters, 3 uniaxial tests + equibiaxial bulge	Barlat <i>et al.</i> 1997 Vegter <i>et al.</i> 1999.

$A, B, C, F, G, H, L, M, N, a$ are material parameters

$\sigma_x, \sigma_y, \sigma_z, \tau_{xy}, \tau_{zx}, \tau_{yz}$ are stress components in the material orthotropic axes

σ_1, σ_2 are principal stresses oriented by an anticlockwise angle β with RD axis

σ_b is the yield value under plane equibiaxial stress state

τ is the yield stress in pure shear test parallel to orthotropic axes (plane stress case)

σ_F is the yield stress under uniaxial tension in a reference direction

S_1, S_2, S_3 are eigenvalues of tensor \underline{S}

$\underline{\sigma}$ is the stress tensor in orthotropic axes and \underline{L} linear operator

$\sigma_x, \sigma_y, \sigma_{xy}$ stress components on the orthotropic axes

σ_{F1} uniaxial plastic stress in a reference direction

As mentioned by Vial [15], comparing to Hill's other criterion, Hill's oldest criterion gives a better correlation with metals having a weighted average Lankford's coefficient \bar{r} greater than 1 but is less acceptable when r is less than 1. Hill's first model (Hill-1948) has advantages that explain its intensive use. First of all, it improves the simple assumption of neglecting anisotropy and is simple to implement in a FEM code and available in numerous commercial codes. Additionally only 3 tensile tests at 0° , 45° , 90° are required to determine the material parameters.

Another representation of Hill-48 is;

$$2f(\sigma_{ij}) \equiv F(\sigma_y - \sigma_z)^2 + G(\sigma_z - \sigma_x)^2 + H(\sigma_x - \sigma_y)^2 + 2L\tau_{yz}^2 + 2M\tau_{zx}^2 + 2N\tau_{xy}^2 = 1$$

2.5

where F , G , H , L , M , N are parameters characteristic of the current state of anisotropy. It is assumed that there is no Bauschinger effect and that hydrostatic stresses do not influence yielding. Therefore, linear terms are not included and Eq. 2.5 reduces to;

$$2f(\sigma_{ij}) \equiv F(\sigma_y - \sigma_z)^2 + G(\sigma_z - \sigma_x)^2 + H(\sigma_x - \sigma_y)^2 = 1 \quad 2.6$$

Three tensile tests at 0° , 45° , 90° directions are sufficient to determine three unknowns in Eq 2.6. Figure 2.3 shows these directions commonly used for sheet metals. MSC.Marc enables the user to enter the tensile test results, namely Lankford parameters, directly to utilize Hill-48 as yielding model.

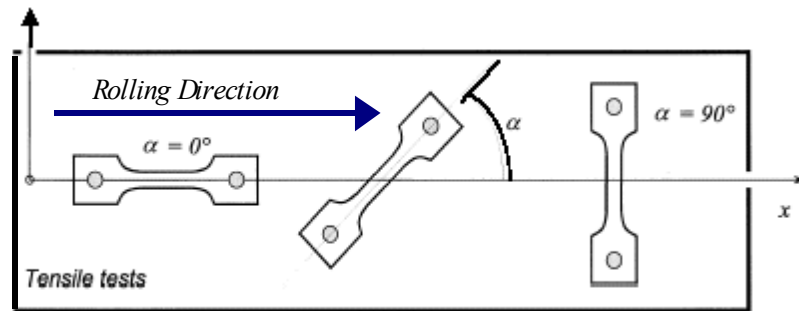


Figure 2.3 Tensile test directions for Hill criteria parameter determination for sheet metals

2.1.2 Elastic-Plastic Flow Rule

Stress states inside the yield surface belong to elastic state of material. Stress states that are on the yield surface are related with plastic state and according to yield surface models there can not be any stress state outside of the yield surface or they are meaningless.

When some amount of load is applied to a material that is already at a stress state on the yield surface, yield surface changes. For hardening materials, produced stress state lies outside of the starting yield surface. During the load application, yield surface changes shape in such a way that, stress state always lie on the surface.

Prandtl-Reuss equation is a flow rule that is associated with von Mises yield function. This function can be derived from Drucker's postulate [1], which establishes a firm relationship between the yield surface and plastic strain increments for hardening materials. Drucker also showed that yield surface must be convex.

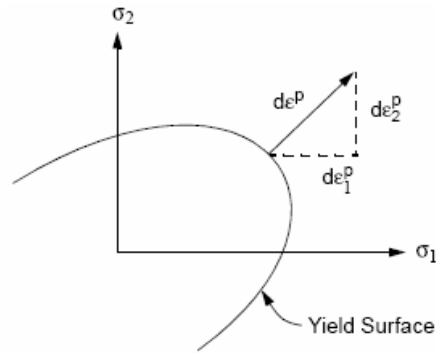


Figure 2.23 Yield surface and normality criterion for 2-D stress space [25]

2.1.3 Hardening Rules

Yield surface defined in section 2.1.1, changes as a result of hardening that develops during the history of plastic deformation. There are two basic models that model the change in the yield surface and a model, which combines these two basic models. Isotropic hardening assumes that the yield surface center is fixed and the surface expands without any change in its shape. Kinematic hardening assumes that the yield surface does not expand or change shape but center moves in six dimensional stress space. Combined hardening is the combination of isotropic and kinematic models. Figure 2.4 relates the true stress-true strain diagram to isotropic hardening of von Mises yield surface in 2D principal stress state.

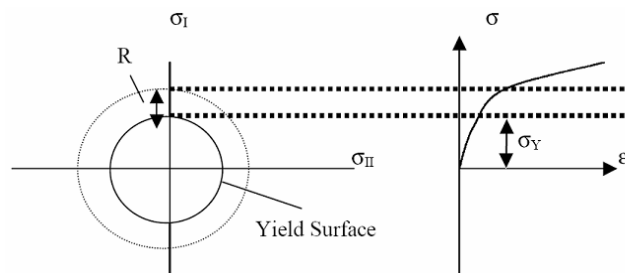


Figure 2.4 Expansion of von Mises yield surface with isotropic hardening

2.1.3.1 Isotropic Hardening

The expansion of the yield surface for isotropic hardening rule is shown in Figure 2.4. Corresponding loading/unloading graph is also given in Figure 2.5 (a).

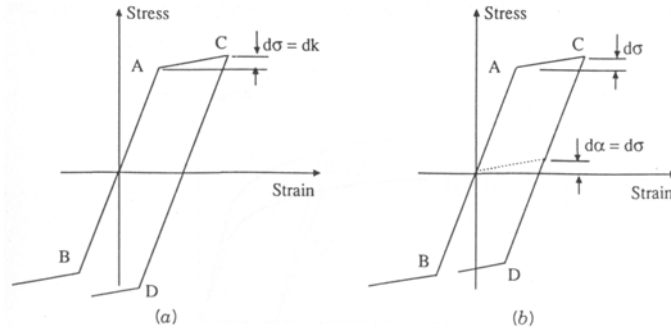


Figure 2.5 Schematic representation of loading/unloading corresponding to (a) isotropic (b) and kinematic hardening rules for tensile response [2]

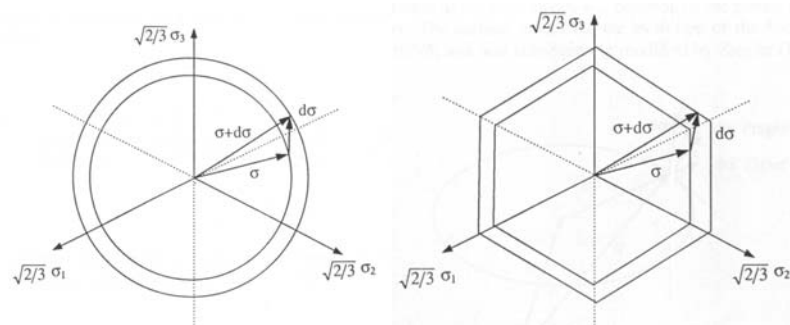


Figure 2.6 Isotropic hardening in 2D principal stress (π plane representation) space associated with (a) von Mises surface (b) Tresca yield surface [2]

According to isotropic hardening, yield surface expands uniformly in stress space as yielding occurs. Initially, the tensile and compressive yield stresses at points A and B are equal in magnitude. Once the stress has exceeded the yield in tension, the yield stress increases in both tension and compression. This is illustrated in Figure 2.5.a by the loading path from A to C , followed by an unload to zero stress and a compressive loading to the new compressive point D . The material remains

isotropic after yielding and the new tensile and compressive stresses are equal in magnitude throughout the deformation history.

For many materials, the isotropic workhardening model is inaccurate if unloading occurs (as in cyclic loading problems). For problems where loading is followed by unloading, the kinematic hardening model or the combined hardening model is preferred because isotropic hardening remains inaccurate.

2.1.3.2 Kinematic Hardening

Under the kinematic hardening rule, the von Mises yield surface does not change in size or shape, but the center of the yield surface can move in stress space. Prager-Ziegler kinematic hardening model is used to define the translation of the yield surface in the stress space.

Since the material is initially isotropic, the initial tensile and compressive yield stresses are equal in magnitude (Figure 2.5.b). The initial yield in tension is at point *A* and initial yield in compression is at point *B*. On the loading past, the initial yield point in tension and the magnitude of the yield stress in compression are assumed to decrease so that the elastic stress range from the tensile to the compressive yield remains unchanged. This is illustrated by the loading path from *A* to *C* followed by an unload to zero stress and a compressive loading to the new compressive yield point *D*. The material is no longer isotropic after yielding since the tensile and the compressive yield stresses are different.

2.1.3.3 Mixed Hardening

The mixed hardening model combines isotropic and kinematic yield functions and is proposed by Hodge in 1957 [1]. Hodge's mixed hardening model is based on the

assumption that the plastic strain increment may be linearly decomposed into components that produce kinematic hardening and isotropic hardening.

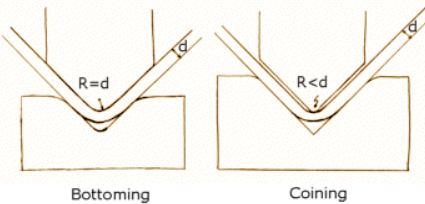
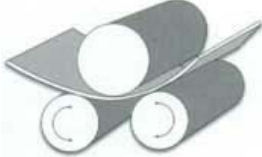
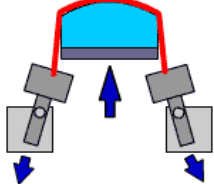
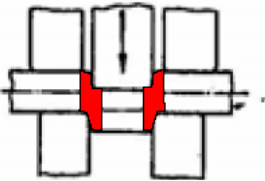
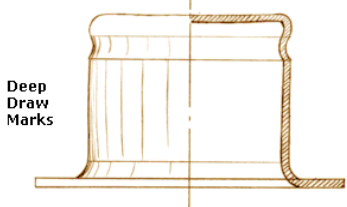
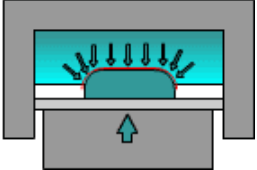
$$d\boldsymbol{\varepsilon}_{ij}^p = d\boldsymbol{\varepsilon}_{ij}^k + d\boldsymbol{\varepsilon}_{ij}^i \quad 2.7$$

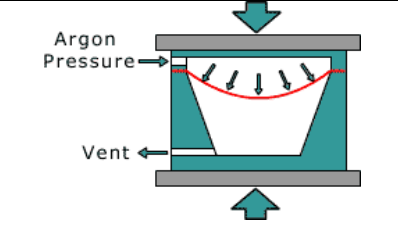
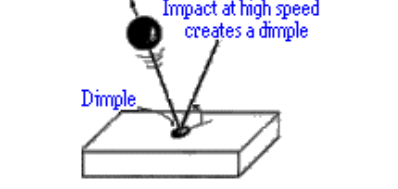
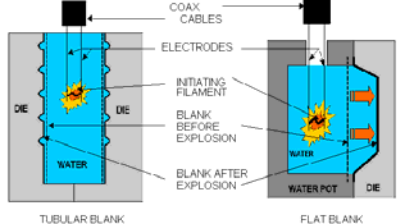
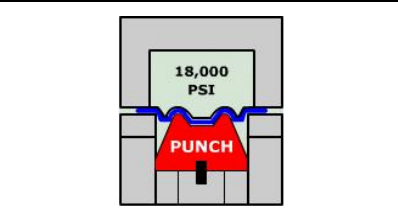
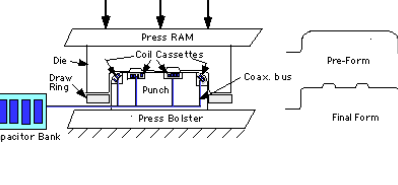
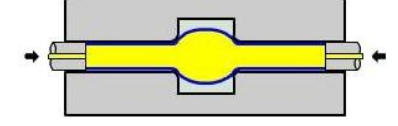
The ratio of isotropic to kinematic hardening is defined by a mixed hardening parameter, which must be obtained experimentally. Mixed hardening parameter may vary between 0 and 1. For pure kinematic hardening $M=0$, for pure isotropic hardening $M=1$.

2.2 Sheet Metal Forming Methods

The most common sheet metal forming methods utilize press machines to form sheet metal. As different geometries and materials are demanded by the market, new technologies are developed like hydroforming, magnetic pulse forming etc. Since the part that is subjected to analysis in this thesis is formed with deep drawing with hydraulic press machine, other methods are only mentioned for the integrity of the concept.

Table 2.2 Representation of common sheet metal forming methods

Method and Description	Schematic Representation
<p>Bending: usually refers to deformation about one axis.</p>	 <p style="text-align: center;">Bottoming Coining</p>
<p>Roll Forming: long parts with constant complex cross-sections; good surface finish; high production rates; high tooling costs.</p>	
<p>Stretch Forming: large parts with shallow contours; suitable for low-quantity production; high labor costs; high tooling and equipment costs.</p>	
<p>Shearing (Blanking/Piercing): includes a variety of operations, such as punching, embossing, bending, flanging, and coining; simple or complex shapes formed at high production rates; tooling and equipment costs can be high, but labor cost is low.</p>	
<p>Drawing: shallow or deep parts with relatively simple shapes; high production rates; high tooling and equipment costs.</p>	 <p style="text-align: left;">Deep Draw Marks</p>
<p>Rubber Forming / Elastoforming: drawing and embossing of simple or complex shapes; sheet surface protected by rubber membranes; flexibility of operation; low tooling costs.</p>	
<p>Spinning: small or large axisymmetric parts; good surface finish; low tooling costs, but labor costs can be high unless operations are automated.</p>	
<p>continued...</p>	

<p>Superplastic Forming: complex shapes, fine detail and close tolerances; forming times are long, hence production rates are low; parts not suitable for high-temperature use.</p>	
<p>Peen Forming: shallow contours on large sheets; flexibility of operation; equipment costs can be high; process is also used for straightening parts.</p>	
<p>Explosive Forming: very large sheets with relatively complex shapes, although usually axisymmetric; low tooling costs, but high labor cost; suitable for low-quantity production; long cycle times.</p>	
<p>Hydroforming: the sheet is formed against female die by the hydraulic pressure of the fluid, During the forming process, the intermediate plate acts as a blank holder to control the material movement from the flange and also seals the fluid medium to avoid leakage</p>	
<p>Magnetic Pulse Forming: shallow forming, bulging, and embossing operations on relatively low-strength sheets; most suitable for tubular shapes; high production rates; requires special tooling.</p>	
<p>Tubular Hydroforming: the process of forming hollow parts by applying internal hydraulic pressure to a tubular blank, mostly used in the automotive industry.</p>	

Deep drawing is defined as the process of cold working or drawing sheet or strip metal blanks by means of dies on a press into shapes which are usually more or less cup-like in character involving considerable plastic deformation of the metal. Deep-drawing quality sheet or strip steel, ordered or sold on the basis of suitability for deep drawing. There are many shapes that can be made through drawing and sheet metal fabrication such as cups, pans, cylinders, hemispheres, as well as

irregular shaped products. During the deep drawing process an initially flat blank is clamped between the die and the blank holder after which the punch moves down to deform the clamped blank into the desired shape. The final shape of the product depends on the geometry of the tools, the material behavior of the blank and the process parameters. The contact between the blank and the tools is the driving force of the deformation process. For this reason, the contact issue is of major importance in numerical simulations.

2.2.1 Press Machines

There are various types of press machines used for forming sheet metals. These machines are generally classified under three main categories;

- According to load application units
 - Hydraulic Presses
 - Mechanical Presses
- According to body shapes
 - C Shaped Presses
 - Straight Sided Presses
- According to number increments (1, 2 or 3 increment presses)

Mechanical presses are actuated by an electrical motor and the rotational motion is converted to in-line motion either by crank or eccentric shaft. The force is uniformly distributed over the pressure area. When lower speed or higher forming pressure is required, generally, a gear system is used. Articulated arm presses have shorter strokes but the pressure can go higher than 1000 tons. These presses are usually used for operations requiring high pressures like stamping, ironing etc.

2.2.2 Related Material Properties

Both elastic and plastic properties of the material have great importance for forming operations. Elastic properties are effective especially on spring back characteristics. Most of the necessary properties for sheet metal forming applications are measured by two common mechanical tests; tensile test and formability test. Important properties and concepts concerning forming are elastic modulus, yielding point, ultimate tensile strength, anisotropy, formability, grain size and residual stresses. Elastic modulus, yielding point, ultimate tensile strength and amount of anisotropy can be found by tensile tests. Formability diagram of the material is drawn by formability test. Another appropriate measure of formability for deep drawing is the Lankford coefficient, r , which is a measure of the resistance of the material to thinning [27]. More about this factor is in the following section. Grain size has influence on both mechanical and visual characteristics of the material. Residual stresses can have positive or negative effect on the formation of the sheets.

The properties of the sheet metal are highly affected by the method used for raw sheet metal production. Figure 2.7 shows classical methods for sheet metal production. Sheet metals are available as flat plates and/or coils. Hot rolled products exist between 12 to 50 mm, while cold rolled products are 1.5-20 mm. These availabilities may change depending on the manufacturer. One of the most favorite products of sheet metals is the galvanized sheets and coils. These products are mostly used in galvanized coils and they are used in automotive industries, office and home equipment, electrical appliances and farming implements. Electrolytic tinplates are produced in 0.2-0.6 mm. and are used to manufacture tin cans for food and beverage industry, containers for chemical products, paints and oil industry, crown caps and bottle caps, various drawn and fabricated parts such as electrical equipment and toys. Following pictures are adopted from Erdemir A.Ş.'s web site.



(a) (b) (c)
Figure 2.7 Sheet metal products from Erdemir A.Ş., (a) plates (b) coils (c) galvanized coils

2.2.3 Standard Tensile Test for Sheet Metals

The standard tensile test is one of the basic tests of metallic materials and is realized by application of tensile load on circular or rectangular cross-section standard test specimen until breakage. The ends of the specimen are so that the specimen does not slide out of grips during the tensile load application. There are standards dictating how the geometry of test specimen should be and how tests should be conducted. General parameters of the specimens are as shown in Figure 2.8. European standard (EN 10002-1) or German standards (DIN 50125:2004-01) describe the specimen dimensions for different shapes of products in details.

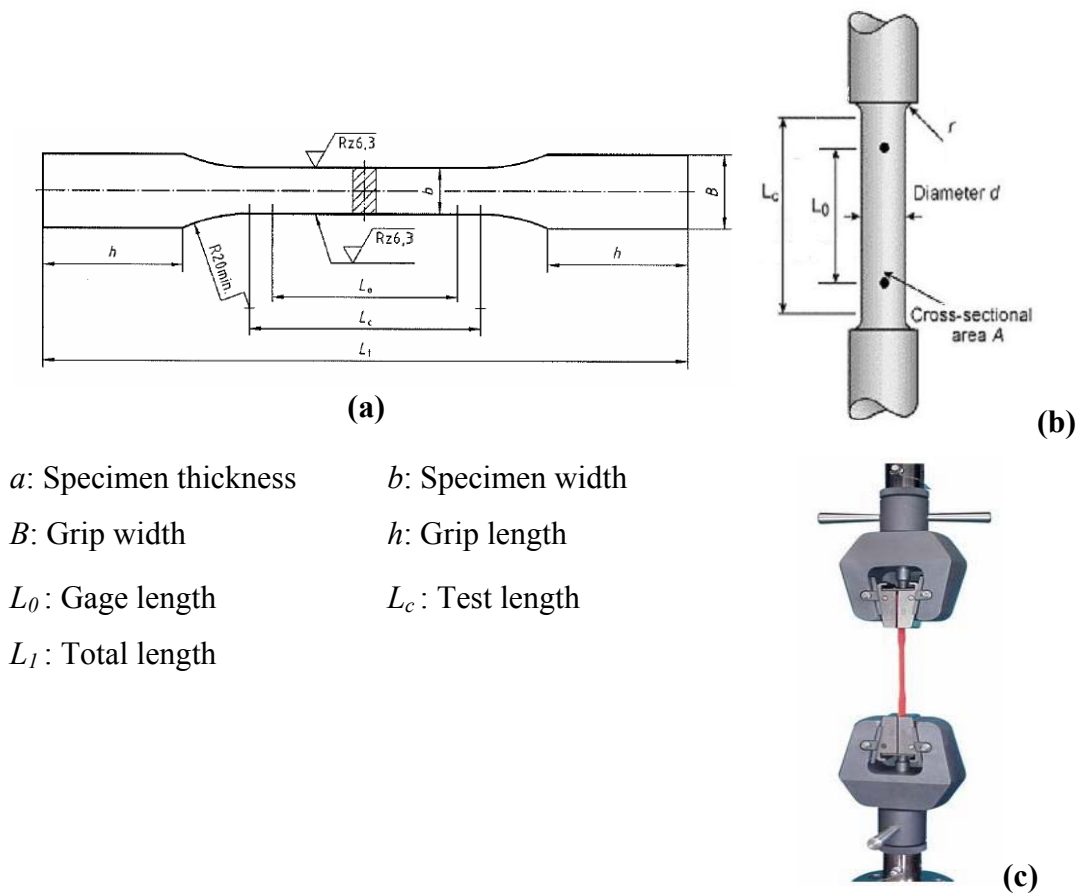


Figure 2.8 Tensile test specimen (a) circular cross section [DIN 50125:2004-01]
 (b) rectangular cross section and (c) grips and fixtures [Instron 2716-0003]

Most of the tensile test machines allow load controlled or displacement controlled tests. The main objective is to measure the load versus elongation of the gage length. Gage length is the portion of the specimen where the cross section is constant and where necking is expected because the cross sectional area in this range is the smallest. To be able to measure the elongation of the gage length only, a special measurement device called extensometer is utilized (Figure 2.9). It can be assumed that the elongation of the gage length is equal to the total elongation of the specimen when only a reasonably small amount of deformation is occurring outside of the gage length portion of the specimen.



Figure 2.9 Mechanical extensometer

Metallic materials generally exhibit similar behavior in the standard tensile test. This typical behavior is shown in Figure 2.10. The stress-strain curve is almost linear in the elastic region. The plastic region starts with yielding and load increases until ultimate tensile strength is reached. As necking of the specimen starts, load drops until breakage. Drop in the load does not mean a stress drop on the necking section.

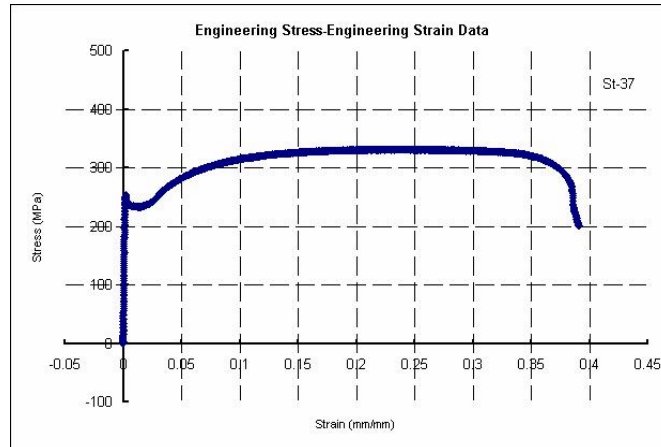


Figure 2.10 Tensile test realized in Ege University Laboratories, engineering stress-engineering strain data of a St-37 steel

Strain is the ratio between the amount of elongation to the initial length. Dividing the gage length elongation to initial gage length gives the engineering strain:

$$\varepsilon_e = \frac{\Delta L}{L_i} \quad 2.8$$

Since the length of the gage changes continuously, instantaneous strain can be defined by:

$$d\varepsilon_i = \frac{dL}{L} \quad 2.9$$

In this case the total strain, which is better known as the true strain or the logarithmic strain, will be:

$$\varepsilon_t = \int_{L_i}^L \frac{dL}{L} = \ln\left(\frac{L}{L_i}\right) \quad 2.10$$

The relation given below between the engineering strain and the true strain can easily be derived from Eq 2.9 and Eq 2.11:

$$\varepsilon_t = \ln\left(\frac{L_i + \Delta L}{L_i}\right) = \ln(1 + \varepsilon_e) \quad 2.11$$

The logarithmic strain is additive while engineering strain is not. This is the reason why iterative implicit algorithms utilize the logarithmic strain.

Dividing the recorded load to cross-sectional area gives the nominal stress through the cross section of the specimen. If this area is the initial cross-section of the specimen at the gage length, than this stress is called engineering stress.

$$\sigma_e = \frac{F}{A_i} \quad 2.12$$

where σ_e is the engineering stress, F is the applied force and A_i is the initial cross sectional area. However, since the cross sectional area changes as the specimen is elongated, instantaneous cross sectional area, A_{ins} , is required to find out true stress, σ_t , at any time of the test. Assuming negligibly small volume change:

$$A_i L_i = A_{ins} L_{ins} \quad 2.13$$

where L_i is the initial gage length and L_{ins} is the instantaneous gage length. Then,

$$\sigma_t = \frac{F}{A_{ins}} = \frac{F}{\left(\frac{A_i L_i}{L_{ins}}\right)} = \frac{F}{A_i} \frac{(L_i + \Delta L)}{L_i} = \sigma_e (1 + \varepsilon_e) \quad 2.14$$

Once the material stress-strain curve is obtained, several properties can also be calculated like modulus of resilience etc. Ludwik's equation can be used to represent the plastic region of the monotonic true stress-true strain curve of metals as [28];

$$\sigma_t = K \varepsilon_t^n \quad 2.15$$

or in logarithmic form;

$$\ln(\sigma_t) = \ln(K) + n \ln(\varepsilon_t) \quad 2.16$$

where K and n are material constants, namely, the strength coefficient and the strain hardening exponent respectively. These constants are calculated from the stress-strain data obtained with tensile test.

Simplifying and using least squares;

$$y = A + Bx \quad 2.17$$

where;

$$y = \ln \sigma$$

$$A = \ln K$$

$$x = \ln \varepsilon$$

$$B = n$$

The difference between a data point to the constructed line is;

$$y_i - (A + Bx_i) = \delta \quad 2.18$$

The sum of squares of all errors;

$$E = \sum_{i=1}^n \delta_i^2 = \sum_{i=1}^n (y_i - A - Bx_i)^2 \quad 2.19$$

To minimize the total error, the first derivatives with respect to a and b are taken and equated to zero;

$$\sum_{i=1}^n (y_i - A - Bx_i)(-1) = 0 \quad 2.20$$

$$\sum_{i=1}^n (y_i - A - Bx_i)(-x_i) = 0 \quad 2.21$$

simplifying;

$$nA + B \sum_{i=1}^n x_i = \sum_{i=1}^n y_i \quad 2.22$$

Replacing parameters;

$$A \sum_{i=1}^n x_i + B \sum_{i=1}^n x_i^2 = \sum_{i=1}^n x_i y_i \quad 2.23$$

The weighted average of n is calculated as follows;

$$\bar{n} = \frac{n_0 + n_{90} + 2n_{45}}{4} \quad 2.24$$

The obtained n value is represented with subscripts as $n_{x/y}$ where x is the angle to rolling direction and y is the upper strain value of data points used for calculations. The mechanical properties of sheet metals exhibit anisotropy unless special operations to prevent directional property differences are done. An example of this case is shown in Figure 2.11.

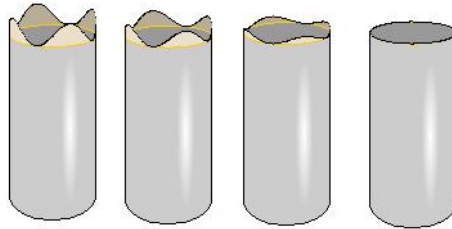


Figure 2.11 Formation of wave like shapes caused by anisotropy [27]

Lankford parameters are calculated at a certain strain level with the given formulation below;

$$r_{x/y} = \frac{\epsilon_{t,w}}{\epsilon_{t,t}} \quad 2.25$$

where ε_{rw} is the true width strain and $\varepsilon_{t,t}$ is the true thickness strain. The subscript x is the angle to rolling direction and y is the strain level at which the calculation is made. The weighted average value of r is calculated as;

$$\bar{r} = \frac{r_0 + 2r_{45} + r_{90}}{4} \quad 2.26$$

2.3 Fatigue Behavior of Metals

The history of fatigue design goes back to the middle of the nineteenth century, marked by the beginning of industrial revolution and, in particular, the development of railroads in central Europe. The first known investigators concerned with fatigue phenomena were designers of axles for locomotives. Wöhler's experiments [10] with axles in 1852 were the first known laboratory tests with the objective to derive and quantitatively describe the limits of fatigue. This was followed by more elaborate analyses of stresses and their effect on fatigue by Berber, Goodman and others [23].

Continuous efforts of researches in the twentieth century have given a new dynamic to the development of theories, such as the effects of plastic deformation on fatigue-resulting in the strain method discovered by Manson and Coffin [22]. In parallel, Paris and others [30] continued the theory of crack propagation started by Griffith [29]. Research accomplishment of Morrow Socie and their followers brought the state of fatigue analysis to the present day level [7]. Fatigue was incorporated into design criteria near the end of the nineteenth century and has been studied since. However, the most significant developments have occurred since the 1950s. At present, fatigue is part of design specification for many engineering structures [3].

2.3.1 Fatigue Failure

The fatigue failure of metals is a type of failure that occurs after the repetition of several cycles – from a few to millions – of stresses applied to the specimen, or to the component. This failure is very different from static failure (or quasi-static failure), that this failure is due to a load, consequently a stress, monotonically growing from zero to the value that produces breakage. Recently, as the improvements in the comprehension of this phenomenon have been done, engineers have several tools to design a component subjected to repeated loads without breakage during the desired life [2].

Fatigue failures are caused by a crack, that can already exist in the specimen or in the part (defect or flaw), or that takes origin somewhere due to the repeated stress (nucleates). This crack – existing or nucleated – propagates in the specimen or in the part, reducing the effective area and finally causing the breakage, when the area is reduced to an amount that is lower than the minimum value that can resist to a static load. It is a very rough approximation that the maximum value of the repeated load that produces a fatigue failure is 50% of the value that produces static failure.

Fatigue failure studies are directed to the study of crack nucleation and propagation until breakage.

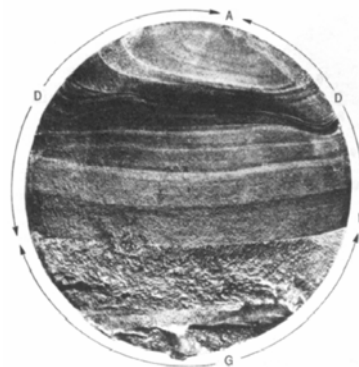


Figure 2.12 Typical fatigue failure stages [6]

2.3.2 Crack Nucleation and Propagation

At a value of monotonic uniaxial loading of a crystalline material, some slip will occur in the direction of maximum shear stress, which is in this simplest case, 45° to the direction of maximum normal stress. This case is shown in Figure 2.13.

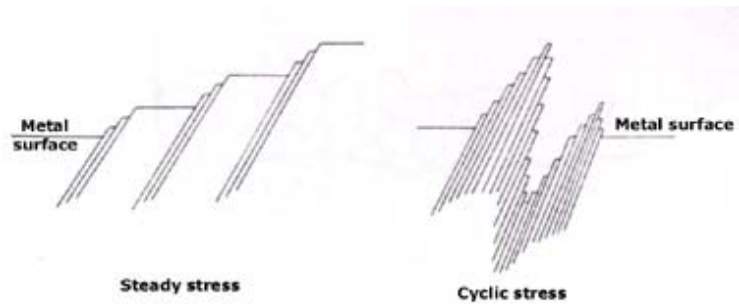


Figure 2.13 Slip formation on the metal surface and slip directions in case of uniaxial loading [6]

When the load cycle is applied as loading, unloading and loading in the opposite direction, then slip bands are formed as shown in Figure 2.13. Slips are not reversible, even in the elastic region of the material; consequently some plastic phenomena occur. As a result of these slip bands, a surface crack can nucleate.

After nucleation, crack can propagate inside the bulk of the specimen or of the part if appropriate conditions occur. Figure 2.14 schematizes crack propagation in two stages. At stage I, crack propagates at 45° with the maximum normal stress while in stage II, crack propagates along planes normal to the maximum stress. In Figure 2.14, crack propagates across the grain boundaries and this crack growth is called transcrystalline. It is possible that crack grows along the grain boundaries, which is called intercrystalline growth.

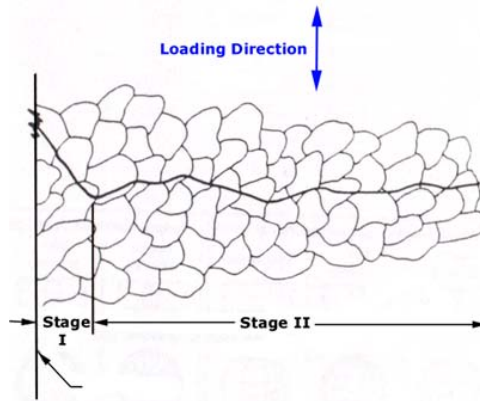


Figure 2.14 Propagation of a crack starting from the surface of the metal [4]

A very summarized representation of fatigue process is shown in Figure 2.15. The figure shows stages of the fatigue process.

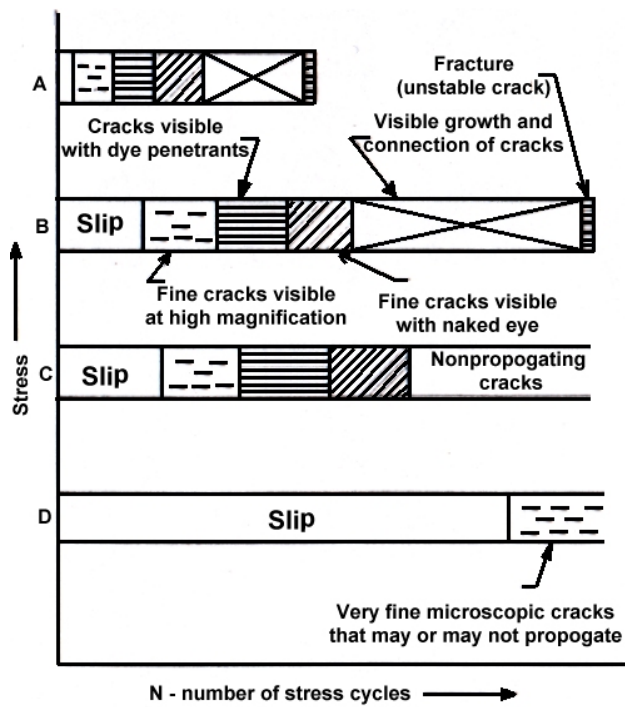


Figure 2.15 Fatigue process developments [7]

2.3.3 Wöhler Diagram

Wöhler diagram, or S-N diagram or Moore diagram, is a typical tool for fatigue design, especially for high cycle fatigue cases, introduced in 1874 by Prof. Ludwig Spangenberg. The name of the diagram comes from a mechanical engineer who did a systematic research in the field of fatigue, August Wöhler (1819-1914).

Data represented in Wöhler diagram is THE stress amplitude versus number of cycles to failure. There are three versions of the diagram; linear-linear, linear-logarithm and logarithm-logarithm. Figure 2.27 shows the most common representation that is logarithm-logarithm. The line in the Wöhler diagram is the interpolation of points of breakage. At a level of stress amplitude, break occurs at different number of cycles and the Wöhler line is handled by statistical analysis and should be treated accordingly. More information on Wöhler diagram is given in section 2.3.6.1.

2.3.4 High Cycle Fatigue and Low Cycle Fatigue

It is possible speak about three main fields of Wöhler diagram. These fields are shown in Figure 2.16; Low Cycle Fatigue (LCF), High Cycle Fatigue (HCF) and infinite life field.

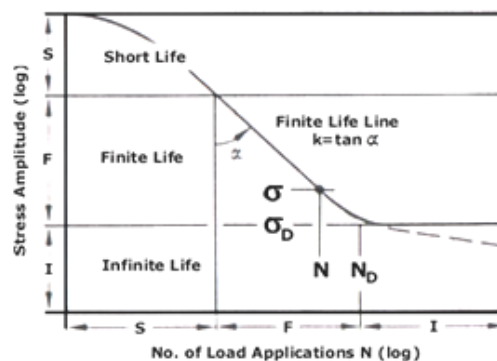


Figure 2.16 Zones of fatigue behaviors

There is no certain rule to separate the LCF from the HCF fields. As a rule of thumb, LCF refers to life from 10 to 10^6 cycles to failure, usually 10^5 ; for higher number of cycles, the field is called HCF [5]. The real difference between these two fields are done according to amount of plastic strain that the most stressed location of the part or the specimen faces. In LCF field relatively high stresses are present, consequently, plastic strain of the total strain exists. Another important sign of LCF is that, in LCF, the portion of crack nucleation of total fatigue life is high. This situation can be seen in Figure 2.17.

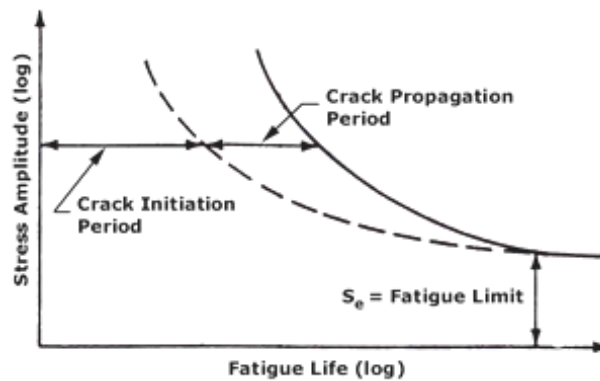


Figure 2.17 Crack initiation and propagation periods [8]

The knee of the Wöhler diagram occurs at the number of cycles called N_D and N_D depends on the type of the material. The corresponding stress value is called fatigue limit and in infinite life field, stress over the specimen or part is equal or lower than the fatigue limit, if exists or where the stress-cycle line has a very small slope. Some materials like aluminum have no knee and no fatigue limit. In these cases, we refer to the endurance limit, which is the stress value at a given number of cycles (10^6 or 10^7 etc.).

2.3.5 Factors Effecting Fatigue Life

Since the fatigue curves are prepared for predefined test specimens and predefined loads, some corrections has to be done. These corrections are generally done with correction factors. Common factors are listed below;

- Component size, C_{size}
- The effect of notches, C_{notch}
- The effect of surface finish, C_{surf}
- Mean stress effects

More detailed survey on correction factors can be found in different fatigue sources. To account for some of these effects, specific modifying factors are typically applied to the test result so that:

$$\varepsilon_e = \varepsilon'_e \cdot C_{notch} \cdot C_{size} \cdot C_{load} \cdot C_{surf} \cdot \dots \quad 2.27$$

where reciprocal of the product, $C_{notch} \cdot C_{size} \cdot C_{load} \cdot C_{surf} \cdot \dots$, is collectively known as the fatigue strength reduction factor K_f :

$$K_f = 1/(C_{notch} \cdot C_{size} \cdot C_{load} \cdot C_{surf} \dots) \quad 2.28$$

It is very important to remember that all the modification factors are empirical, conservative and generally only applicable to steel. They provide little or no fundamental insight into the fatigue process itself other than providing approximate trends.

2.3.5.1 Technological Size Effects

The size of the part, or the size of the rough metal sheet or bar from which the part has been machined, can effect the fatigue resistance, due to technological effects: the larger the dimension, in general, the lower the fatigue limit; this effect can be up to 10% of the fatigue limit [1]. Experiments show that from rotating beam tests and from torsion tests, the values of fatigue limit change inversely to diameters of specimens, while from axial loading tests the size has no influences on the fatigue limit [9].

“Critical Volume” concept is introduced by Kuguel [13] to explain size effect in notches. According to Kuguel, larger components has a greater volume of material at critical stress level as shown in Figure 2.18. Kuguel formed an empirical relationship between endurance limit and volume of the component as;

$$S_{eo} = S_{er} \left(\frac{V_0}{V_r} \right)^{-0.034} \quad 2.29$$

where S_{er} is the endurance limit for reference volume V_r , and S_{eo} is the endurance limit for some other volume V . There are other authors suggesting other techniques for size effects on fatigue behavior. As another example Shigley and Mitschke [14] present a simple expression that is fairly conservative.

Table 2.3 Suggested size factors of Shigley and Mitschke

For $d \leq 0.3$ in. (8 mm)	$C_{size} = 1$
For $0.3 \text{ in} \leq d \leq 10 \text{ in.}$	$C_{size} = 0.869 d^{-0.097}$
For $8 \text{ mm} \leq d \leq 250 \text{ mm}$	$C_{size} = 1.189 d^{-0.097}$
For larger sizes use	$C_{size} = 0.6$

These equations are valid for cylindrical parts. For parts of other shapes, Kuguell [13] suggested that equating the nonround part’s cross-sectional area stressed above 95% of its maximum stress with the similarly stressed area of a rotating

beam specimen would provide an equivalent diameter to use in the above equations. For a rectangular cross-section Kuguel suggests the use of the following relation [13];

$$d_{eq} = 0.81A \quad 2.30$$

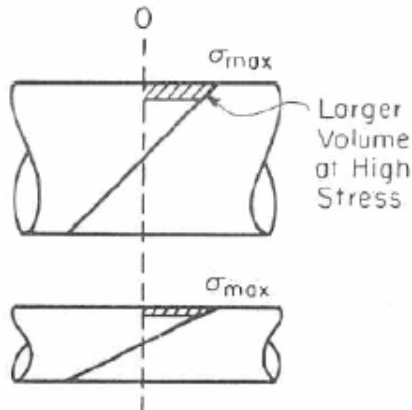


Figure 2.18 Area under critical stress [13]

2.3.5.2 Nominal Stresses and Real Stresses (Effect of Notches)

Nominal stresses are calculated throughout the cross section of the specimen or of the part, without any stress gradient. But, stress raisers such as notches, holes or sharp corners can cause large rise in stress above the nominal stress. These effects are taken into account with a factor. A detailed survey of gradient effects on fatigue limit can be found in the work of Filippini [11].

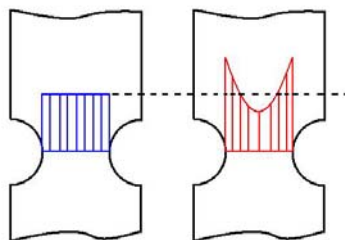


Figure 2.19 Nominal stresses to real stresses

2.3.5.3 *Surface Effects*

A large number of fatigue breakages nucleate from the surface of the part, because the stresses are higher as a consequence of the kind of applied stress and of notches [1]. Any change in the surface conditions can influence fatigue behavior. The conditions of the material at the surface layer can be very different from the conditions of the core by means of the followings;

- Surface roughness
- Residual stresses
- Mechanical property changes

There are many operations that may cause above changes. Below processes are the most familiar processes;

- Surface finish and related operations
- Thermal processing
- Chemical processing
- Plating or coating

Pits and scratches on the surface serve as points of stress concentration and crack initiation sites. The effect of surface processing is tabulated by Zahavi and Turbilo [8] and it is given in Table 2.4;

Table 2.4 Surface process effects on fatigue limit [8]

Processing Method	R_a [μm]	Strain Hardening	Residual Stresses	Fatigue Limit Effect
Turning	0.32 - 3.2	Present	Tens./comps.	Variable
Boring	0.32 - 3.2	Present	Tens./comps.	Variable
Milling	0.32 - 5.0	Present	Tens./comps.	Variable
Broaching	0.63 - 2.5	Present	Tens./comps.	Variable
Grinding	0.2 - 1.25	Absent	Tensile	Decrease

Honing	0.2 - 0.8	Variable	Tensile	Decrease
Polishing	0.04 - 0.32	Variable	Tens./comps.	Increase
Lapping	0.01 - 0.16	Variable	Tens./comps.	Increase
Superfinish	0.02 - 0.16	Variable	Tens./comps.	Increase
Electropolishing	0.15 - 0.3	Absent	-	Increase
Rolling	0.08 - 0.63	Present	Compressive	Increase
Shot peening	1.25 - 5.0	Present	Compressive	Increase

Table 2.5 Surface process effect on fatigue limit [5]

Processing Method	R_a [μm]	Residual Stress [MPa]	Fatigue Limit [MPa]	Relative to Basic Process [%]
Grind. Polish. (basic proc.)	0.12	+100	640	100
Grind. Polish. lapping	0.02	+100	670	105
Grind. Polish. Electropolish	0.08	+40	850	133
Grind. Polish. rolling	0.12	-1600	900	140

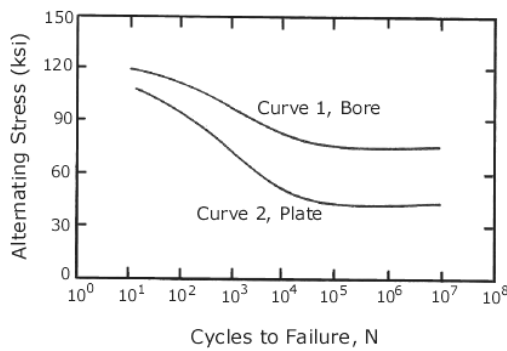
In Table 2.5, relative increase of fatigue limit for steels are shown. Thermal processes may cause residual stresses because of thermal gradients and differential expansion/contraction. In addition to quenching and casting, welding, severe grinding, flame cutting, flame hardening, induction hardening are some processes that can thermally create residual stresses and/or change phase of the material, in consequence mechanical properties.

Chemical processes like carburizing/decarburizing, nitriding creates residual stresses and changes the fatigue strength of the material at the surface. Decarburization is done at high temperatures in oxygen rich environments by migrating carbon out of the iron matrix. As a result, residual tensile stresses are formed and strength drops. Forging and hot rolling processes are also sources of decarburization. Table 2.6 summarizes the decarburization effect on several steels;

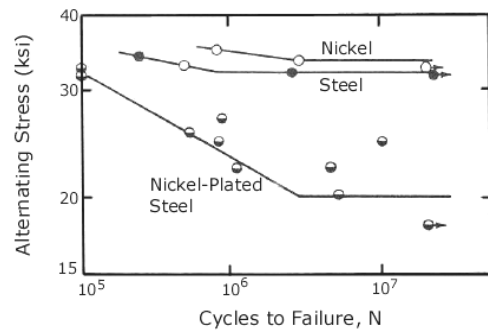
Table 2.6 Decarburization effect on fatigue limit [20]

		Endurance Limit (ksi)			
		Non-decarburized		Decarburized	
Steel	S_u (ksi)	Smooth	Notched	Smooth	Notched
AISI 2340	1724	841	476	241	172
AISI 2340	951	572	296	303	172
AISI 4140	1634	717	455	214	152
AISI 4140	965	572	276	221	131

Plating or coating can have different effects on the fatigue strength of steels. Generally, electroplating of hard metals on steel reduces the fatigue strength as shown in Figure 2.20. The reasons for this reduction are tensile stress formation on steel surface and early formation of cracks on plate metal that grow into steel core. Plating with soft metals has less effect on fatigue behavior of the part or of the specimen.



(a)



(b)

Figure 2.20 (a) Effect of chrome plating on SN curve for 4140 steel (b) Effect of nickel plating on SN curve of steel ($S_u=63\text{ksi}$) [23]

2.3.5.4 Mean Stress Effects

Since, classical S-N and ϵ -N curves are obtained at zero mean stress, it has to be modified to adopt for non-zero mean stress cases. There are several empirical studies done to relate mean stress to fatigue limit via yield strength or ultimate

strength. A brief history on these studies can be found in the work of Fuchs and Stephens [7]. Table 2.7 summarizes these relationships and following figure gives graphical representation of these equations. Although these rules are valid for tensile stress cases, they are applied for other stress states.

Table 2.7 Mean stress correction methods

Mean Stress Method	Equation
Soderberg, 1930	$\frac{\sigma_a}{S_e} + \frac{\sigma_m}{S_y} = 1$
Goodman, 1899	$\frac{\sigma_a}{S_e} + \frac{\sigma_m}{S_u} = 1$
Gerber, 1874	$\frac{\sigma_a}{S_e} + \left(\frac{\sigma_m}{S_u}\right)^2 = 1$
Morrow, 1960's	$\frac{\sigma_a}{S_e} + \frac{\sigma_m}{\sigma_f} = 1$

σ_a , stress amplitude; σ_m , mean stress; σ_f true fracture limit
 S_y , yield strength; S_u , ultimate tensile strength; S_e , endurance (fatigue) limit

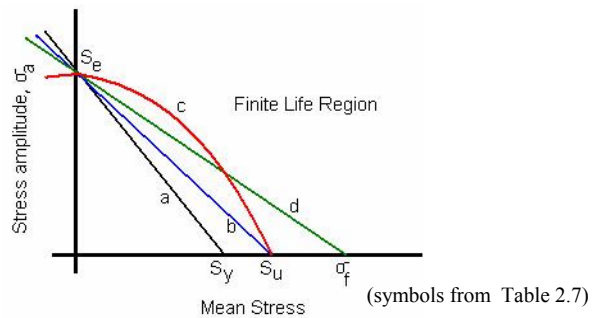


Figure 2.21 a. Soderberg b. Goodman c. Gerber d. Morrow

For the strain-life analysis, there are two common methods for mean stress correction. One of these methods is Morrow and the other one is Smith-Watson-Topper. Comer [20] explains the mean stress effect on strain-life curve as in Figure 2.22. As a rule of thumb, for long life cases compressive mean stresses improve

fatigue life while tensile mean stresses degrades. For short life cases, lower than 10^3 cycles, mean stresses have little effect on the fatigue behavior.

Morrow equation [20];

$$\frac{\Delta \varepsilon}{2} = \frac{\sigma'_f - \sigma_0}{E} (2N_f)^b + \varepsilon'_f (2N_f)^c \quad 2.31$$

Smith-Watson-Topper [24] equation;

$$\frac{\Delta \varepsilon}{2} \sigma_{\max} = \frac{\sigma_f'^2}{E} (2N_f)^{2b} + \sigma'_f \varepsilon_f' (2N_f)^{b+c} \quad 2.32$$

In these equations $\sigma'_f, \varepsilon_f', b, c$ are material parameters and $\Delta \varepsilon, \sigma_{\max}$ are load parameters. Uniform material parameters for steel are listed in Table 2.11. For fully reversed strain cases, both equations will give same results. More information about mean stress effects can be found in the work of Comer [20].

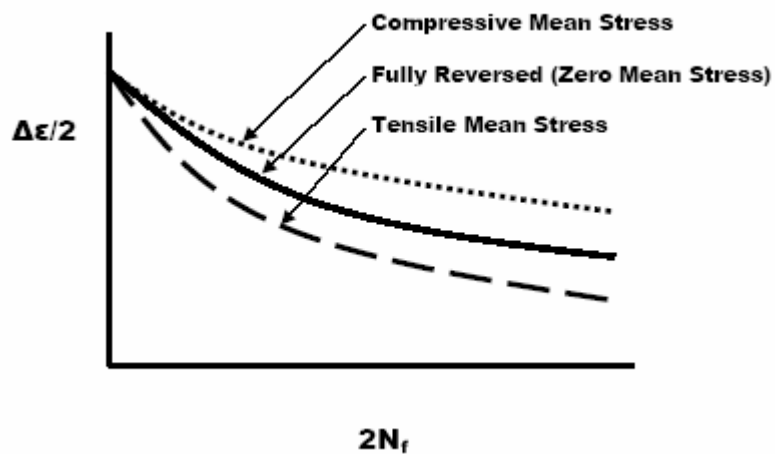


Figure 2.22 Mean stress effect on strain life curve [20]

2.3.6 Fatigue Analysis Approaches

2.3.6.1 The Stress-Life Approach

It is a well-known approach based on Wöhler diagram [10] and nominal stresses in the part. This approach is utilized for parts requested to have a long life, HCF, or infinite life. In cases where stresses evolve large plastic strains, this method may only be used to have a very rough idea about the fatigue life of the part, because it does not count for plastic strains.

Wöhler is the person who designed and built the first rotating beam test machine that produced fluctuating stresses of constant amplitude in test specimens. Moore , 1983

[16] later adopted this technique to a simply supported rotating beam in fully reversed, pure bending. Figure 2.23 is the schematic representation of Moore rotating bending machine. The constant force is applied by hanging weight, no shear over the length of the specimen is applied. Another testing is axial loading testing, which enables the application of cyclic load with a non-zero mean stress. Figure 2.24 shows a test machine operated by hydraulic actuators.

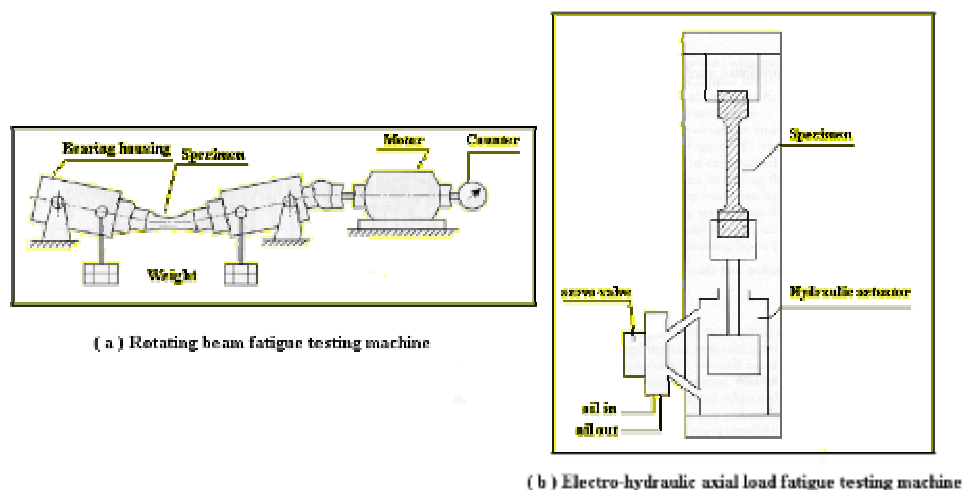


Figure 2.23 Schematic representation of fatigue test machines [7]

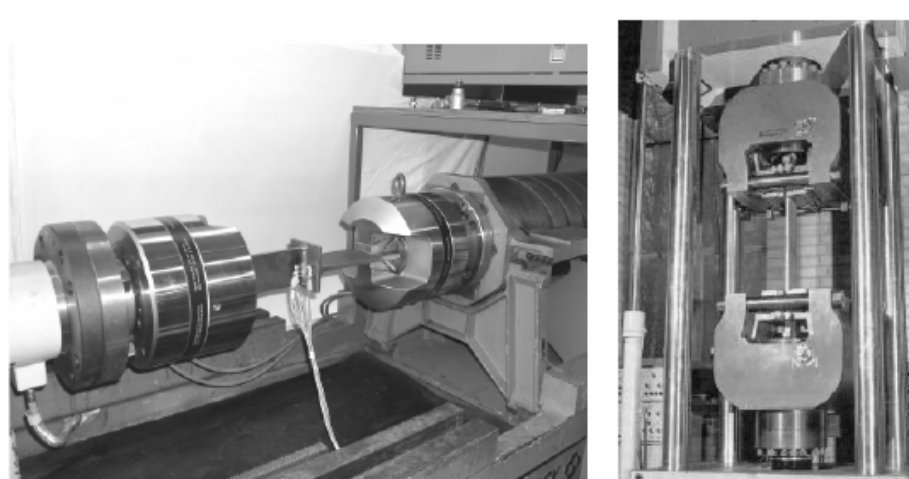


Figure 2.24 Fatigue test machines [7]

A principle difference between axial and rotating bending test is that the entire section is uniformly stressed in axial loading rather than linear stress distribution. Figure 2.25 shows this difference and it can be seen that S-N curve obtained from axial loading test is lower than those from rotating bending test.

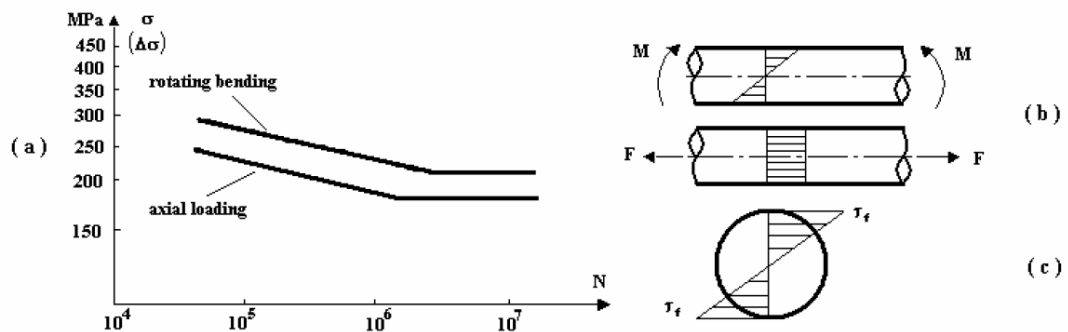


Figure 2.25 Stress gradient of rotating bending and axial loading tests [7]

There are fatigue tests other than two mentioned above. Torsional fatigue tests are performed on a cylindrical specimen subjected to fully reversed, torsional load. There is also rotating bending test that is very similar to rotating bending test but the specimen is pushed at one free end alternatively.

The common specimens have the geometry shown in Figure 2.26. There are mainly two types of specimen; un-notched or smooth and notched which has stress raisers. Most of the fatigue tests are performed in the high cycle fatigue field, where there is a linear relationship between stress range and fatigue life in log-log diagram.

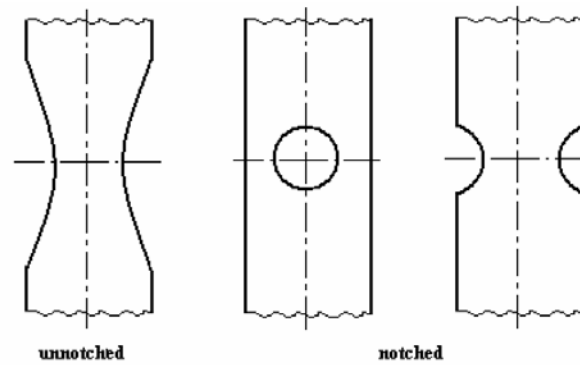


Figure 2.26 Common fatigue test specimens [6]

Even though the same specimen is used in tests, the results show large range of dispersion due to the different geometrical micro irregularities of surfaces for the same type of specimen. Therefore it is necessary to carry out the statistical analysis of fatigue data. The curves formed by integrating the failure probability are called P-S-N curves. The standard S-N curve corresponds to a 50 percent of probability of failure ($P=0.5$). A sample P-S-N curve is shown in Figure 2.27.

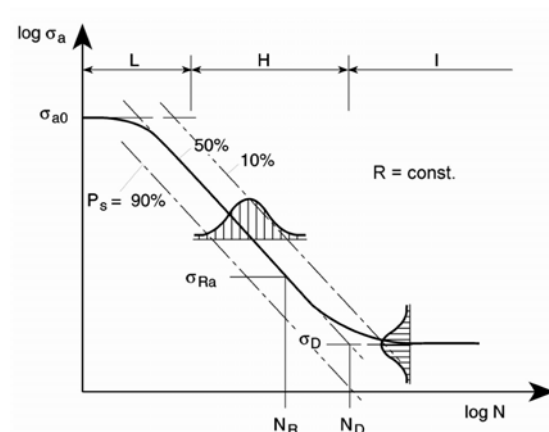


Figure 2.27 Logarithmic P-S-N Curve (Wöhler diagram) [3]

The objective for the infinite life is to ensure the working stress due to loading is under the fatigue limit. While the objective of the limit life design is to predict the number of cycles available within the fatigue life based on the stress level, or conversely to determine the stress based on a given number of cycles. To determine the fatigue limit experimentally, the test results are evaluated statistically using either the data of specimens that survived or of those that failed. A common procedure is staircase method, which can be described as follows [2];

- Estimate mean value, $\Delta\sigma_m$, and standard deviation, d , of the fatigue limit based on the preliminary knowledge
- Perform the first fatigue test at the stress level $\Delta\sigma_m + d$
- If the specimen fails, decrease the stress level by d . If the specimen survives, increase the stress level by d .
- Continue until 15 to 30 specimens have been tested
- A statistical evaluation of all tests yields the mean value of $\Delta\sigma_{D,50}$ and standard deviation of the fatigue limit as;

$$\Delta\sigma_{D,50} = \Delta\sigma_0 + d \cdot (A/F + 0.5) \quad 2.33$$

Figure 2.28 summarizes the method.

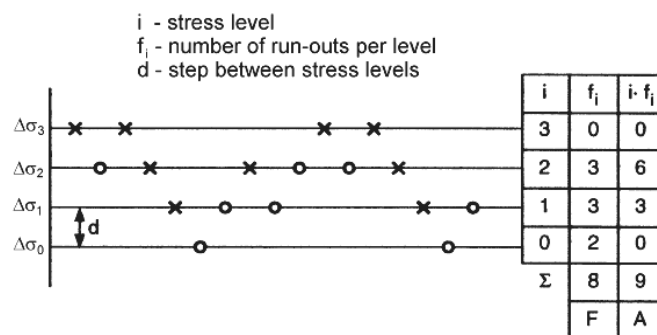


Figure 2.28 Statistical method used for determination of fatigue limit [3]

There are empirical estimates on fatigue limit of steels, but these estimations are very rough and not always reliable.

$S_e \sim 0.5 S_u$	for $S_u < 1379$ MPa
$S_e \sim 689$ MPa	for $S_u > 1379$ MPa

Table 2.8 Empirical fatigue limits for steel, related with ultimate strength

$S_e \sim 1,72$ BHN	for BHN < 400
$S_e \sim 689$ MPa	for BHN > 400

Table 2.9 Empirical fatigue limits for steel, related with Brinell hardness number

Many fatigue analysis programs generate S-N curves using different methods. The coefficients used by the program that fatigue calculations are based in this study is given in Table 2.10;

Table 2.10 Empirical coefficients to generate synthetic S-N curves

	Cycles	Stress Amplitude [MPa]
Ferrous Alloys	1	$1 \times S_u$
	10^3	$0.9 \times S_u$
	10^6	$0.357 \times S_u$
Titanium Alloys	1	$1 \times S_u$
	10^3	$0.8 \times S_u$
	5.10^8	$0.307 \times S_u$
Aluminum Alloys	1	$1 \times S_u$
	10^3	$0.7 \times S_u$
	5.10^8	$0.258 \times S_u$
Other Alloys	1	$1 \times S_u$
	10^3	$0.8 \times S_u$
	10^8	$0.274 \times S_u$

S-N curve is obtained by fatigue tests under certain conditions with predefined specimens. Generally, any change on the mechanical properties or microstructure is likely to affect the S-N curve. Some of these factors are; chemical environment, cyclic frequency, temperature, residual stresses, surface effects and etc. In order to adapt the S-N curve to different situations, there are many multipliers called modification factors. More about modification factors can be found in Section 2.3.5.

It is very well known that machine parts and components are seldom subjected to external loads that produce uniaxial state of stress as for example tension-compression or pure bending (torsion induces a biaxial state of stress). On the contrary, it is common that one, or more, external loads produce in the part a multiaxial state of stress, i.e. a state of stress having at least two principle stresses different from zero [2]. The state of stress in notches is often not the same as the state of stress in the main body, and the stress concentration factor changes with the state of stress. A transverse hole in a shaft in torsion produces a stress concentration. On the surface of the hole the state of stress is uniaxial, although it is biaxial in the shaft [1].

Although it has been conceived that von Mises criterion states the limit conditions referring to static stress (yielding), not to fatigue, a common rule (very often utilized because of the availability of FEM analyses that give this results as default) is to evaluate the state of stress at each point of a component utilizing the von Mises criterion. The utilization of this criterion (based on an energetic point of view) for fatigue analysis is, in general, not correct [3]. Another common stress used for fatigue analysis is the maximum absolute principle stress.

Monotonic and cyclic stresses show differences. The differences can be better visualized in Figure 2.29. Most of the stress-life analyses are elastic analysis with

monotonic stress-strain data. This situation effects the stress distribution over the part and adds another error into stress-life fatigue analysis.

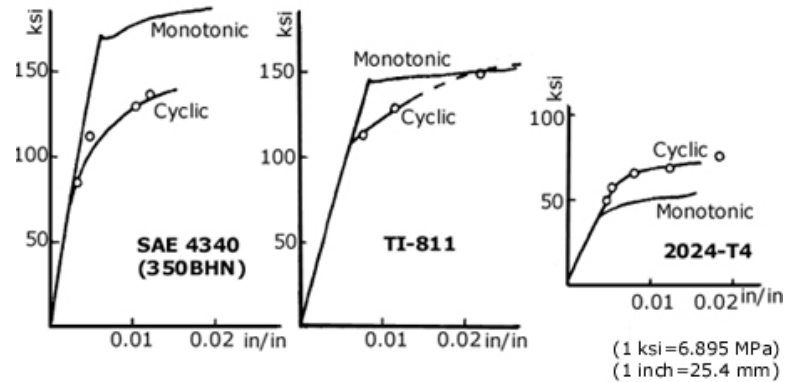


Figure 2.29 Material laws for static and cyclic loading, Langrad [19]

2.3.6.2 The Strain-Life Approach

The stress raisers such as notches create stress concentrations and elevate the strain into plastic range. The solution to this phenomenon is strain method, because this approach takes plastic strains into account. This method is preferred especially for low cycle fatigue problems where high amount of stresses, so high plastic strains, are present. The method was first developed by Coffin and Manson [22] in 1950's and is refined in 1960's by Morrow, Neuber [17], etc. the strain-life method is applicable to a larger range of problems than stress life method since it accounts for plastic strains in addition to elastic strains.

Strain-life method uses the strain-Wöhler curve to determine damage for each load and sum these damages to find out the total damage. Strain-life curves of materials can be derived when there is no test conducted. A usual method is to use uniform material law constants in so called Manson-Coffin [22] relation;

$$\varepsilon_a = \varepsilon_p + \varepsilon_e = \sigma_f' (2N_f)^b / E + \sigma_f' (2N_f)^c \quad 2.34$$

Figure 2.30 shows an example of strain-life curve. The coefficients in above relation are be estimated by Baumel-Seeger uniform material law [12] for steels and aluminum/titanium alloys as;

Table 2.11 Modified uniform material law, Baumel-Seeger

	Steel	Aluminum/titanium alloys
σ'_f	$1.5 S_u$	$1.67 S_u$
b	-0.087	-0.095
ε'_f	0.59	0.35
c	-0.58	-0.69
S_e	$0.45 S_u$	$0.42 S_u$
ε_e	$0.45 S_u / E + 1.95 \cdot 10^{-4} \cdot \psi$	$0.42 S_u / E$
N_e	5.105	1.106
K'	$1,65 S_u$	$1.61 S_u$
n'	0,15	0.11
ψ	1.0 for $S_u / E \leq 3 \cdot 10^{-3}$	
	$(1,375 - 125 \cdot S_u / E)$ for $S_u / E > 3 \cdot 10^{-3}$	

S_u : maximum allowable stress, σ'_f : fatigue strength coefficient,

ε'_f : fatigue ductility coefficient, K' : cyclic strength coefficient,

n' : cyclic strain hardening exponent, c : fatigue ductility exponent,

b : fatigue strength exponent, S_e : fatigue limit, ε_e : fatigue strain limit, N_e : finite life limit

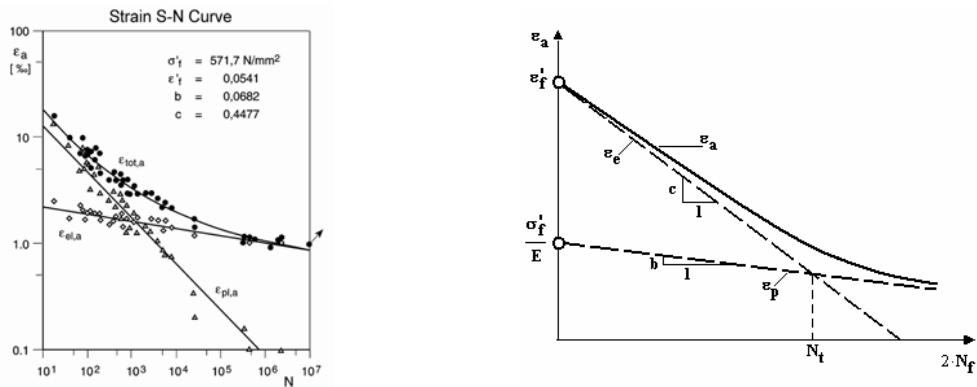


Figure 2.30 A typical Strain-Life (ε - N) curve [3]

Cyclic material data is utilized in strain-life analyses instead of monotonic data. The cyclic stress-strain data can be derived with Ramberg-Osgood [21] relation using the same material constant as Manson-Coffin relation [22].

$$\varepsilon_a = \sigma_a/E + (\sigma_a + K')^{1/n'} \quad 2.35$$

where σ_a is stress amplitude, K' is cyclic strength coefficient and n' is the cyclic strain hardening exponent. An example of cyclic and monotonic material curve is presented in Figure 2.31.

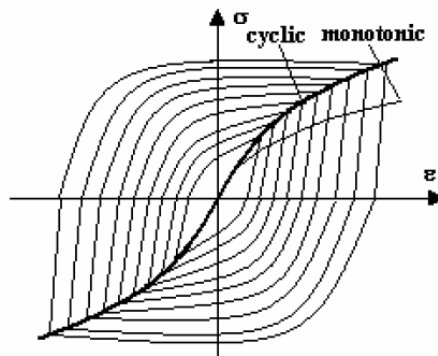


Figure 2.31 Cyclic to monotonic stress-strain diagram of a strain hardened material [4]

Strain-life analyses utilize elastic stress analyses to calculate the total life after elastic-plastic correction of stress-strain data. The elastic stresses and strains are looked up on the elastic line and then corrected to fall onto the cyclic stress strain curve to determine the elastic-plastic stresses and strains. This elastic-plastic strain is used to look up damage on the strain-life damage curve. Neuber's [17] elastic-plastic correction (sometimes called a notch correction) is based on the simple principle that the product of the elastic stress and strain should be equal to the product of the elastic-plastic stress and strain from the cyclic stress-strain curve.

Then through an iterative method, the elastic-plastic stress and strain can be determined. This is illustrated below.

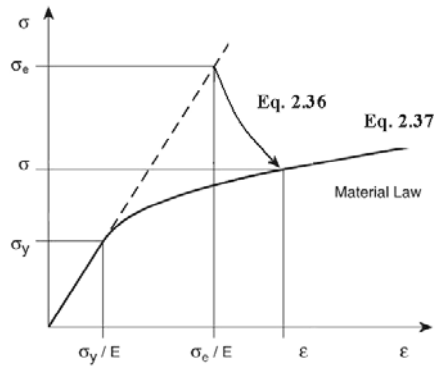


Figure 2.32 Schematic presentation of Neuber's rule [31]

Neuber's rule;

$$\sigma \cdot \varepsilon = K_t^2 \cdot \frac{S^2}{E} \quad 2.36$$

where

$$K_t^2 = K_\sigma \cdot K_\varepsilon \quad 2.37$$

and

$$K_\sigma = \frac{\sigma}{\sigma_n} \quad 2.39$$

$$K_\varepsilon = \frac{\varepsilon \cdot E}{\sigma_n} \quad 2.38$$

and σ is local stress, S is nominal stress, ε is local strain, e is nominal strain, K_t stress concentration factor.

2.3.6.3 The LEFM Approach

The LEFM (Linear Elastic Fracture Mechanics) approach is based on the propagation of cracks. A typical application of this method is the evaluation of crack propagation starting from an assumed or estimated initial dimension of the crack, to find out the remaining life of the component. [3] [28]

2.3.6.4 Variable Amplitude Loading, Cumulative Damage Hypothesis, Cycle Counting Methods

Constant amplitude loading is an abstract loading condition for a part or for a machine: the general rule is variable amplitude loading, for example for an automobile suspension system part or for an airplane. To handle cases where the load is variable, some methods are developed.

Palmgren-Miner [18] rule is a linear damage rule, in which the damage fraction D is defined as the fraction of life that is spent at a given level of stress (or strain). The hypothesis is that failure occurs if the sum of the damage fraction is greater or equal to unity ($\sum D_i \geq 1$). The linearity comes from the definition of damage fraction:

$$D_i = \frac{n_i}{N_i} \quad 2.40$$

and consequently,

$$\sum \frac{n_i}{N_i} \geq 1 \quad 2.41$$

Palmgren-Miner damage rule [18] assumes that the load cycles are complete, purely alternating cycles and the sequence of load cycles does not have any effect

on cumulative damage. The scheme of Palmgren-Miner's rule is shown in Figure 2.33. The stresses less than the fatigue limit may also be assumed to have no effect on cumulative damage or they can be taken into calculation by using a slope line after fatigue life instead of a horizontal line as shown in Figure 2.34.

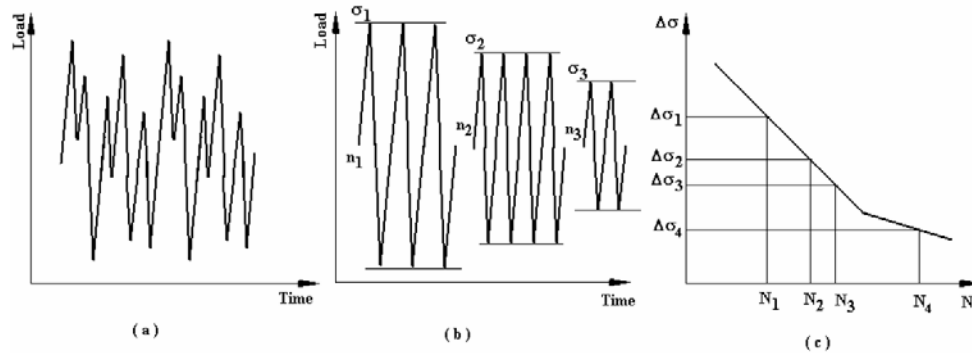


Figure 2.33 Palmgren-Miner's rule [3]

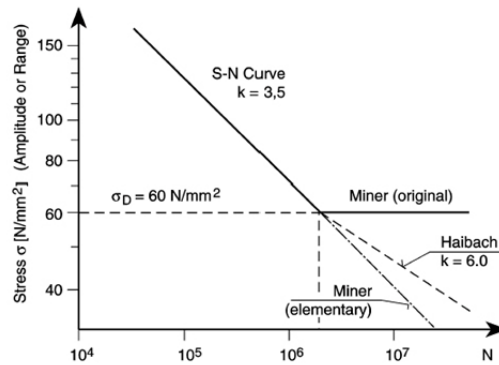


Figure 2.34 Stresses under fatigue limit [31]

There are two main shortcomings of the linear damage rule: assuming sequence independence and independence of damage. Some improvements of the linear damage rule come from non-linear damage rule, where;

$$D_i = \left(\frac{n_i}{N_i}\right)^p \quad 2.42$$

and $p = p(\sigma)$ (for the linear rule $p=1$). But values of p must be known for the actual material [5].

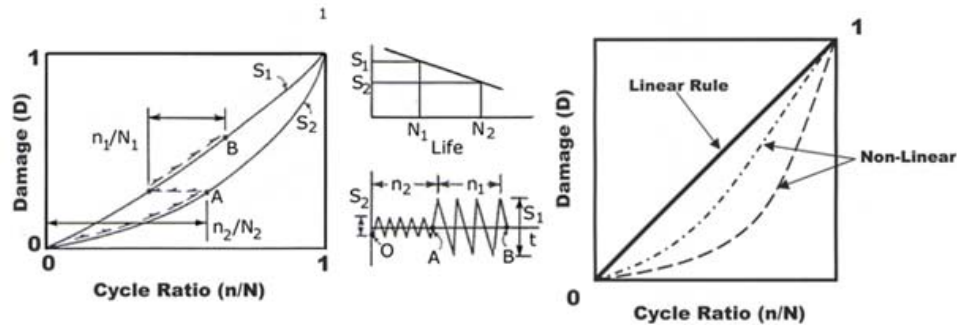


Figure 2.35 Linear/Non-linear damage rules [2]

Variable load cycles are inserted into cumulative damage calculations as a series of constant amplitude loads by means of cycle counting techniques. Level crossing, peak counting, simple range counting and rainflow counting are common cycle counting methods. These counts are used to draw a re-organized cycle graphics by means of forming complete cycles out of counted level value. This process is shown in Figure 2.33.b. A very important disadvantage of the former three cycle counting methods is that they do not recognize closed hysteresis loops. This case sometimes results in two different load histories to cause same results for level crossing, peak counting and simple range counting methods. There are several rainflow-counting algorithms all reference closed hysteresis loops. The analogy is developed by Matsuishi and Endo in 1968 [32].

The rainflow counting method is easy to do manually for relatively simple load histories but for complex load histories, numerical methods have to be used. Software to analyse and re-organize load data with one of the many cycle counting methods are available with fatigue analysis software packages. More detail about cycle counting methods can be found in the work of Fuchs [7]. After counting, the

stress (or strain) range and corresponding number of cycles are obtained and damage can be estimated according to damage models.

2.4 Residual Stress Determination with X-Ray Diffraction Method

X-rays are electromagnetic radiation with photon energies in the range of 100eV-100keV. Short wavelength (e.g. 0.1 angstrom) X-rays are ideally suited for probing the structural arrangement of atoms and molecules in a wide range of materials. In the case of crystal structures, the smallest groups of repeating atoms form "unit cells" in the structure. Various families of planes may be drawn through the corners of the unit cells that form a crystallite. Such planes are separated by an interplanar spacing, d , as in the Figure 2.36 [28].

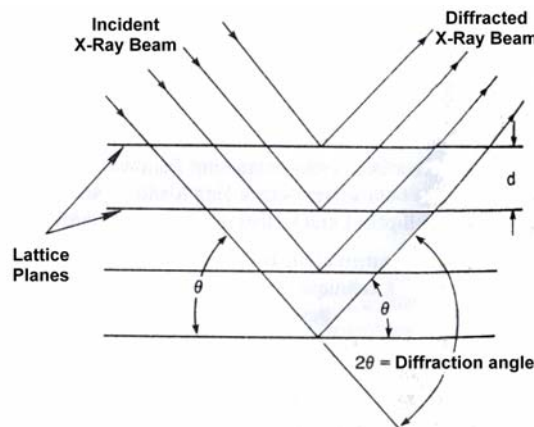


Figure 2.36 X-Ray beam diffraction in accordance with Bragg's law [28]

The angle of diffraction of an X-ray is a measure of the interplanar spacing. The diffraction angle, θ , is related to the interplanar spacing and the wavelength of the radiation by Bragg's law [33]. A departure of the interplanar spacing from the unstressed value represents a stress in the material and is the essence of the X-ray diffraction method for measurement of residual stresses. In accordance with the Piosson effect, the interplanar spacing will elongate in the direction of the applied stress and contract in the transverse direction. In classical treatment, it is assumed

that the stress normal to the surface is zero; i.e., the only possible stresses are biaxial in the plane of stress. If the material is stressed in tension, the X-ray beam normal to the surface will be diffracted by an angle (2θ) that corresponds to the slightly reduced interplanar spacing, and the beam incident at 45 degrees will be diffracted by a slightly different angle corresponding to the increased spacing in the direction of the tensile stress component. By differentiation of Bragg's law, it is found that a difference in diffraction angles at the two tilt angles (ψ) is a measure of the change of the interplanar spacing. The equation for determining stress then is a simply a constant times the shift in the diffraction angle. [28]

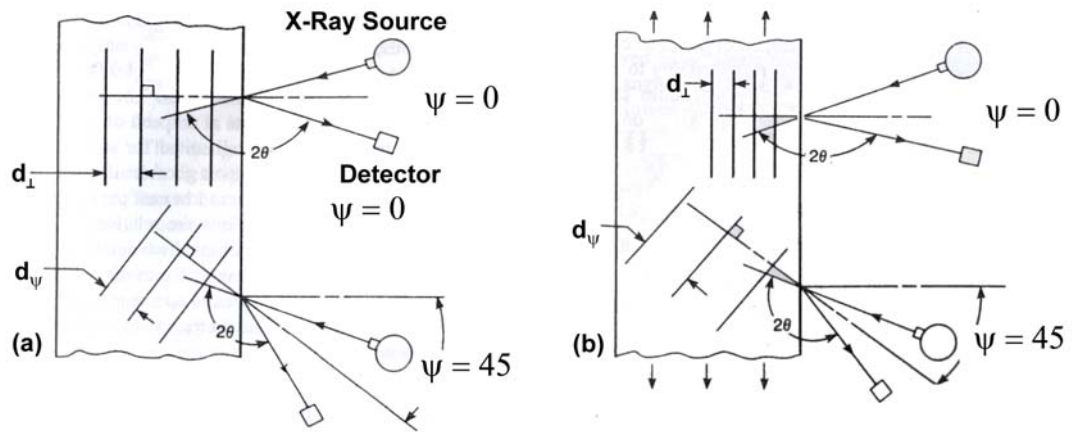


Figure 2.37 X-Ray beam angles [28]

CHAPTER 3

DRAWING OF SHEET METAL

3.1 Process Description

Drawing process is realized on a double action hydraulic press machine with 2000 kN capacity (see Figure 3.1). Total process time is measured to be 8 seconds including edge trimming which is done before forming. Both sides of the blank are lubricated and the friction coefficient between blank and male pattern is assumed to be 0.12. Since thinner lubrication oil used for other faces, the friction coefficient between blank-female pattern, blank-blank holder is assumed to be 0.15. These friction values are proposed by the producer company of the tube parts used.

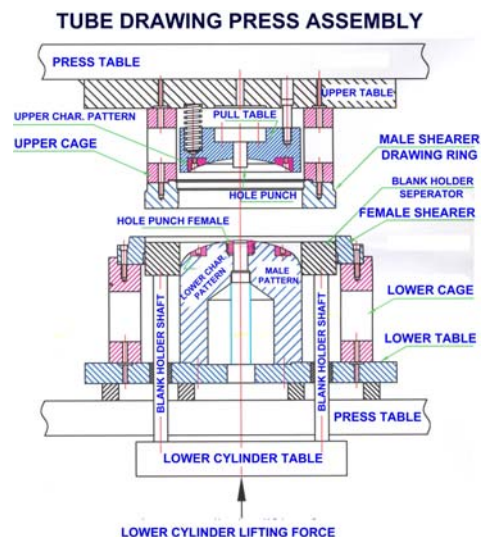


Figure 3.1 Double action hydraulic press

The part drawn in Figure 3.2 is half of a pressure tube. The thickness of the sheet metal used is 2 mm. Blank is a 335 mm square before edge trimming. In the first action of the press, blank is trimmed into a 333mm circular disk. Second action of the press forms the sheet into a half sphere-like shape as shown in Figure 3.2 and Figure 3.3. Material is gas cylinder steel with grade number P245NB.

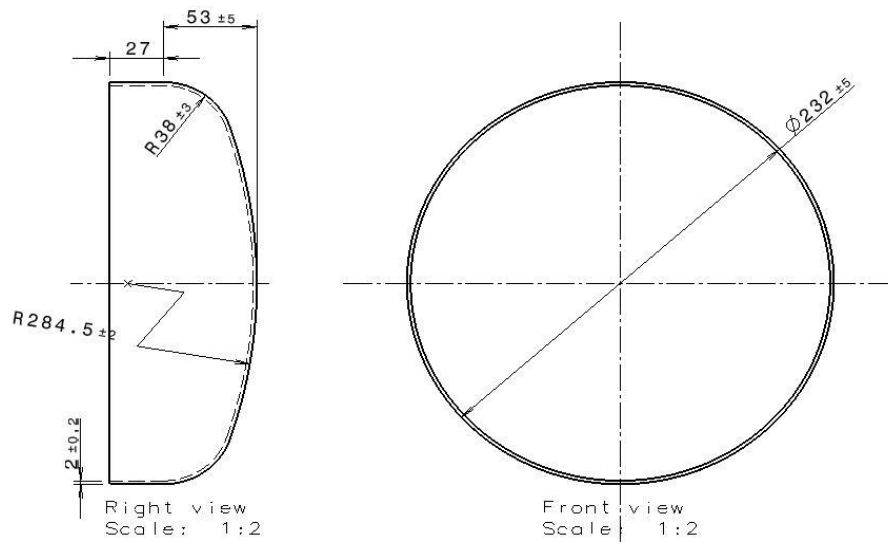


Figure 3.2 2D drawing of the part



Figure 3.3 Photographs of the final part

3.2 Finite Element Modeling

CAD model is prepared in Catia V5r12. The finite element model of the process is prepared in MSC.Patran 2004r2 and MSC.Marc 2003. Following sections explain details of FE models.

3.2.1 Geometry and Mesh Structure

There are 3 rigid and 1 deformable body in the finite element model. These bodies are shown in Figure 3.4. The mesh of the deformable body is prepared considering the deformation of the forming process. No remeshing and rezoning is required in the advanced steps of the analysis.

Reduced integration quad4 thick shell flat elements (Marc 140) with 7 layers and without midnodes are used (Figure 3.5). Total number of elements is 12,672. The reason why symmetric boundary conditions are not used is that the output of the simulation model is utilized in another FE analysis, which has non-symmetric boundary conditions. Since the results of simulation at each node and element must be directly transferred into another program, full model had to be utilized. Another reason of using a 3D model is that the usage of anisotropic material properties are not available in symmetric FE models.

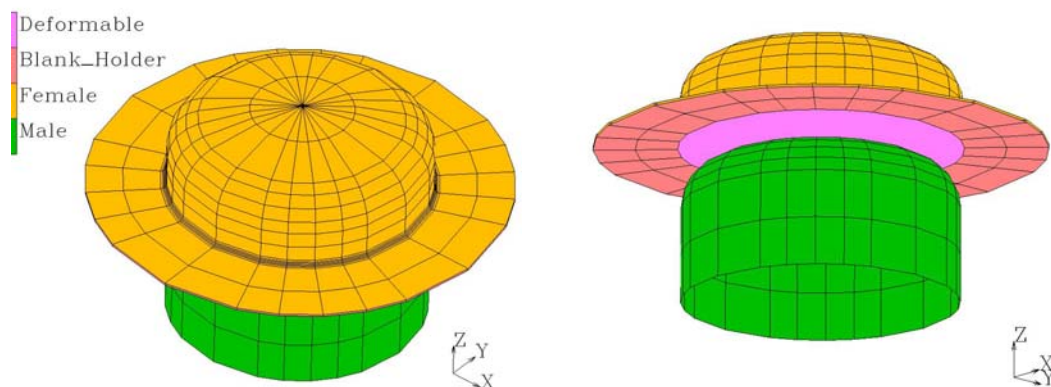


Figure 3.4 FEM analysis bodies

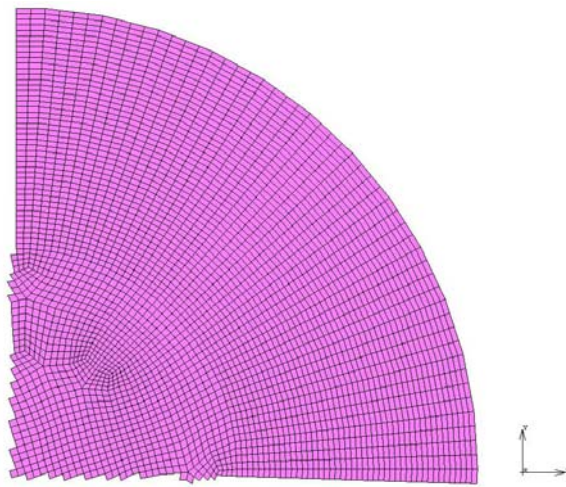


Figure 3.5 A portion of blank mesh

3.2.2 Boundary Conditions

This analysis is a load controlled analysis. The FE model has three boundary conditions. One is the applied force to the female pattern. A time dependant linear increase in the force applied is described and can be seen in Figure 3.6. Blank holder applies half of the female load. So second boundary condition is also force boundary condition, using the same load table as female pattern with a factor of 0.5.

Third boundary condition is defined to prevent the free body motion of the blank in horizontal plane, especially before the parts get into contact. This is achieved by defining fixed displacements to the 1st and 2nd degrees of freedom of the center node of the blank body.

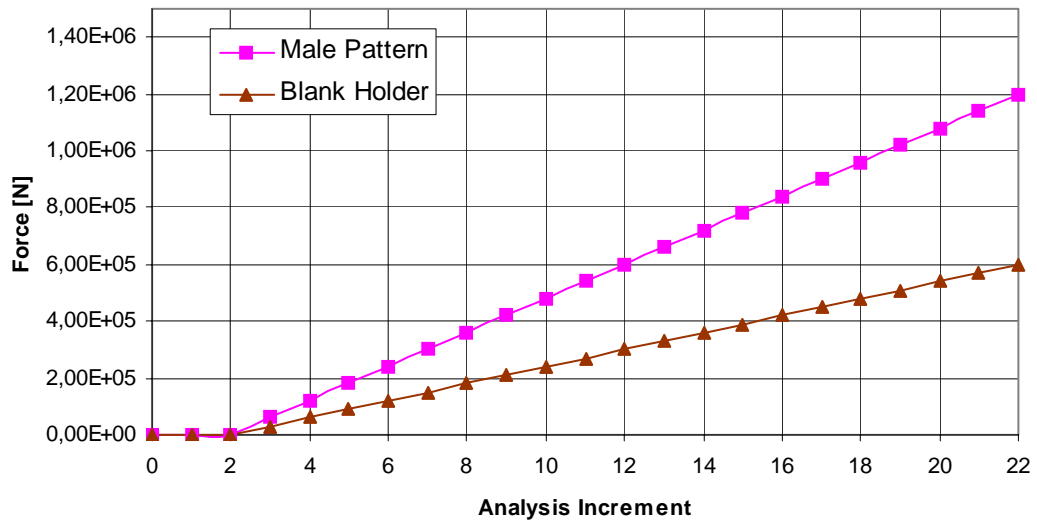


Figure 3.6 Load of the female pattern and blank holder

3.2.3 Material Modeling

Orthogonally anisotropic material properties are assumed and Hill-48 model is used. Elastic-plastic material plasticity is utilized with elastic-plastic stress-strain curve shown in Figure 3.7. Von Mises yield criteria and isotropic hardening rule are utilized.

The yield points of the material for different directions are found by offsetting the elastic curve of the true stress-true strain data by a value of 0,2%. Three tensile tests with two samples taken in 0°, 45° and 90° directions to rolling direction of the sheet metal are done to find out the parameters for the Hill-48 model. Lankford parameters for each direction are calculated as described in Section 2.2.3. The values obtained are tabulated in Table 3.1. Values are calculated at a true strain level of 1%.

The engineering stress-engineering strain curve is input into program with power method (Ludwik's function). The parameters K and n are calculated as described

in Section 2.2.3. Ten data points are utilized for each direction of measurement and the average of three values is taken to find the values to be inputted into FE program. The values for K and n are tabulated in Table 3.1 and Figure 3.7 shows the curves obtained from tensile tests and power method. Subscript x in $n_{x/10}$ is the angle with respect to the rolling direction and 10 is the upper limit of true strain data in percentage used to calculate n .

Table 3.1 Calculated values for K , n and r different angles to the rolling direction

	K	$n_{x/10}$	$r_{x/10}$
0°	448	0,0502	2,037
45°	538	0,0823	0,971
90°	564	0,0938	0,137
Average	517	0,08	1,03

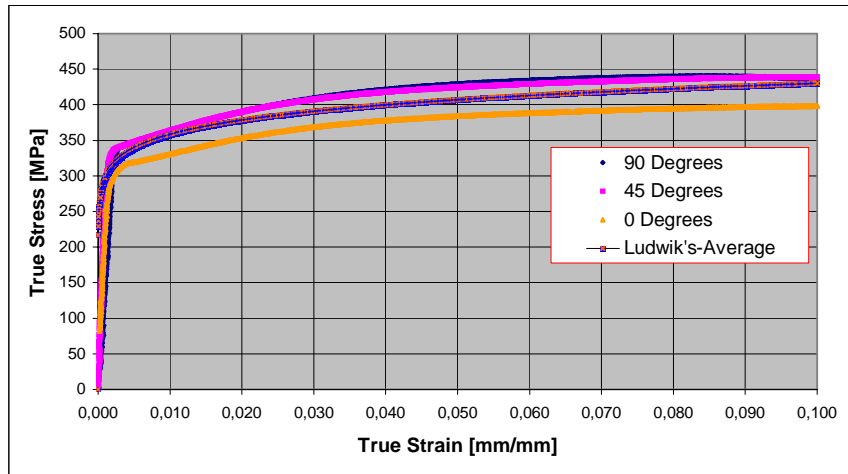


Figure 3.7 Engineering stress-engineering strain data

3.2.4 Program Parameters

3D analysis is done with Marc2001 solver. Since displacements are large, large displacement option and large strain additive procedure for plasticity are used to invoke updated Lagrange procedure and to account for the effects of the internal stresses. The large displacement option automatically invokes the residual load correction procedure, which calculates the residual forces of the previous increment and corrects the loads of the next increment accordingly to enforce the global equilibrium that is very critical for load controlled problems where residual convergence checking is done. Coulomb for rolling type of friction model is utilized for friction modeling. Distance tolerance for the contact bias is set to 0.95 which gives better accuracy for contact detection. Relative sliding velocity is set to 1. Max cut-back number is increased to 30 because of stabilization problems. Relative residual force convergence is used for convergence checking with a value of 5%. 22 increments are set for totally 11 second analysis time. One load case is prepared for the formation of the sheet metal. Second one is set up for the release of contacts.

Analysis is restarted to reset relative sliding velocity, separation checking and penetration checking and convergence criteria for several times. Marc solver is able to restart from increment of recycle that is converged. Some of the parameters can be reset before restarting. Since the loads are very high at the advanced steps, 5% convergence in residual force is hard to obtain. At increment number 13, convergence check is changed to 2,5% displacement. At increment number 17, convergence checking is set back to 5% residual force check with relative sliding velocity of 1.10^{-6} .

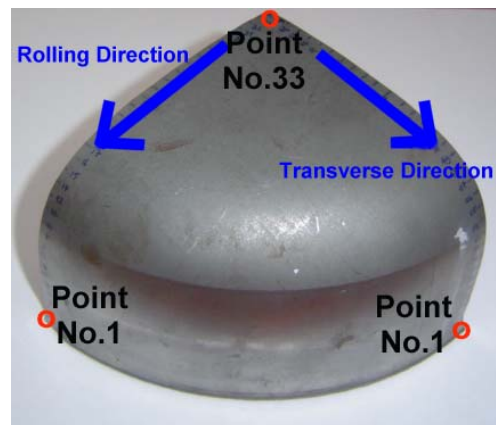
Another problem is high number of recycles because of touching, releasing or sliding nodes. These recycles in the analysis increment are called chattering. Chattering is more effective when bodies are getting into contact. At the beginning of the analysis, they are prevented by depressing the separation of nodes from a contact surface in an increment if the node comes into contact with that surface in

that increment. But at the advanced steps, this option is turned off to let the nodes separate from any contact body in any increment of the analysis.

3.3 Measurements, Tests and Evaluations of Results

3.3.1 Thickness Measurements

Thickness of the formed sheet is measured at several locations and comparative results from FE analysis and measurement are given in Figure 3.8. Although there are some differences between analysis and measurements, general thickness distribution over the part is similar. The maximum and minimum values and their locations are also calculated.



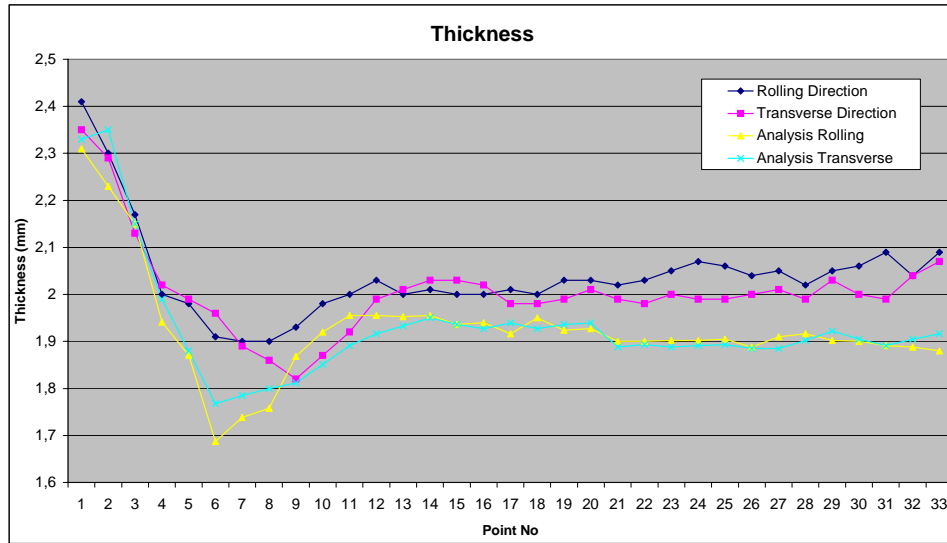


Figure 3.8 Measured thickness of the formed sheet metal and the FE analysis results

3.3.2 Residual Stress Measurements with X-Ray Diffraction Method

The residual stress measurement is done with a Psi type XRD equipment. Reflection data is collected with Cr-Kalfa radiation at 5 μ m depth at an angle of 155.89° from 211 crystal plane. Several measurements on each sample are done automatically by the equipment and the averages are presented. The outputs of the measurements are the principal stresses in rolling and transverse direction. 5 samples are cutout from the part and the locations where these samples are extracted are shown in Figure 3.9. The samples are cutout with electrowire cutting without disturbing the residual stress distribution. One sample, no 6, from undeformed sheet metal is also used in measurements. Another sample, no 7, is cut out from a part that is heat treated for stress relaxation. The location of this sample on the part is the same as the location of sample 5. Measurements at different angles showed that the texture effect is less than 10%.

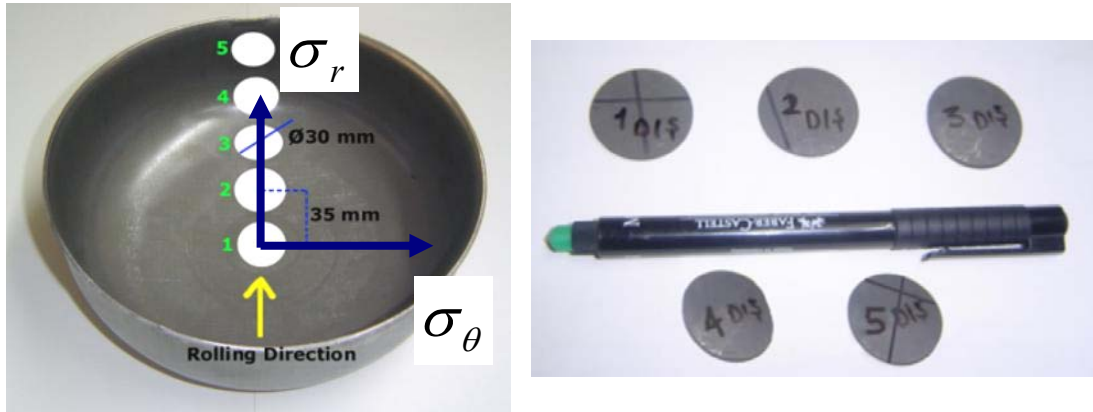


Figure 3.9 Residual stress measurement sample locations

The results of X-Ray diffraction measurements are tabulated in Table 3.2. Measurements are done at the center of the outer sides of the samples. Full Width at Half Maximum (FWHM) values are a measure of microscopic residual stress value and can be utilized as a numerical value of the amount of plastic deformation of the material. Although undeformed, sample 6 has an amount of residual stress that is probably left on the sheet metal even after normalization heat treatment. It can be observed from these results that the sample 7, which is cut out from the heat treated part, has least plastic deformation while sample 5 is mostly deformed over all samples as expected. The minus sign in front of stress values means compressive stresses, which are expected to increase the fatigue life of the component.

Sample No	σ_r [MPa]	σ_θ [MPa]	FWHM [°]
1	-14 ± 2	-30 ± 3	0.88
2	-25 ± 2	-50 ± 2	0.90
3	-95 ± 3	-97 ± 3	1.00
4	-110 ± 4	-40 ± 3	1.13
5	-220 ± 4	-190 ± 4	1.58
6 undeformed	$+47 \pm 3$	-21 ± 3	0.85
7 stress free	$+22 \pm 3$	$+7 \pm 2$	0.7

Table 3.2 Residual stresses measured with Psi XRD equipment

3.3.3 Evaluation of Results

Thickness values calculated are lower than the actual values as shown in Figure 3.8. Maximum error occurs at the thinner region as 16%. There are not too much directional differences observed from the thickness change point of view. A very slight difference exists in the finite element analysis that part becomes 11% thinner at the rolling direction. This was expected since the material is normalized and material properties are close to each other as found by tensile tests.

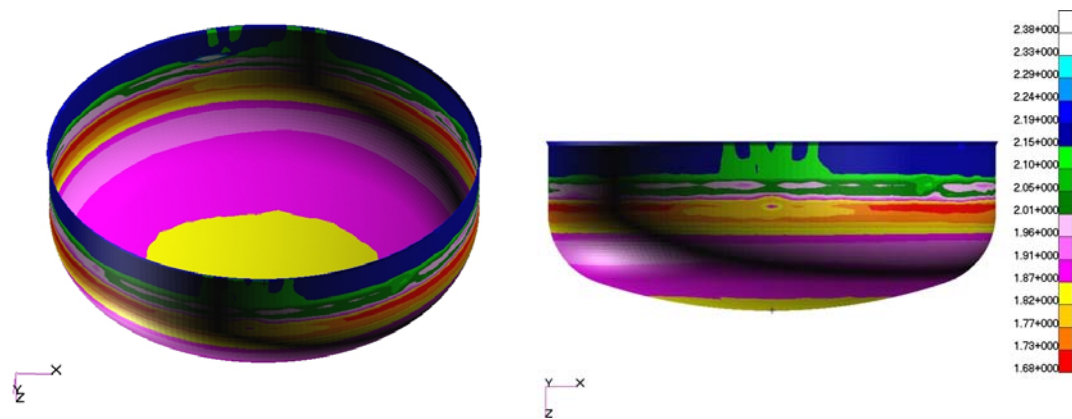


Figure 3.10 Thickness distribution after forming

Stress distribution over the part shows irregularities because of touching/releasing nodes on the deformable body. Below is the total equivalent plastic strain.

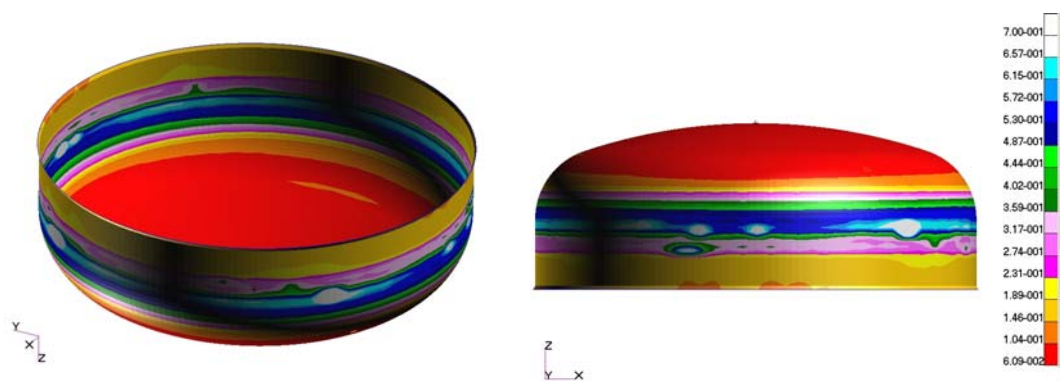


Figure 3.11 Total equivalent plastic strain distribution before release of contact bodies

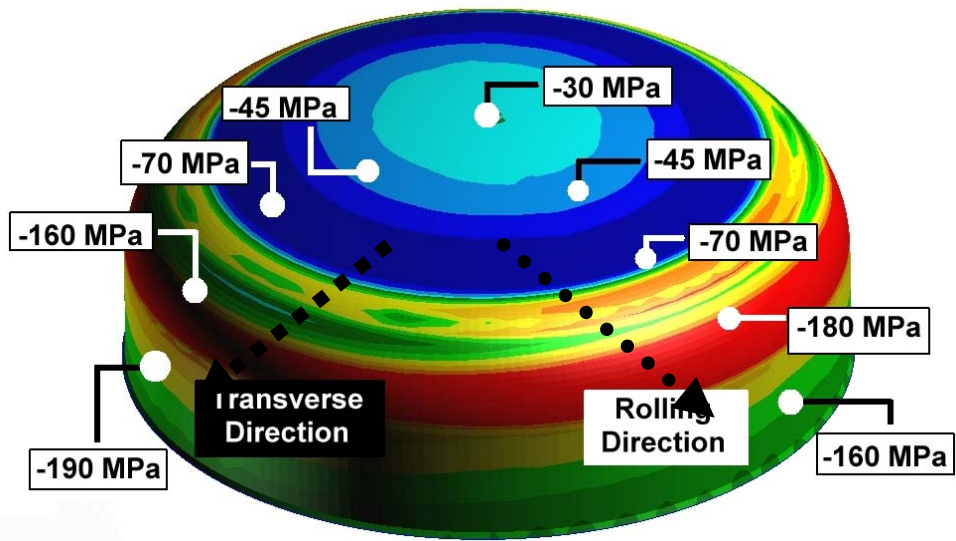


Figure 3.12 Principal residual stresses in cylindrical coordinates, σ_r

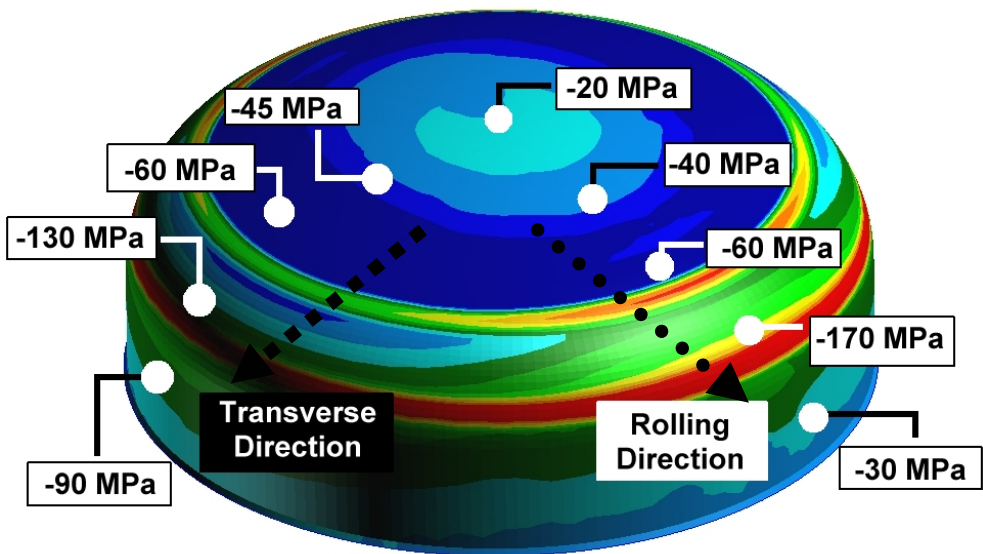


Figure 3.13 Principal residual stresses in cylindrical coordinates, σ_θ

Below figure compares residual stresses from the test results and FE analysis. Since the test results are in cylindrical coordinates, analysis results are also

transferred into cylindrical coordinates. Values are radial and circumferential principal stress values at outer surface of the part.

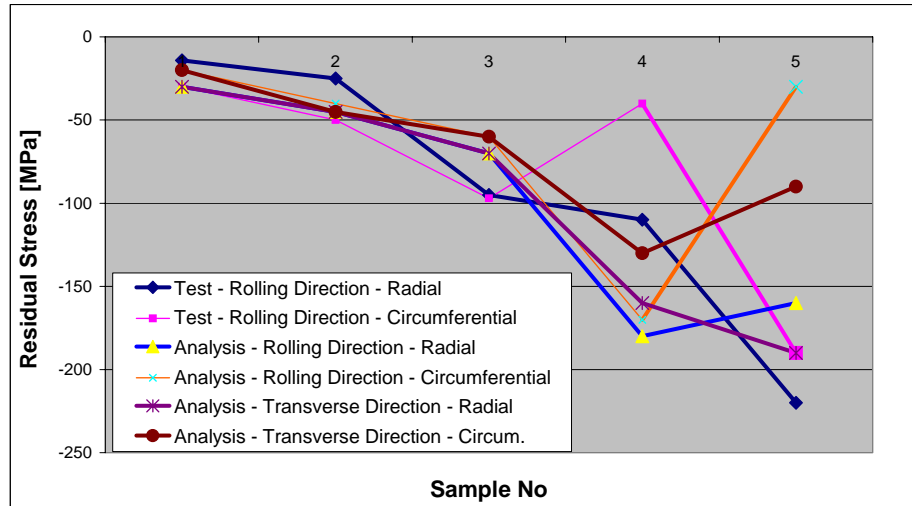


Figure 3.14 Measured and calculated residual stresses

CHAPTER 4

FATIGUE BEHAVIOR OF THE COMPONENT

4.1 Fatigue Test Procedure

Fatigue test is done as repeated cycles of loads in one direction and in both tension and compression. The experimental setup is shown in Figure 4.1 and Figure 4.2. The pneumatic cylinder is able to supply different pressures in desired directions. The total forward-backward cycle takes about 3 seconds. The loads applied are tabulated in Table 4.1.

Table 4.1 Fatigue test loads

Case No	Cylinder Perssure	Compressio n Load (N)	Tension Load (N)
1	7 bar	5498	5154
2	6 bar	4712	4418

Fatigue tests are applied as repeated 2,000 cycles to inspect any crack growth. Two groups of tests are completed. One group of tests done with parts with residual stresses and the other group with parts that are heat treated for residual stress relieve. Each loadcase is repeated two times and thus 4 tests are done for each group that totally makes 8 tests. Heat treatment is done by subjecting parts to a temperature of about 650 °C for 60 minutes. The parts are air cooled in still air.

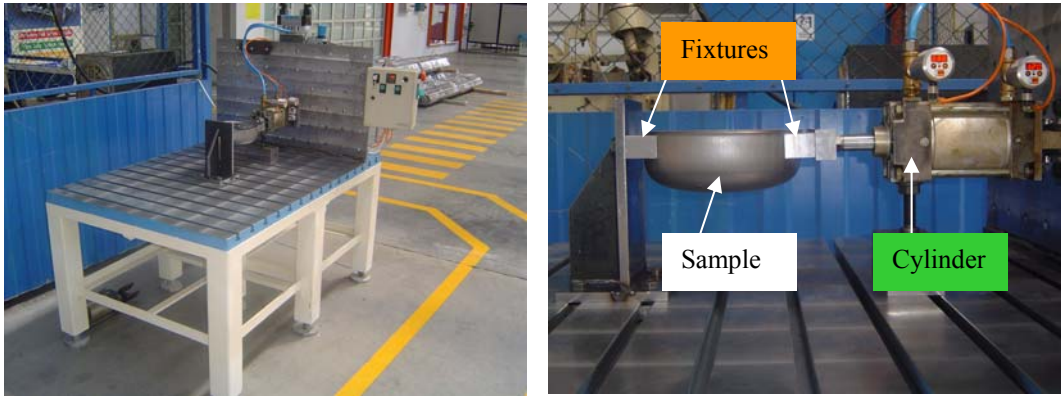


Figure 4.1 Fatigue test setup

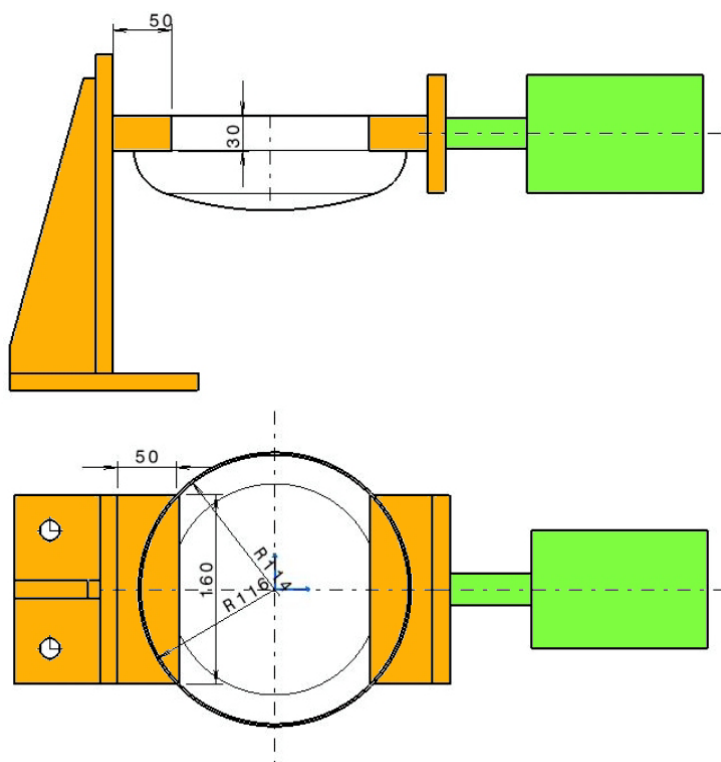


Figure 4.2 Fatigue test fixtures

4.2 Finite Element Modeling

Finite element model is prepared in MSC.Patran 2004r2 with fatigue analysis menus of MSC. Five different models are analyzed (Table 4.2). Model number 1 is prepared with the most usual method that does not include any effect of sheet metal forming. There are several reasons why it is preferred to not to include sheet metal forming effects into fatigue model. First of all, it is necessary to find out the thickness changes and the residual stresses formed before being able to include these effects into the model. Finding these parameters requires another analysis to be run, that is sheet metal forming analysis. These analyses are non-linear and much complicated and time consuming than linear analyses. There are also problems existing with the transfer of the outputs of the forming simulation into fatigue analysis program. There are some primitive methods to realize this transfer but still a robust and easy-to-use method not developed.

Second model is prepared with using the thickness change measurements, mentioned in 3.3.1. The elements around the cup are defined with the measured thickness as shown in Figure 4.3 (a).

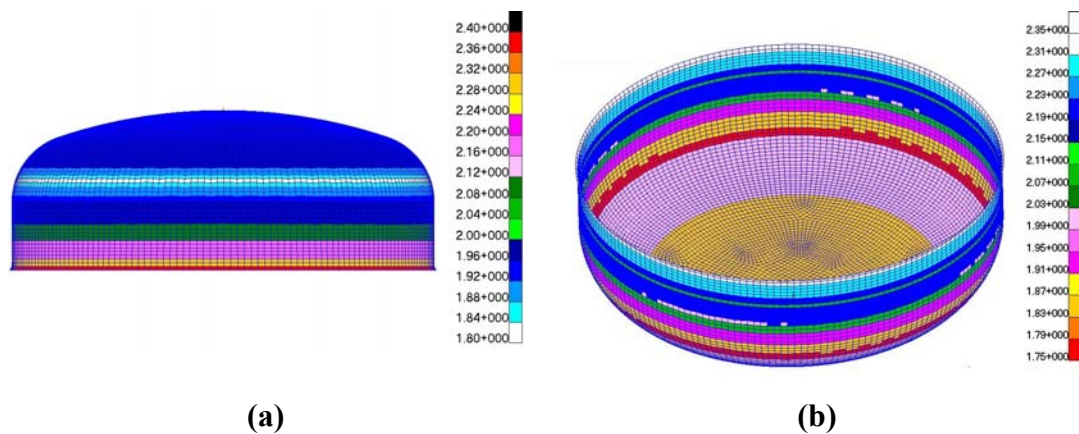


Figure 4.3 FE model with measured thickness distribution after sheet metal forming (a) measured (b) FE results

Third model is prepared from the outcome of the sheet metal forming analysis and this outcome is directly used as the input model of the fatigue loadcase. The residual stresses that are calculated in metal forming analyses are used as static mean stresses. In the fourth model, in addition to residual mean stresses, measured thickness changes are applied. Fifth model includes the thickness and residual stress results directly from the metal forming simulation. The thicknesses used are in Figure 4.3 (b). This model is producible before any production process of the part starts. Below table summarizes the fatigue simulation models.

Model No	Model Description
1	without drawing effects
2	with measured thickness change effects
3	with residual stress effects
4	with measured thickness change and residual stress effects
5	with direct results from sheet forming FE simulation (thickness and residual stresses)

Table 4.2 Models prepared for analysis

4.2.1 Geometry and Mesh Structure

The mesh structure is the same mesh structure that gets out of drawing simulation (Figure 4.4). It is necessary to use the same mesh structure and the same numbers for nodes and elements in order to correctly transfer the results of the simulation analysis into fatigue analysis. The residual stress/strain distribution over the nodes should be directly transferred into the fatigue program. This transfer is done with a transfer file in t16 format, which is default output file for MSC.Marc.

The number of nodes and elements in the fatigue analysis is less critical than forming simulation analysis because the time consumed by fatigue program is much less than forming FE simulation.

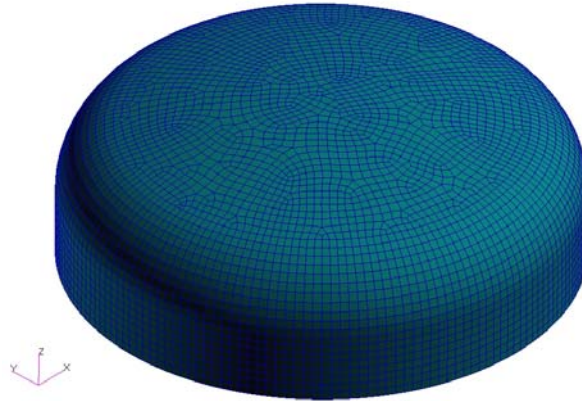


Figure 4.4 Mesh structure used for fatigue analysis, totally 12.672 quad4 elements

4.2.2 Boundary Conditions

Boundary conditions for the fatigue studies are determined from the FE fatigue analysis results. The fixed side and the load application side of the part are reinforced in order to prevent failure right on the load application points. Figure 4.5 shows the FE boundary conditions. Loads are applied with special rigid tying elements. These are called in Patran as RBE elements. Type 2 is preferred to simulate the rigidity at the boundaries supplied by fixtures. RBE2 type elements creates nodal degree of freedom tying with equations inserted into solution group of equations. All the nodes connected to this element, moves together according to degree of freedoms assigned. In this analysis, three translational degrees of freedoms are assigned for tying. The fixed side is defined by zero displacement degrees of freedom in translations.

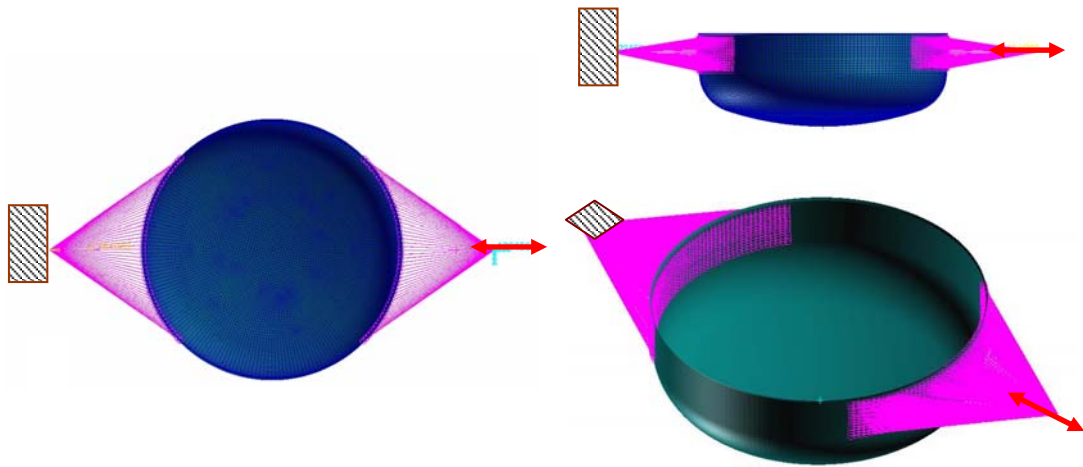


Figure 4.5 Boundary conditions used for fatigue analysis; RBE2 elements are used to create nodal degree of freedom tying

The load is applied as tension and compression. One load cycle is completed with completion of one tension and one compression loads. The time signal used is reversed with $R=-0,9375$. This value is the proportion of the total area of the air pressure cylinder at the back and front section of the cylinder piston. The S-N curve itself was generated by testing numerous polished test specimens at different constant amplitude, fully reversed ($R=-1$) loading conditions. Therefore mean stress correction is required. Load graph is shown below;

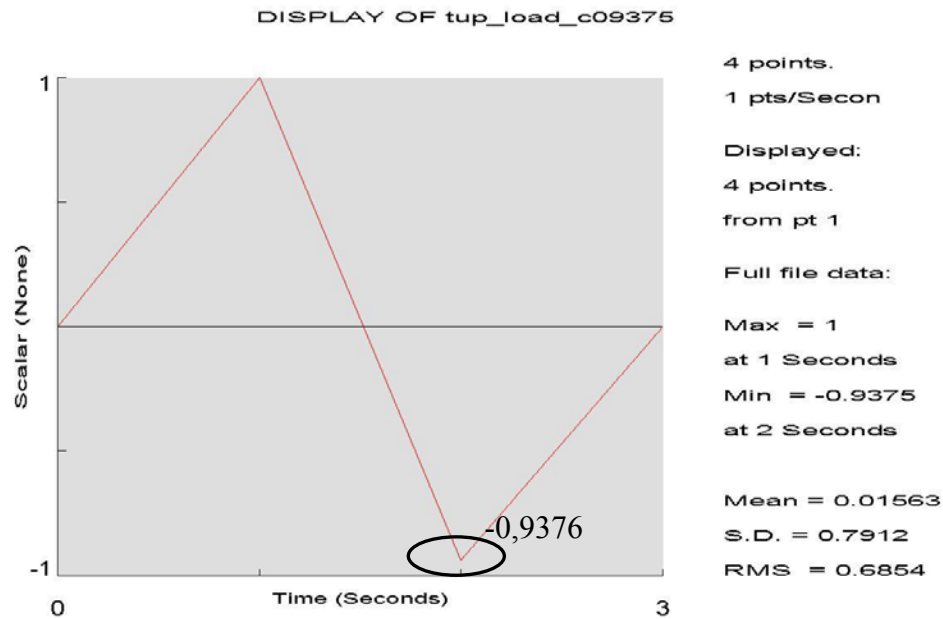


Figure 4.6 Fatigue analysis load graph

For the analysis with residual stress, residual stress results of the sheet metal forming simulation is entered as a boundary condition. The residual stresses are activated as static stress case which behaves as mean stress for all locations over the whole part.

4.2.3 Material Modeling

Stress-life and strain life data of the material is derived with the methods described in section 2.3.6.1 and section 2.3.6.2. These derived curves are called synthetic curves of the material. Derivation is done by a tool program supplied with fatigue program. Many fatigue programs supply similar tools to create different fatigue data of the material. It is possible to derive synthetic strain-life, corrected Morrow curves etc. The material data used for the derivation process are the ultimate tensile strength and the modulus of elasticity. Stress-life and strain-life curves are generated according to statistical studies on UTS and modulus of elasticity values of metals. When both values are supplied, program generates many material data by using a base material, which is in P245NB "Cast steel with less than 0.2%

carbon". Ultimate tensile strength and modulus of elasticity values are calculated from the tensile test result as 400MPa and 210GPa. SN data of the material used is shown in Figure 4.7. This data is generated with the coefficients in Table 2.10. The dotted lines at the two sides of the SN curve are drawn according to standard error calculations. No surface finish or treatment factor is applied.

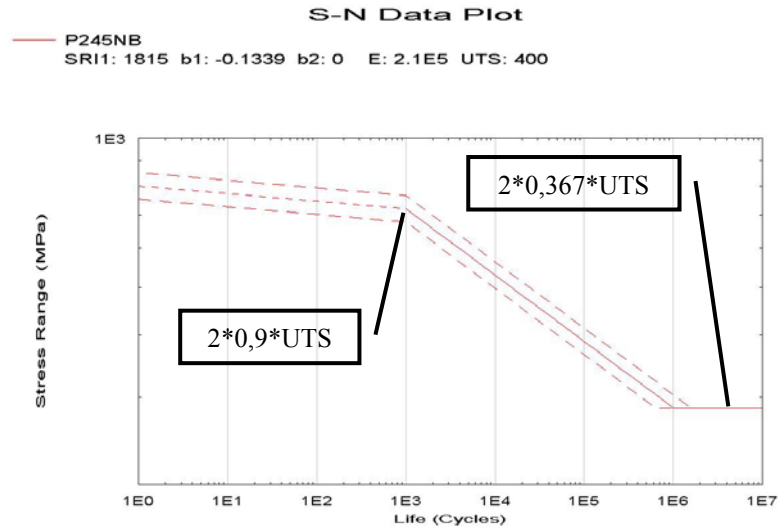


Figure 4.7 Synthetic S-N curve, stresses are in range

Details of strain life curve is described in section 2.3.6. Below figure is the curve derived based on those calculations.

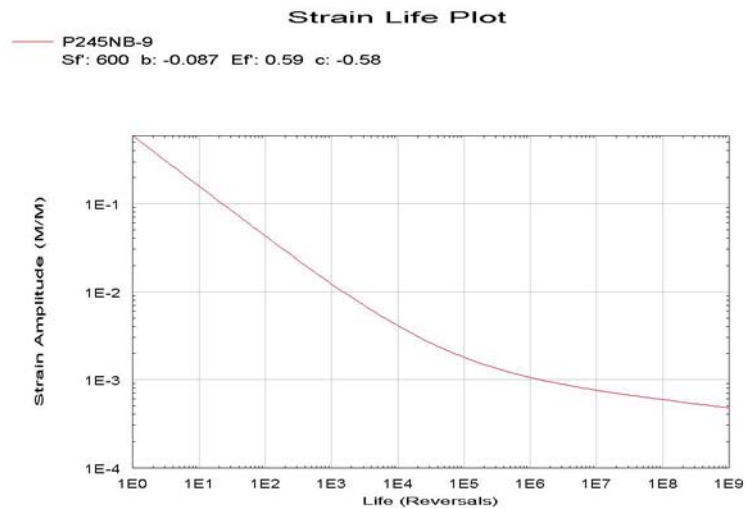


Figure 4.8 Synthetic strain-N curve

Cyclic material data is generated as described in section 2.3.6. Cyclic stress-strain curve is shown below. The difference between the monotonic and cyclic material data can be seen in Figure 4.9.

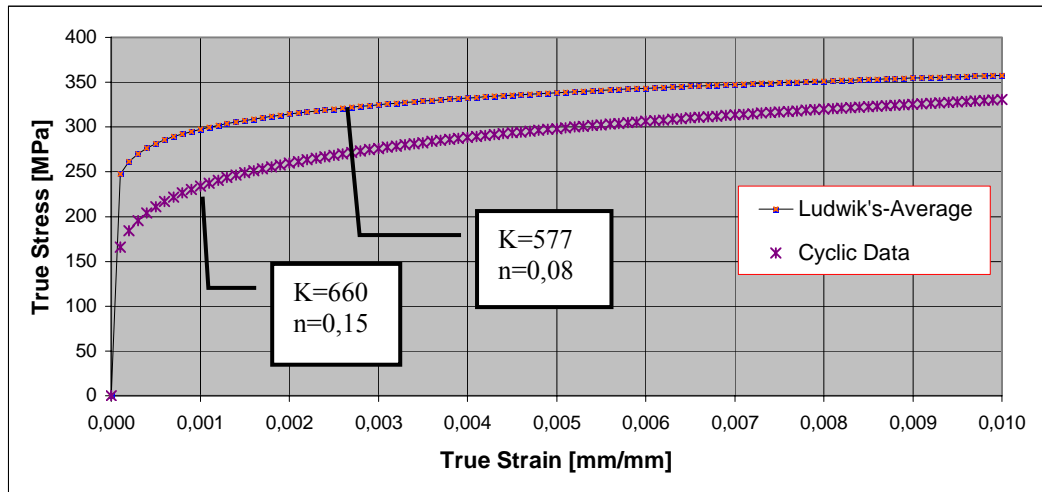


Figure 4.9 Cyclic stress strain curve and Ludwik's fit of P245NB

4.2.4 Program Parameters

Stress-life and strain-life analyses are set for the type of the fatigue analyses. Both Goodman, Gerber mean stress correction methods are used in addition to an analysis without any mean stress correction. In strain-life analyses, Smith-Watson-Topper and Morrow methods are used. All strain-life analyses utilize Neuber's plastic strain correction method. The survival expectancy is set to 50%. All used methods are explained in detail in section 2.3.6.

Maximum absolute principal stress is the stress parameter that will be used in the fatigue analysis. The stress tensor from the FE analysis results is extracted at each node. However only a single stress value can be looked up on the S-N curve. So the six component values of the stress tensor are resolved to the maximum absolute principal value which will be used as the stress look up parameter. The case is the same for strain-life approach. The outer surface results of shell elements are defined in the fatigue model.

4.3 Evaluation of Result

4.3.1 Fatigue Analysis Results

Fatigue analysis consists of two parts. First is the determination of stress distribution with the predefined load and boundary conditions and the second is the calculation of fatigue life with the material, load information and nodal stress results. The maximum principal stress results of fatigue loading are tabulated in Table 4.3. Corresponding figures are given in Appendix A.

	Case 1 (7 bars)		Case 2 (6 bars)		Figure No	
	Comp. [MPa]	Tension [MPa]	Comp. [MPa]	Tension [MPa]	Comp.	Tension
Constant thickness	290	223	249	191	A.1	A.2
Variable thickness (Measured)	264	202	226	173	A.3	A.4
Variable thickness (FEA)	256	196	220	169	A.5	A.6

Table 4.3 Fatigue load maximum principal results of constant and variable thickness models

The general stress distribution for all models are similar. The maximum absolute stress distribution of the models gives much information about where lower cycles of lives are expected. Thus, the fatigue life expectations calculated with fatigue program are found out as tabulated in

Table 4.4 and Table 4.5. Fatigue analysis result figures corresponding to case 1, 7 bars cylinder pressure, are presented in Appendix B. The location of the minimum life cycles are the same for case 2, 6 bars cylinder pressure, and they are not represented but only tabulated in Table 4.5.

Table 4.4 Fatigue simulation models, Case 1, 7 bars, 5498N-5154N cyclic load

Model No		Stress Life			Strain life	
		Mean Stress Correction			Method	
		Goodman	Gerber	None	S-W-T	Morrow
1	without drawing effects	1460	1840	1860	27900	29500
2	with measured thickness change effects	4990	6360	6400	69800	74800
3	with residual stress effects	9800	12100	12200	87000	98000
4	with measured thickness change and residual stress effects	13200	15100	15200	92000	107000
5	with direct results from sheet forming FE simulation (thickness and residual stresses)	12500	13600	13750	90400	105000

Table 4.5 Fatigue simulation models, Case 2, 6 bars, 4712N-4418N cyclic load

Model No		Stress Life			Strain life	
		Mean Stress Correction			Method	
		Goodman	Gerber	None	S-W-T	Morrow
1	without drawing effects	4970	6260	6300	53900	57600
2	with measured thickness change effects	14500	18200	18400	127000	137000
3	with residual stress effects	29500	42500	42600	152000	186000
4	with measured thickness change and residual stress effects	42000	57200	57400	164900	196000
5	with direct results from sheet forming FE simulation (thickness and residual stresses)	39800	52300	52400	159400	192700

Most of the regions of the part are found to be in infinite region of the Wöhler curve. The first crack growth is expected at the same locations for all five models but at different cycle numbers.

4.3.2 Fatigue Test Results

Fatigue tests take about 2 months to complete. Each test could be repeated two times because of long time consumption. Tests are stopped at the first visible crack growth starts. These cracks are very tiny and difficult to detect. There are oscillations at the test results, which are common to fatigue tests.

Table 4.6 Fatigue test results

Test No	Case 1 (7 bars) (cycles in thousands)			Case 2 (6 bars) (cycles in thousands)		
	<i>1</i>	<i>2</i>	<i>Aver.</i>	<i>1</i>	<i>3</i>	<i>Aver.</i>
without residual stresses	154	165	159,5	212	251	231,5
with residual stresses	176	192	184	320	371	345,5

The effects of residual stresses are more effective for lower load case, in other words, at higher fatigue cycles. Since the effect of residual stress is different for different loads, the slope of the cycle-load curves are different for specimens with and without residual stresses. This result can be seen in Figure 4.10.

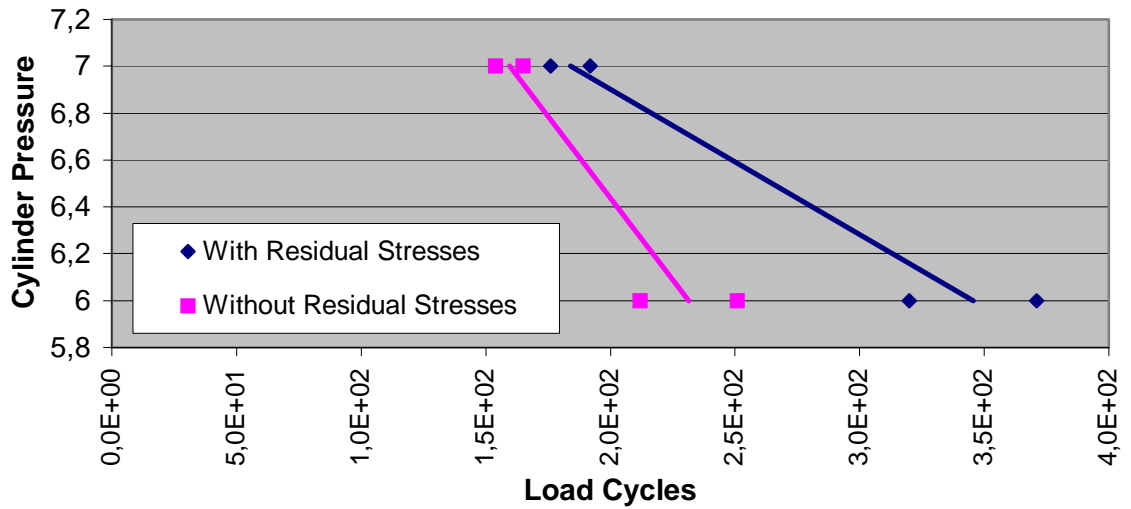


Figure 4.10 Fatigue test results, load cycles vs. cylinder pressure

Test is stopped before crack is advanced. Figure 4.11(c) is an exception to see how crack will propagate. The location of crack root is very close to fixture ends but they are not in contact with fixtures. This is the case found by FE fatigue analysis also. The maximum principal stress occurs several millimeters away from the fixture ends. Some of the specimens are failed from right side while some are failed from the left side of the fixtures. In the case of Figure 4.11(c), both sides are failed about same thousand of cycles.

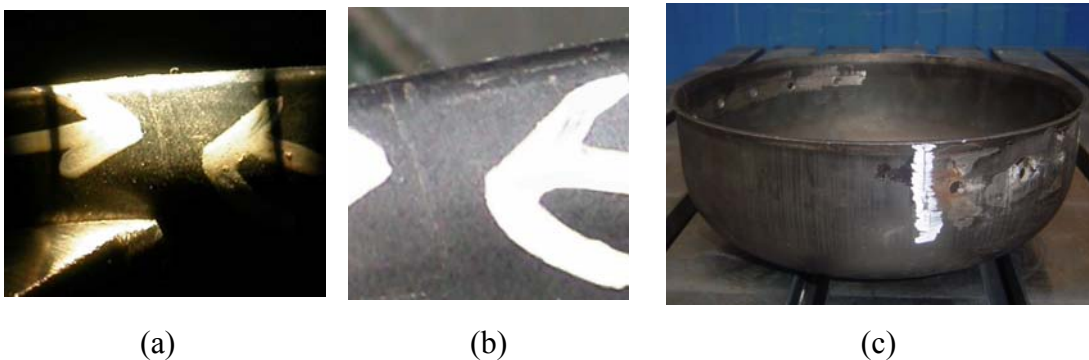
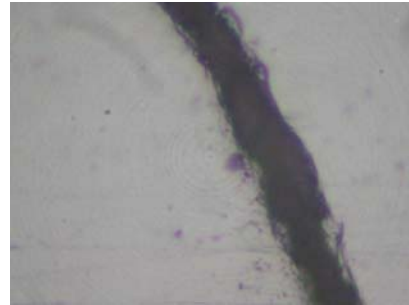


Figure 4.11 First visible fatigue cracks, part with (a) stress relieve (b) residual stresses (c) advanced fatigue crack

Below figure shows one of the cracks with a microscope. Crystalline structure is not seen with these magnifications.



(a)



(b)

Figure 4.12 First visible fatigue cracks with zoom factor (a) 500 (b) 1000

CHAPTER 5

CONCLUSIONS AND FURTHER RECOMMENDATIONS

In this study, two effects of sheet metal forming are investigated on a part with the help of finite element method and fatigue tests. These effects are local thinning/thickening and residual stress formation. Thickness changes are examined with FE analysis and residual stress effects are studied with both FE analysis and fatigue tests.

Sheet metal forming process is simulated with an implicit algorithm. By this analysis, thickness changes and residual stresses are calculated. The errors on the results are found by measurements on the produced part. X-Ray diffraction method is used to compare the residual stresses calculated with FEM. Another finite element study is done for fatigue life calculations.

On the other hand, fatigue tests are completed for certain loadcases. These loadcases are the same with the loadcases used for fatigue life calculations for comparison. Two sets of samples are tested. One set consists of parts as drawn while the other set consists of parts with stress relieve heat treatment. By comparing the results of these two sets, the effect of residual stresses are investigated.

One important aim of the study is to develop a method to include forming effects into fatigue simulations. The success of the method is highly dependent on the

success of forming simulation. The comparisons of sheet metal forming analysis with measurements have shown that simulation results are reasonably close test results.

Examining the fatigue simulations, it is seen that the effect of thickness is very significant. Since the thickness of the regions where fatigue failure expected changed distinctly, the effect is increased. Although the fatigue simulation results of the model with only measured thickness changes are not close to test results of stress relieve part, almost all model results have shown that the fatigue life is doubled with only thickness changes. The percentage thickness change on the location where failure occurred is about 35-40% according to measurements, but the expected fatigue life is increased about two times. The reason of such a drastic increase is that this thickness change shifted the stress level of the region to a lower value that resulted in a big shift down in Wöhler curve. It is clear that the thickness changes directly effect the stress distribution over the region and this directly changes the fatigue life of the part especially if these regions are critical from the fatigue point of view.

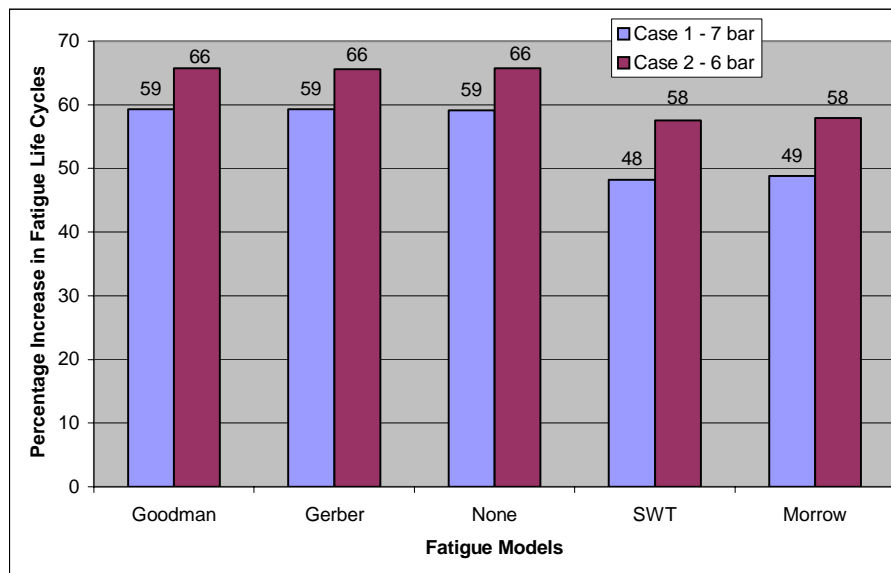


Figure 5.1 Calculated thickness effect on fatigue life for two load cases

The effect of thickness is the same for stress life methods and almost the same for strain life methods. The effect of thickness on fatigue life is not the same for different amplitudes of applied cyclic load. Although the principal stress change percentages are the same for both load cases, load case with lower fatigue load, in other words higher fatigue life cycles, is more effected by thickness change.

The effect of the residual stresses is found by fatigue tests. Tests are conducted at two load levels, each with 2 samples. Since two sets of samples are tested, totally 8 tests are done. Although, the values found by X-Ray diffraction method are not very reliable numerically, these measurements, with FE forming analysis results, have shown that there exists an amount of residual stress left on the part after forming operation. These residuals affected the fatigue life in positive direction as expected since they are all compressive. As in the case of thickness change, maximum compressive residual stress formed at the region where fatigue failure expected and occurred. This caused an increase in the severity of the effect. Residual stresses caused 13-33% increase in the fatigue life of the part. Since all the tests and analysis are done with the same residual stresses, a relation between the amount of plastic strain and fatigue life could not be generated. Further studies can focus on this objective.

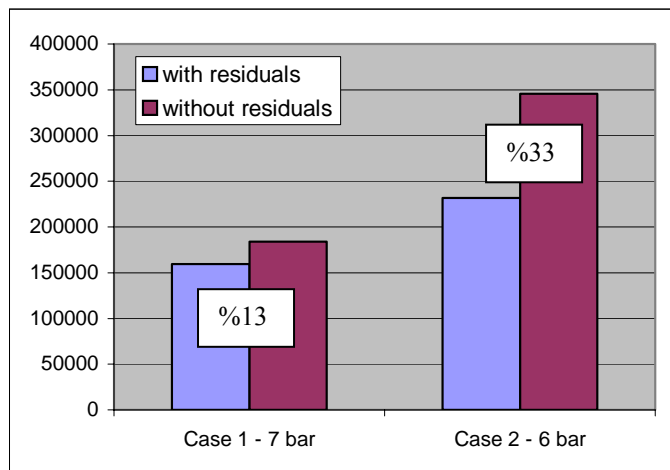


Figure 5.2 Residual stress effect on fatigue life, driven from test results

The residual stress effect calculated with fatigue analysis is much more than found by tests. The comparison of two models with strain life fatigue calculation is presented in the below figure. Another important point is that the effects of residual stresses are less for the load case 2, which is oppose to test results.

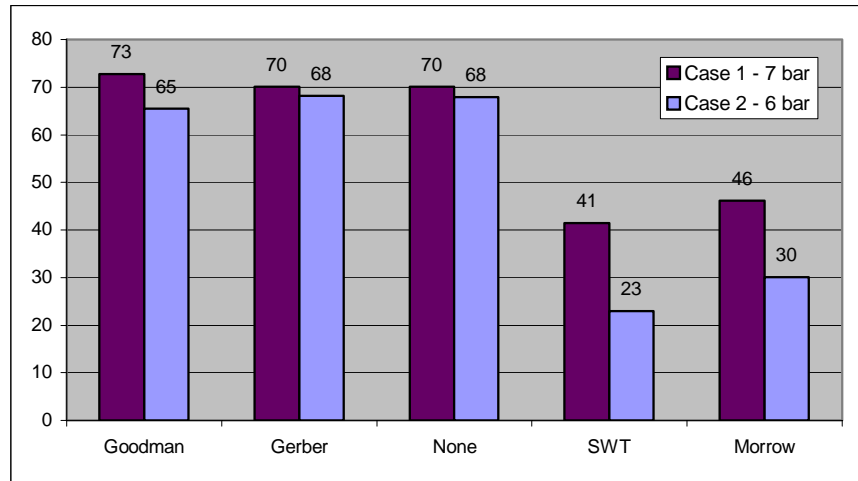


Figure 5.3 Residual stress effect on fatigue life, driven from fatigue simulation results of model 2 and model 4

5 fatigue life prediction methods gave different results. The most successful models are prepared with strain life approach for both load cases. The principal stresses found are all in the plastic region of the synthetic cyclic stress-strain curve. This shows that the plasticity effects are present and the success of strain life approaches comes from this advantage. The percentage differences between stress life and strain life approaches are lower for the fatigue load case 2 as expected, since the contribution of plastic strains is lower. This comparison is given between strain life method with SWT and stress life method with Gerber mean stress correction for all five models in Table 5.1.

Table 5.1 Fatigue life cycle differences in percentage between S-N Gerber and ϵ -N SWT methods

	Case 1 (7 bar)	Case 2 (6 bar)
<i>Model 1</i>	%93	%88
<i>Model 2</i>	%92	%86
<i>Model 3</i>	%86	%72
<i>Model 4</i>	%84	%65
<i>Model 5</i>	%85	%67

Comparing the all five simulation methods, the closest cycle numbers to the test results obtained with strain life method with Morrow mean stress correction. The errors in strain-life analysis models are tabulate in Table 5.2.

Table 5.2 Percentage error reside in strain-life methods, comparison with test results with and without residual stresses

	Comparison with test results of parts without residual stresses		Comparison with test results of parts with residual stresses	
	<i>Loadcase 1</i>	<i>Loadcase 2</i>	<i>Loadcase 1</i>	<i>Loadcase 2</i>
S-W-T (Model 3)	-129 %	-82 %	-164 %	-172 %
Morrow (Model 3)	-113 %	-69 %	-146 %	-152 %

In Table 5.2, fatigue simulation models without residual stresses are compared with test results of parts with and without residual stresses. It is seen that the life estimate results without residual stresses are more consistent with the life cycles of the parts without residual stresses. However, the percentage errors are between -69 and -129. From the engineering design point of view, the simulation results stay on the safe side, but they are far from being accurate. One important reason of such errors in simulation results can be the synthetic Wöhler curves generated. These curves are the basis of the fatigue calculations and can be misleading when the curve does not reflect the behavior of the material. Another possible reason can be that the stress state at the location where crack starts is such that, it may be better to use Wöhler curve generated with bending type of loading or different boundary conditions can be tried. More information on rotating bending tests is given in Section 2.3.6.1.

Table 5.3 tabulates the percentage error in simulation results of strain-life methods with residual stresses. The calculated life cycles are closer to test results for the loadcase 2, the loadcase with 6 bars of cylinder pressure. As in the case of models without residual stresses, the simulation results stay on the safe side, but they are far from being accurate. The possible sources of errors for the simulations without residual stresses exist for the cases with residual stresses. The percentage errors are higher than the errors without residual stresses. This additional errors are possibly a result of additional residual stresses. It is possible that the residual stresses are not accurately calculated at every point of the part.

Table 5.3 Percentage error reside in strain-life methods with residual streeses, comparison with test results with residual stresses

	Loadcase 1 (7 bars)	Loadcase 2 (6 bars)
S-W-T (Model 5)	-104 %	-75 %
Morrow (Model 5)	-117 %	-79 %

Examining five fatigue methods utilized for fatigue calculations, including thickness and residual stress effects in fatigue simulations has a favorable influence over the all results. The best results handled with strain life method with Morrow. The results of this method with model number 5, which is produced all by simulations and contains residual stress effects, and model number 2, which does not contain residual stress effects, are compared with test results in Figure 5.4.

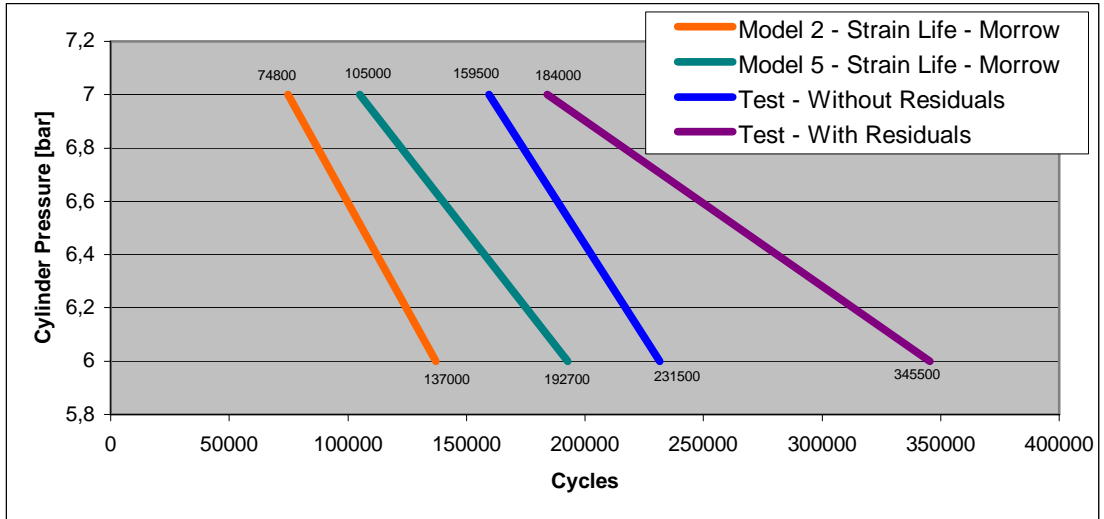


Figure 5.4 Comparison of strain life Morrow method with fatigue test results with and without residual stresses

REFERENCES

- [1] Stouffer, C.D., Dame, L.T., *Inelastic Deformation of Metals*, John Wiley & Sons, 2000
- [2] Anne-Marie HABRAKEN, *Contributions to Constitutive Laws of Metals: Micro-macro and Damage Models*, Universite de Liege, Belgium, 2001
- [3] Lu, W., Makelainen, P., *Advanced Steel Structures*, Helsinki University of Technology Laboratory of Steel Structures Publications 29, Helsinki, 2003
- [4] Thomsen, E.G., Shabaik, A.H., Sohrabpour, S., *A Direct Method for Obtaining an Effective Stress-Strain Curve from a Tension Test*, Manufacturing Engineering Transactions, SME, 1977
- [5] Dang Van K., Papadopoulos I.V., *High Cycle Metal Fatigue-From Theory to Applications*, Springer, 1999
- [6] Forsyth, P.J.E., *The Physical Basis of Metal Fatigue*, Blackie and Son Limited, London, 1969
- [7] Fuchs, H.O., Stephens, R.I., *Metal Fatigue in Engineering*, John Wiley&Sons, New York, 1980
- [8] Zahavi, E., Torbilo, V., *Fatigue Design Life Expectancy of Machine Parts*, CRC Press, 1996
- [9] Boresi, A.P., Schmidt R.J., Sidebottom, O.M., *Advanced Mechanics of Materials*, Wiley, 1993
- [10] Wöhler, A., *Wöhler's Experiments on Strength of Metals*, J. of Engineering, 1967
- [11] Filippini, M., *A Critical Analysis of Multiaxial Fatigue Criteria*, Graduate Thesis, Dipartimento di Meccanica, Politecnico di Milano, 1994

- [12] Baumel, A., Seeger, T., *Material Data for Cyclic Loading*, Amsterdam, Elsevier, 1987
- [13] Kuguel, R., *A Relation Between Theoretical Stress Concentration Factor and Fatigue Notch Factor Deduced from the Concept of Highly Stressed Volume*, Proceedings of the American Society for Testing and Materials, vol 61, ASTM, 1961
- [14] Shigley, J.E. & Mischke, C.R., *Standard Handbook of Machine Design*, McGraw-Hill, Inc., New York, 1986
- [15] Vial, C. and Hosford, W.F., and Caddell, R.M. , *Yield Loci of Anisotropic Sheet Metals*, Int. J. Mechanical Science., vol. 25, no. 12, 1983
- [16] Moore, H.F., Kommers, J.B., *Fatigue of Metals*, McGraw-Hill Book Co., New York, 1927
- [17] Neuber, H., *Theory of Stress Concentration for Shear-strained Prismatic Bodies with Arbitrary Nonlinear Stress-strain Law*, J. of Applied Mechanics, ASME, vol.28, 1961
- [18] Miner, M.A., *Cumulative Damage in Fatigue*, J. of Applied Mechanics, vol.67, 1945
- [19] Landgraf, R.W., Morrow, J.D., Endo, T., *Determination of the Cyclic Stress-Strain Curve*, Journal of Materials, No.4, 1969
- [20] Comer, J., *Fatigue Lecture Notes*, Iowa State University, Mechanical Engineering Dept., 2000
- [21] Ramberg, W., Osgood, W.R., *Description of Stress-Strain Curves by Three Parameters*, No.902, NACA, 1943
- [22] Manson, S.S., *Behavior of Materials Under Conditions of Thermal Stresses*, National Advisory Committee for Aeronautics, Report no.1170, 1954
- [23] Bannantine J. A., J. J. Corner, J. L. Handrock, *Fundamentals of Metal Fatigue Analysis*, Prentice Hall, Englewood Cliffs, 1990
- [24] Topper, T.H., Sandor, B.I., Morrow, J., *Cumulative Fatigue Damage Under Cyclic Strain Control*, Journal of Materials, vol.4, 1969
- [25] *Theory and User Manual*, MSC.Marc vol A., version 2003

- [26] Koçaker, B., *Product Properties Prediction After Forming Process Sequence*, Master of Science Thesis, Mechanical Engineering Dept., METU, 2003
- [27] *Internet Learning of Steel Applications and Processes*, The University of Liverpool, with permission of MATTER, 2005
- [28] *Fatigue Design Handbook*, Society of Automotive Engineers, 3rd ed., 1997
- [29] Griffith, A.A., *The Phenomena of Rupture and Flow in Solids*, Trans.R. Soc., Vol. A221, 1920
- [30] Paris, P.C., Erdogan, F., *A Critical Analysis of Crack Propagation Law*, Trans.ASME, J. Basic Eng., vol.85, No.4, 1963
- [31] Fricke, W., *Lecture Notes on Fatigue of Materials and Structures*, Helsinki University of Technology, 2003
- [32] Matsuishi, M., Endo, T., *Fatigue of Metals Subjected to Varying Stresses*, Japan Soc. of Mech.Eng., Fukuoka, 1968
- [33] Halliday, D., Resnick, R., Walker, J., *Fundamentals of Physics*, 5th ed., Wiley, New York, 1997

APPENDIX A

FATIGUE LOAD PRINCIPAL STRESS RESULTS

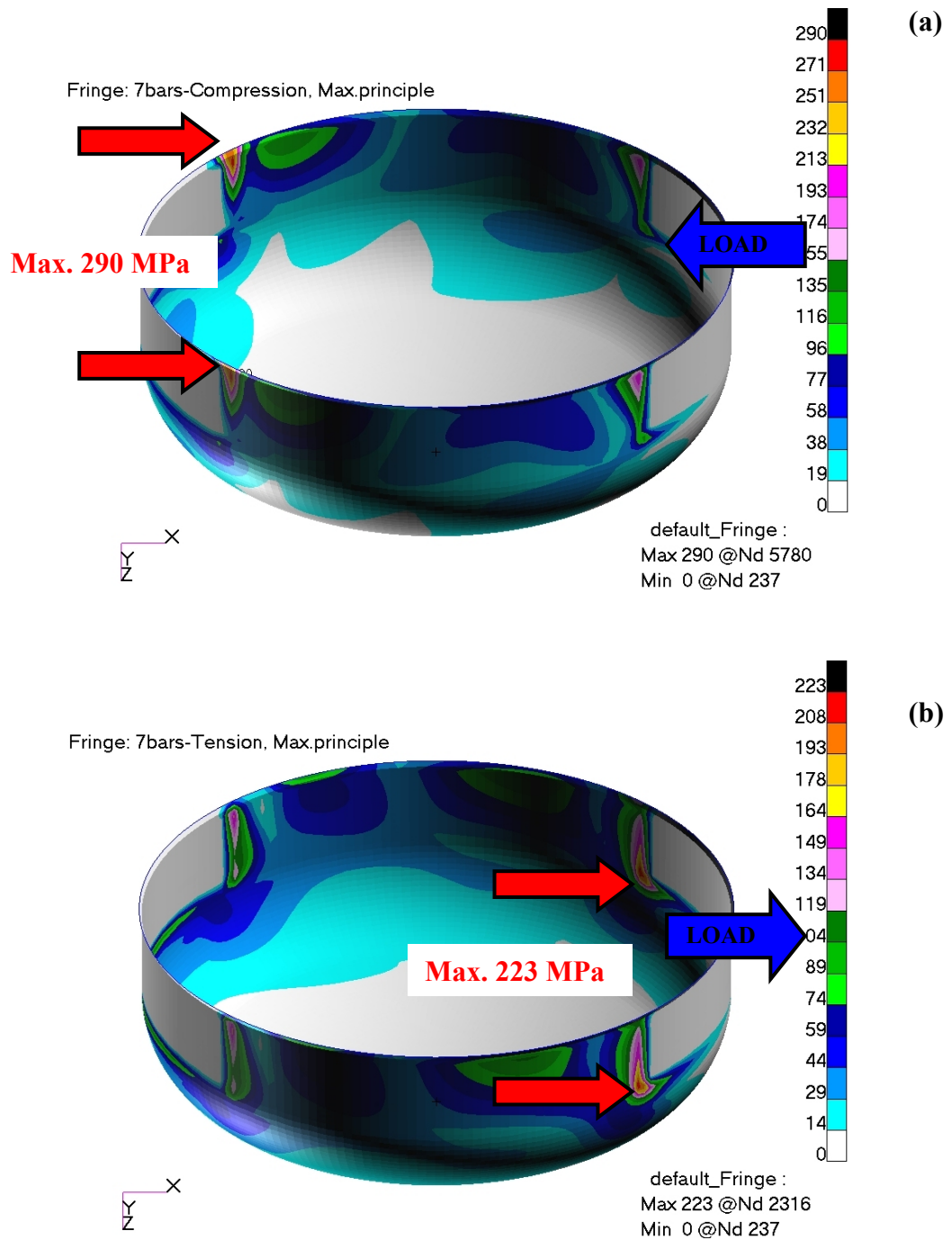


Figure A. 1 Model 1, maximum principal stress results for 7 bars (a) 5498N forward, (b) 5154N backward load

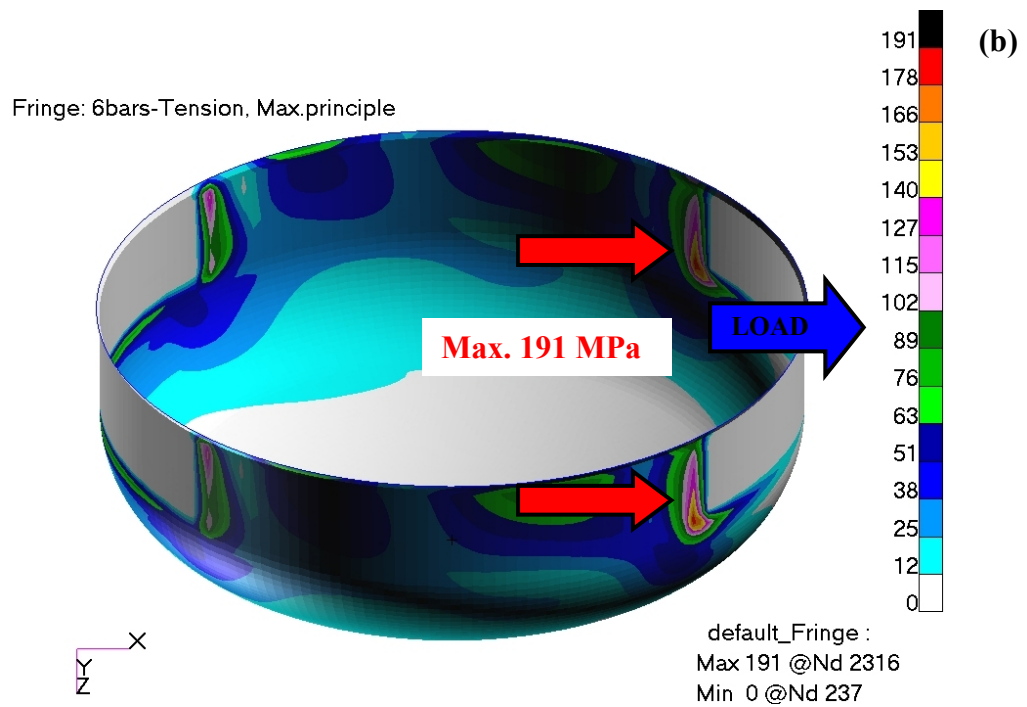
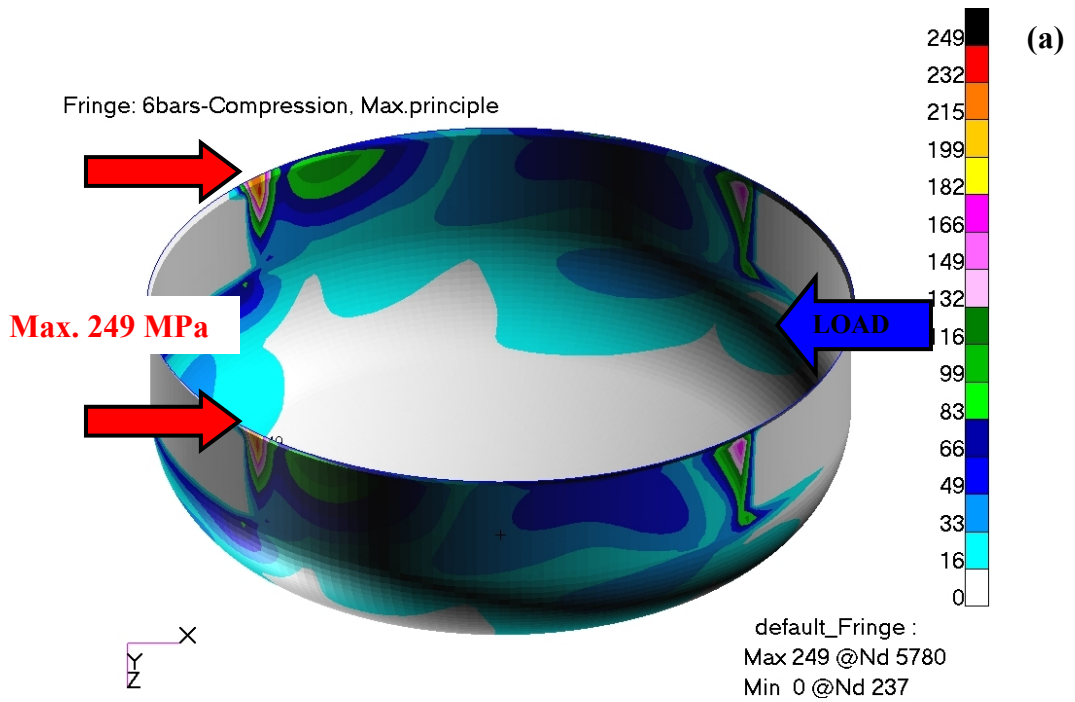


Figure A. 2 Model 1, maximum principal stress results for 6 bars (a) 4712N forward, (b) 4418N backward load

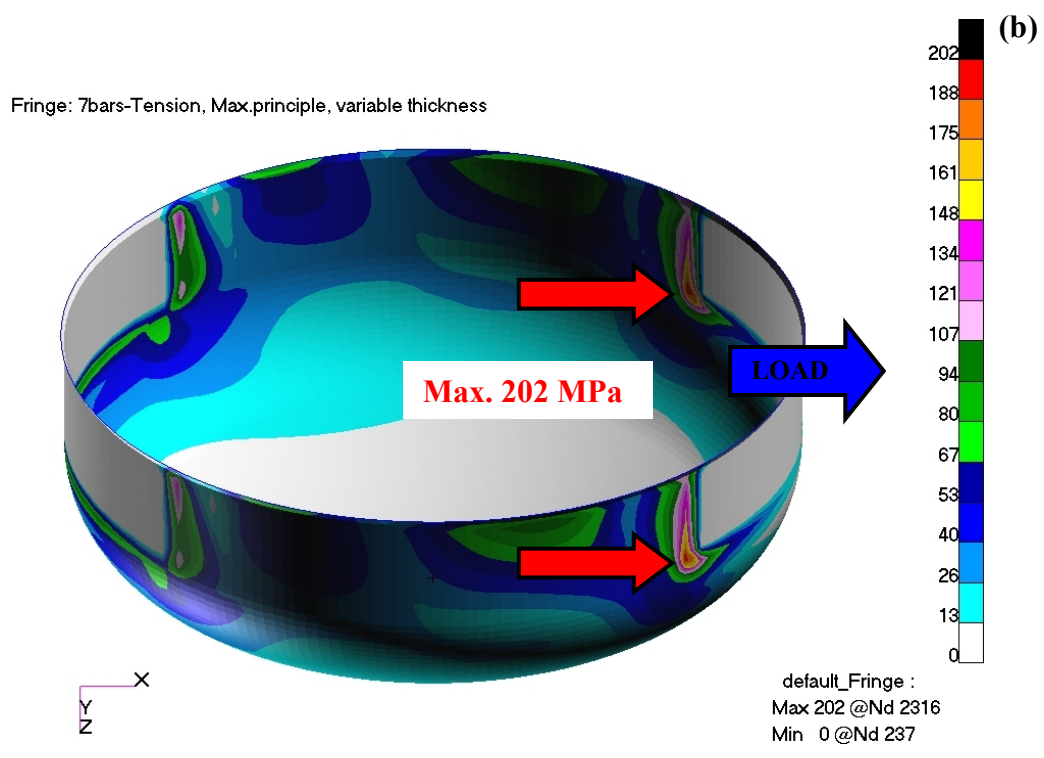
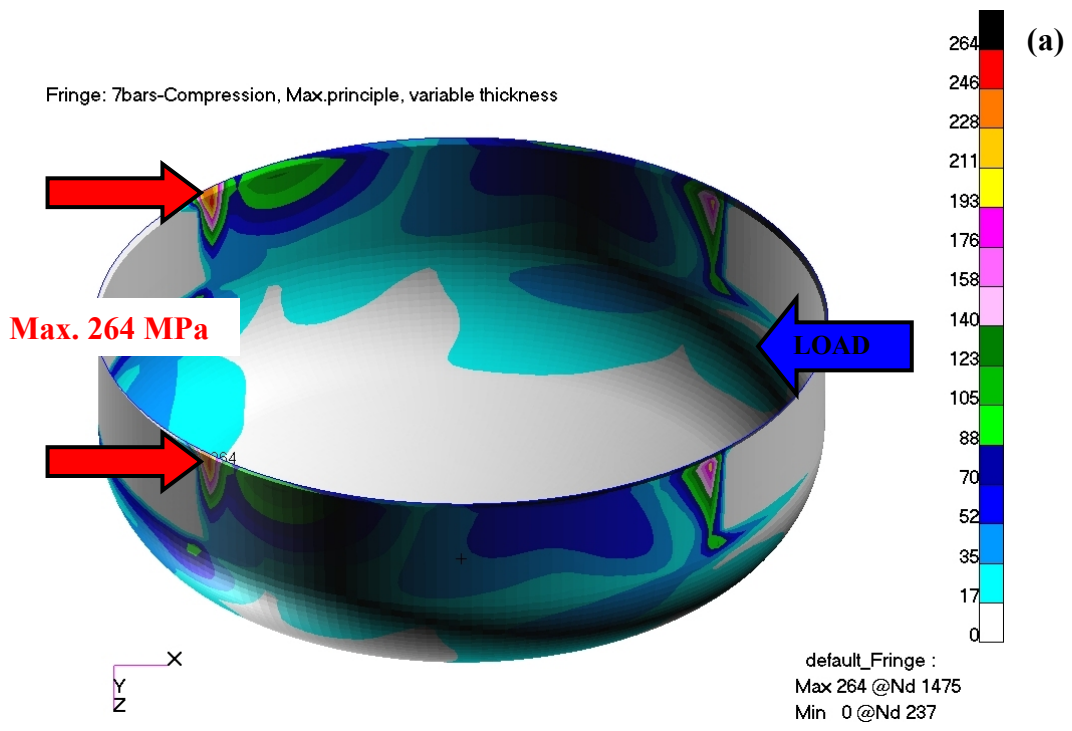


Figure A. 3 Model 2, maximum principal stress results for 7 bars (a) 5498N forward, (b) 5154N backward load

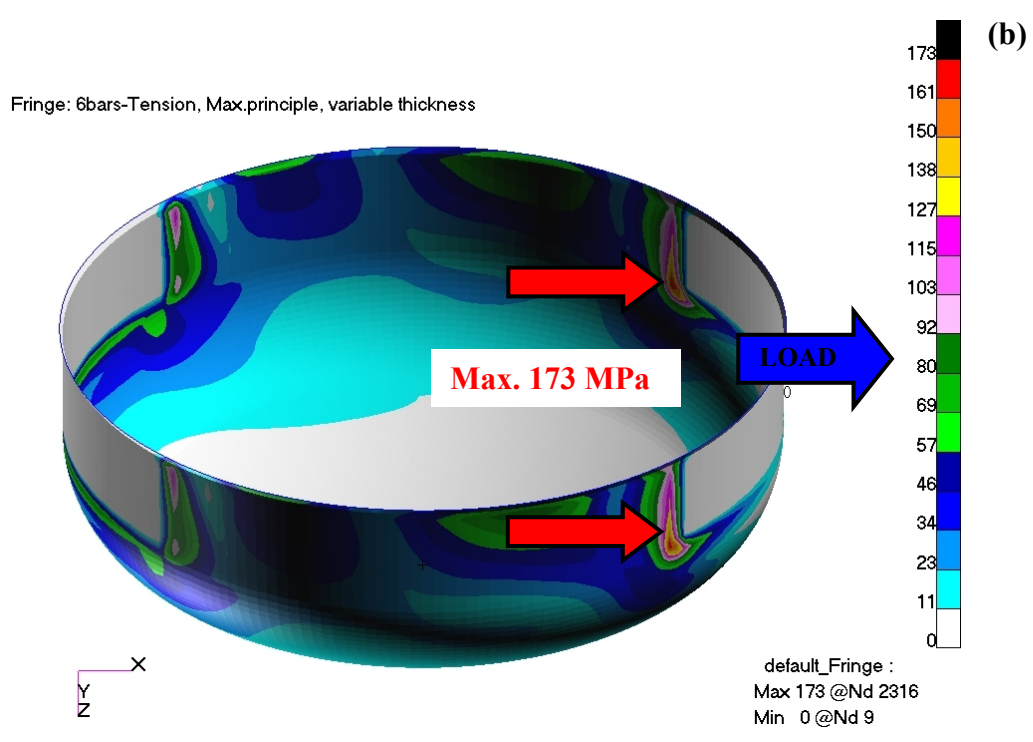
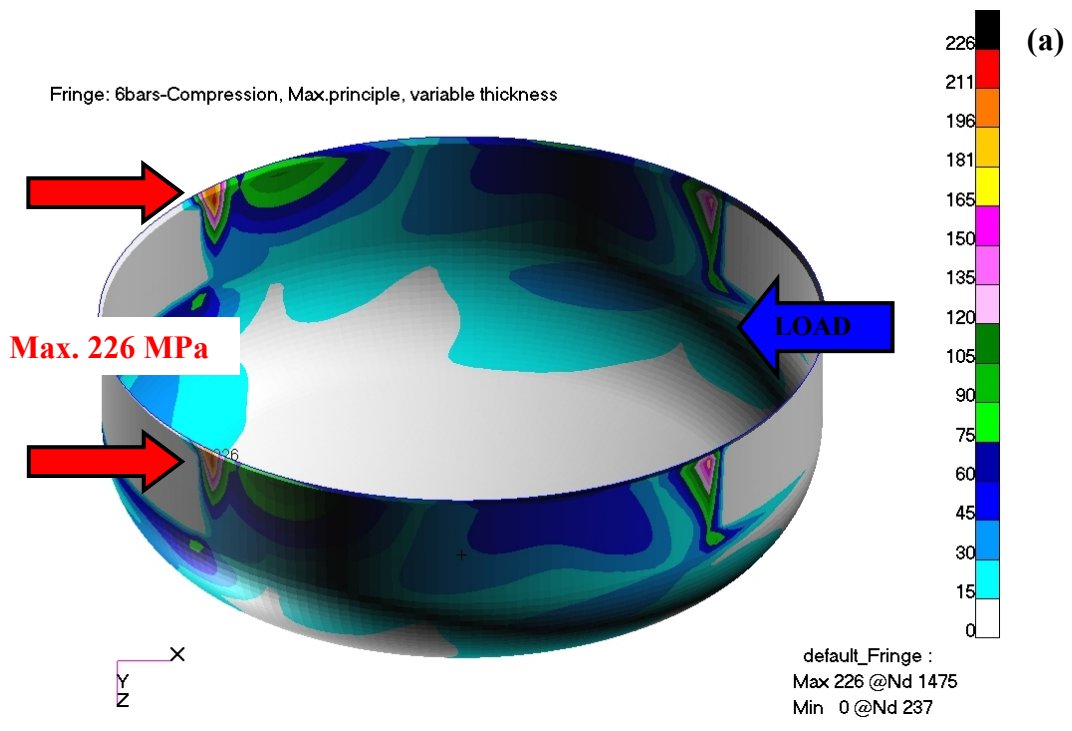


Figure A. 4 Model 2, maximum principal stress results for 6 bars (a) 4712N forward, (b) 4418N backward load

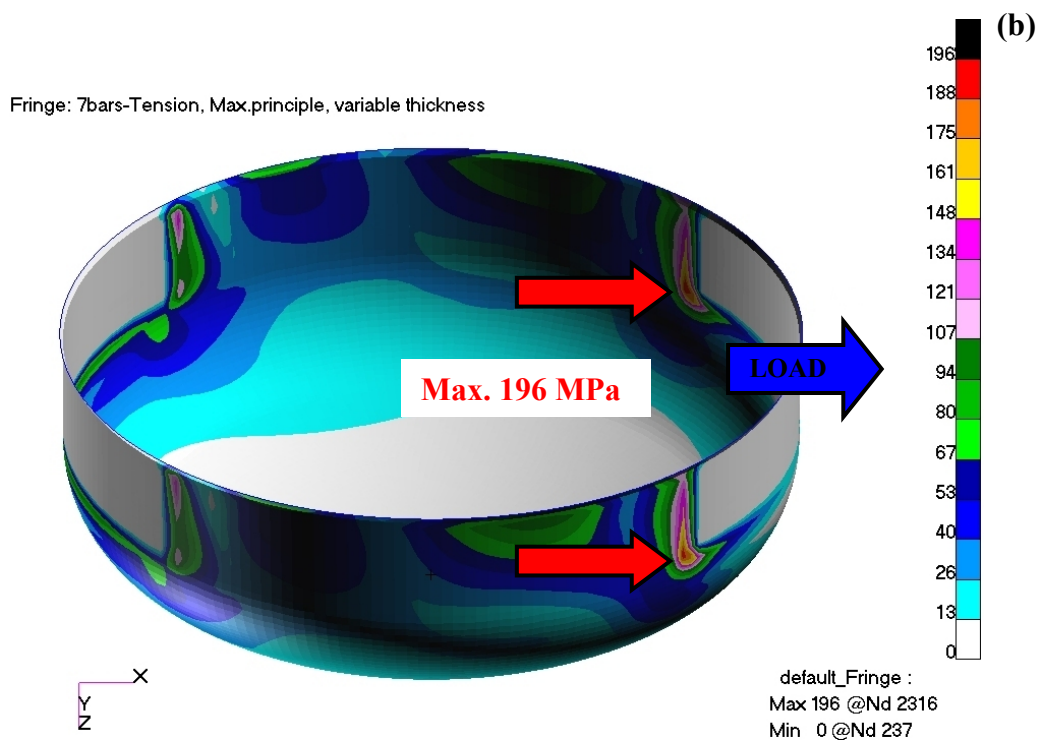
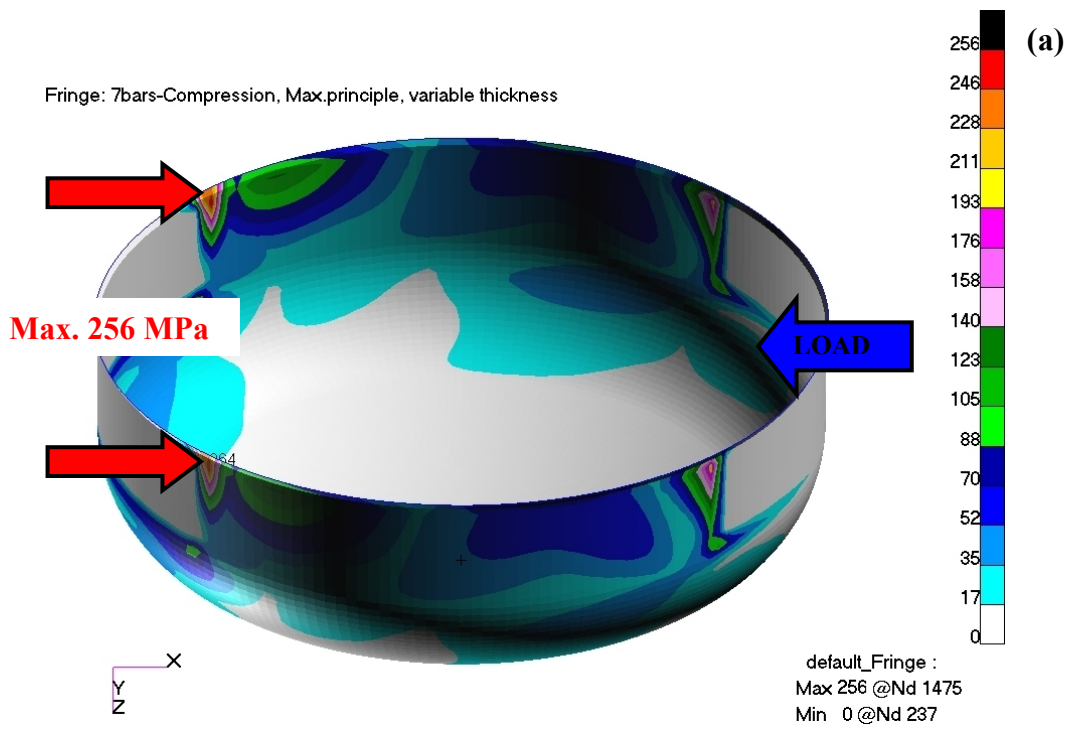


Figure A. 5 Model 3, maximum principal stress results for 7 bars (a) 5498N forward, (b) 5154N backward load

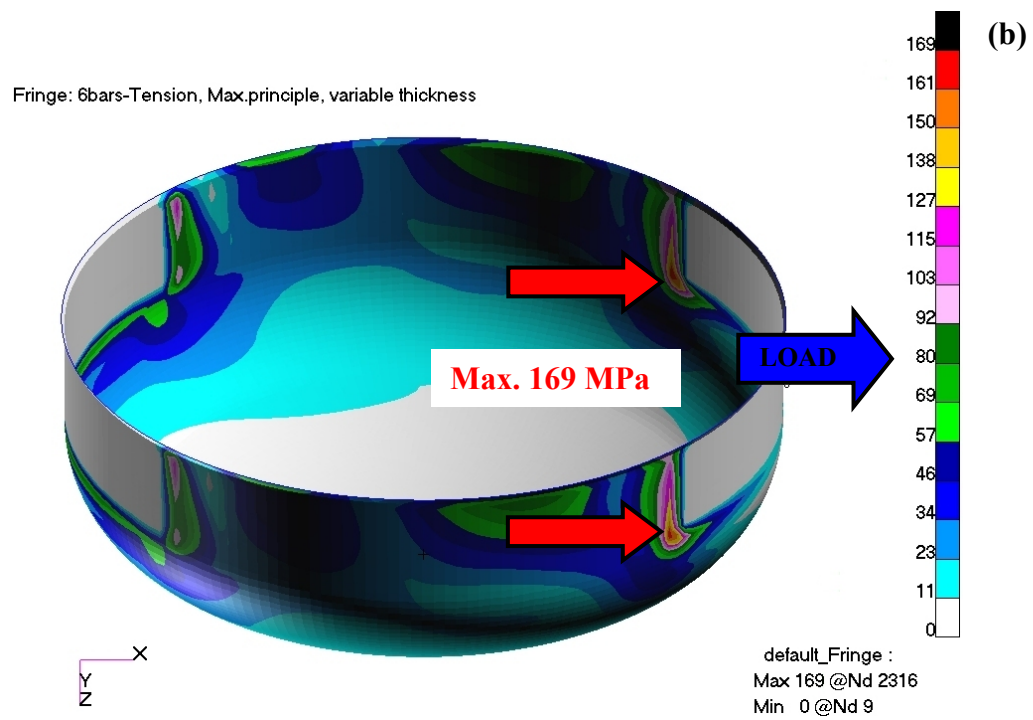
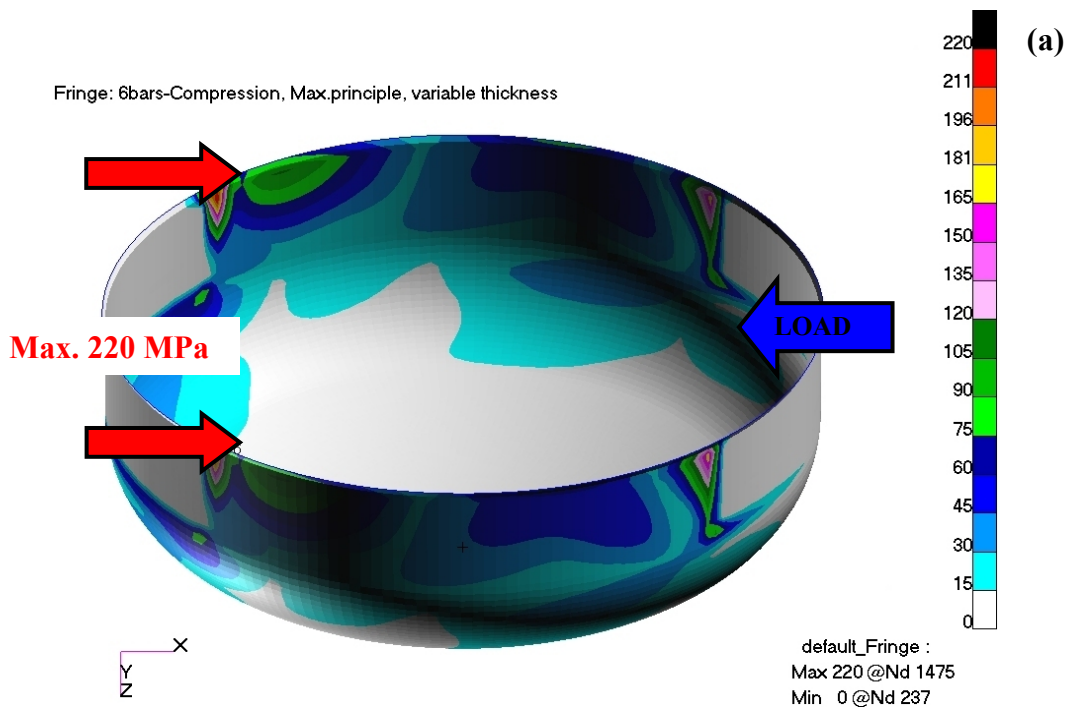


Figure A. 6 Model 3, maximum principal stress results for 6 bars (a) 4712N forward, (b) 4418N backward load

APPENDIX B

FATIGUE LOAD PRINCIPAL STRESS RESULTS

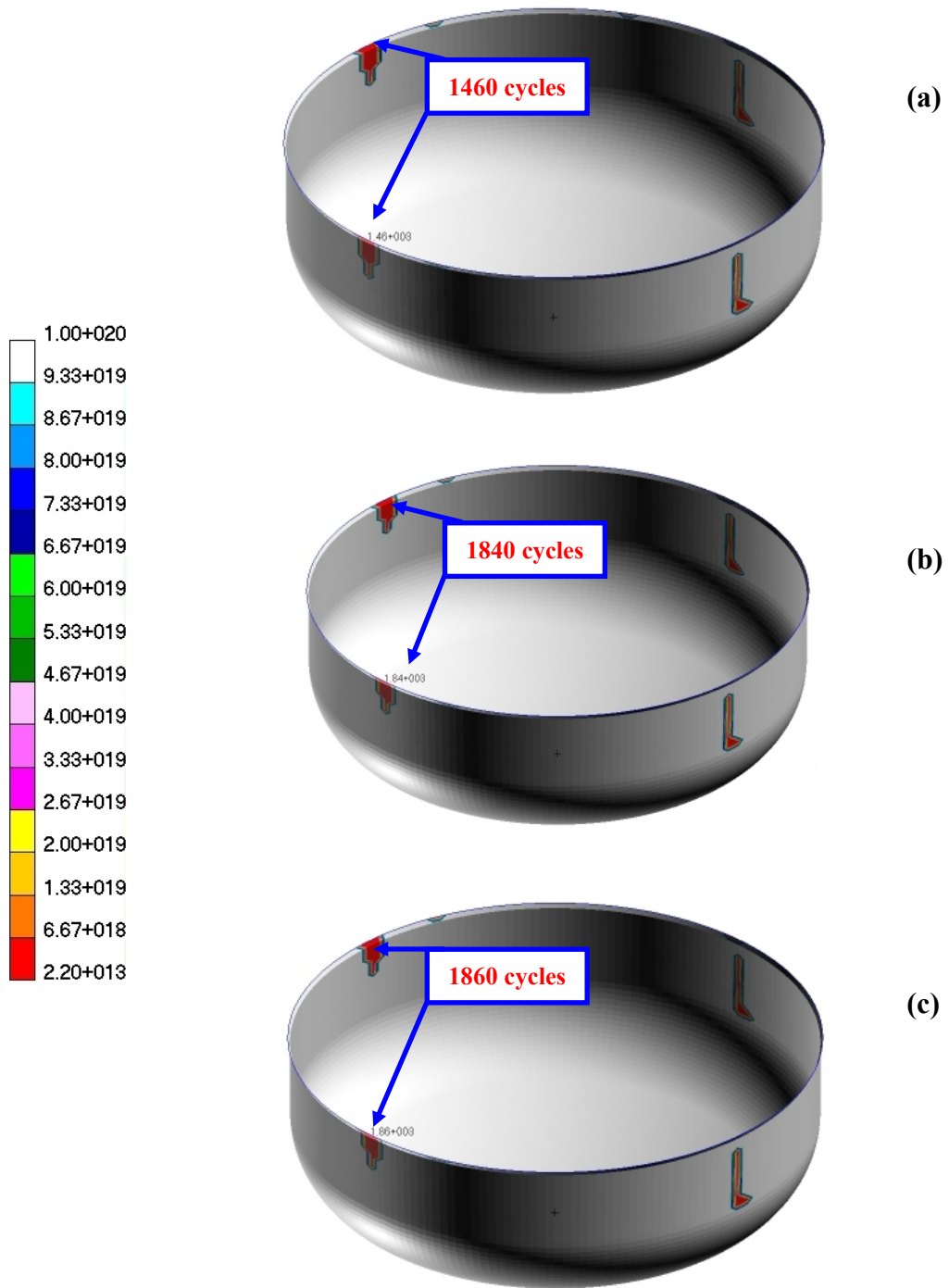


Figure B. 1

Case 1 (7 bars)

Model 1

Stress-Life

(a) Goodman (b) Gerber (c) none

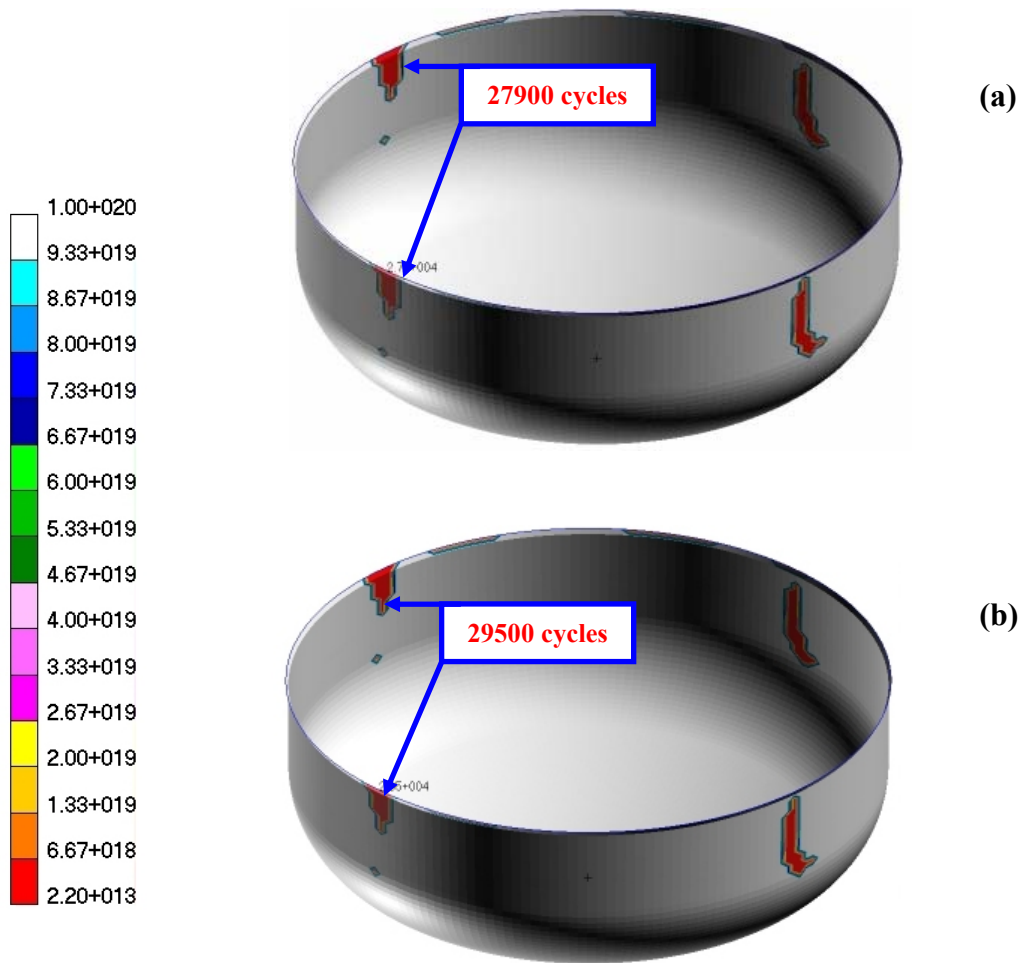


Figure B. 2 Case 1 (7 bars) Model 1 Strain-Life
 (a) S-W-T (b) Morrow

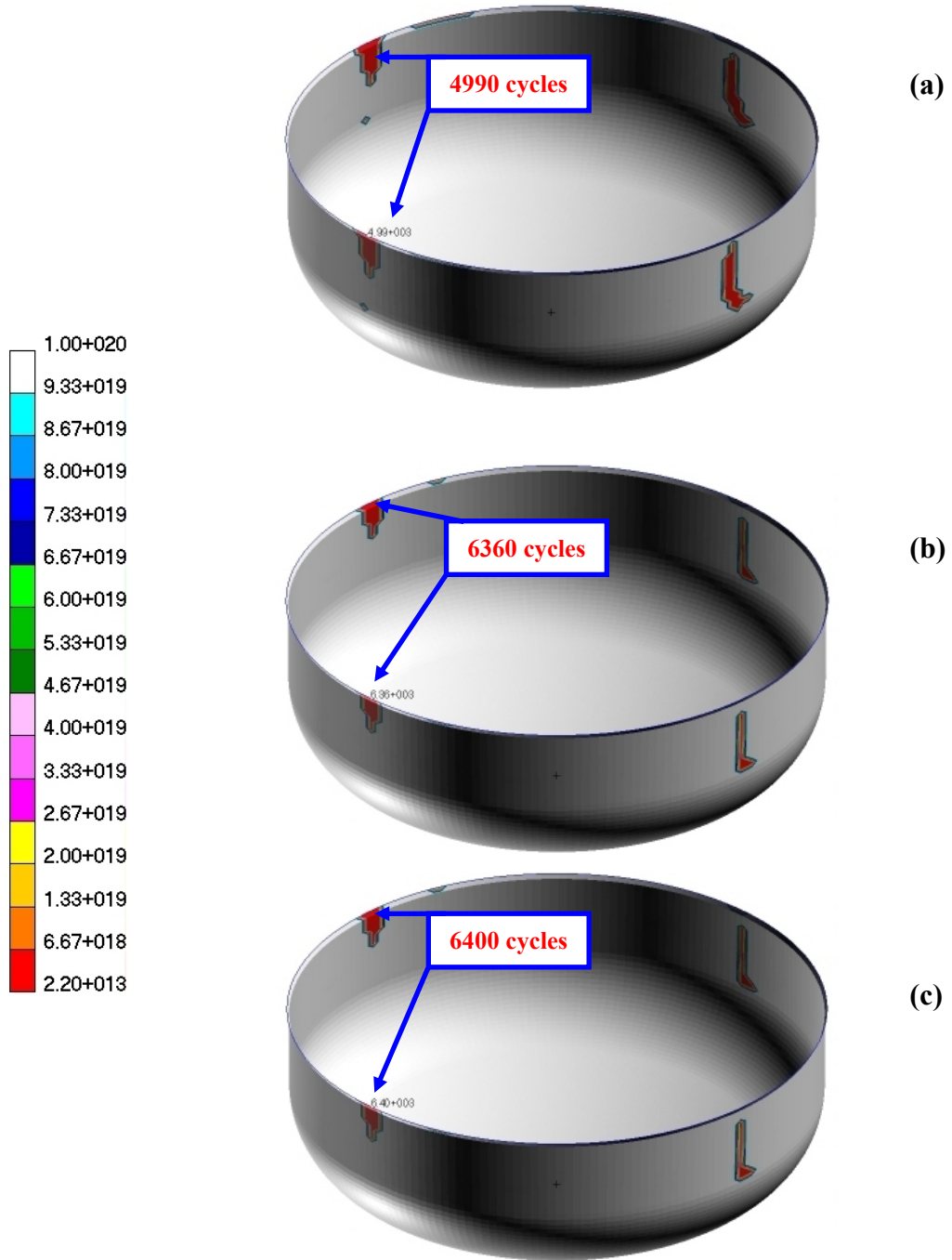


Figure B. 3

Case 1 (7 bars)

Model 2

Stress-Life

(a) Goodman (b) Gerber (c) none

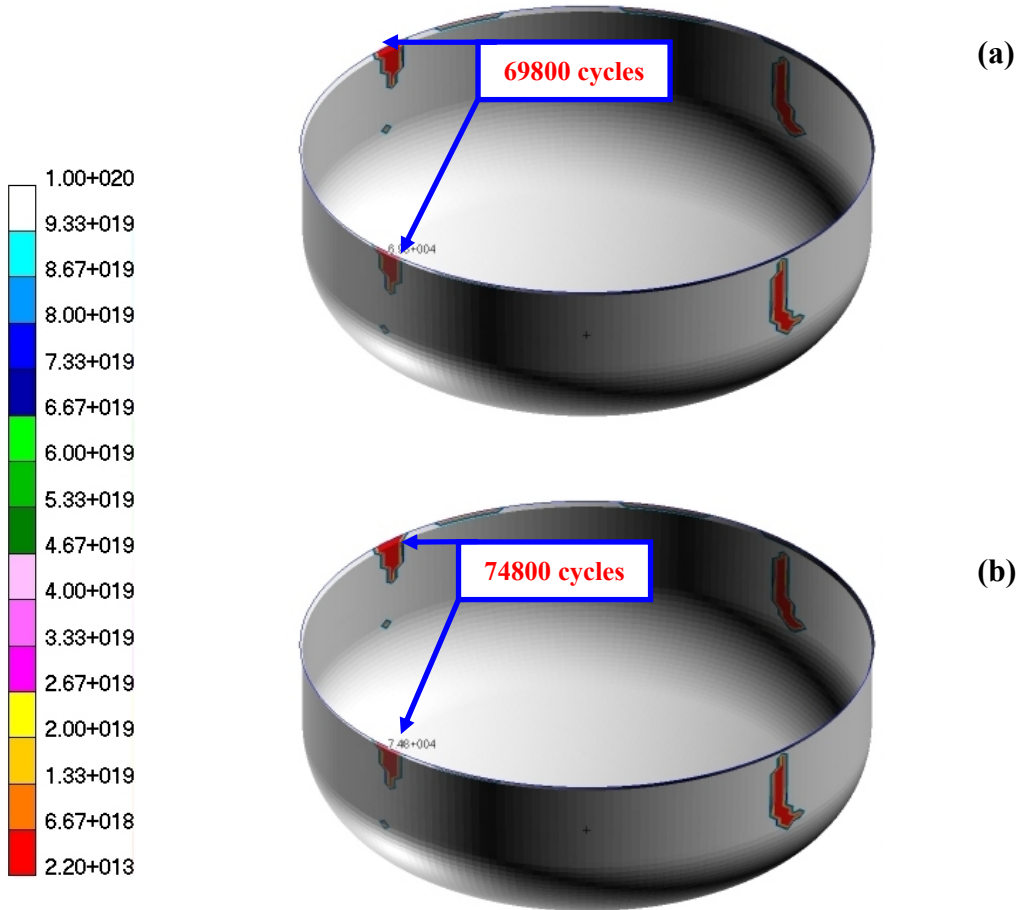


Figure B. 4 Case 1 (7 bars) Model 2 Strain-Life
 (a) S-W-T (b) Morrow

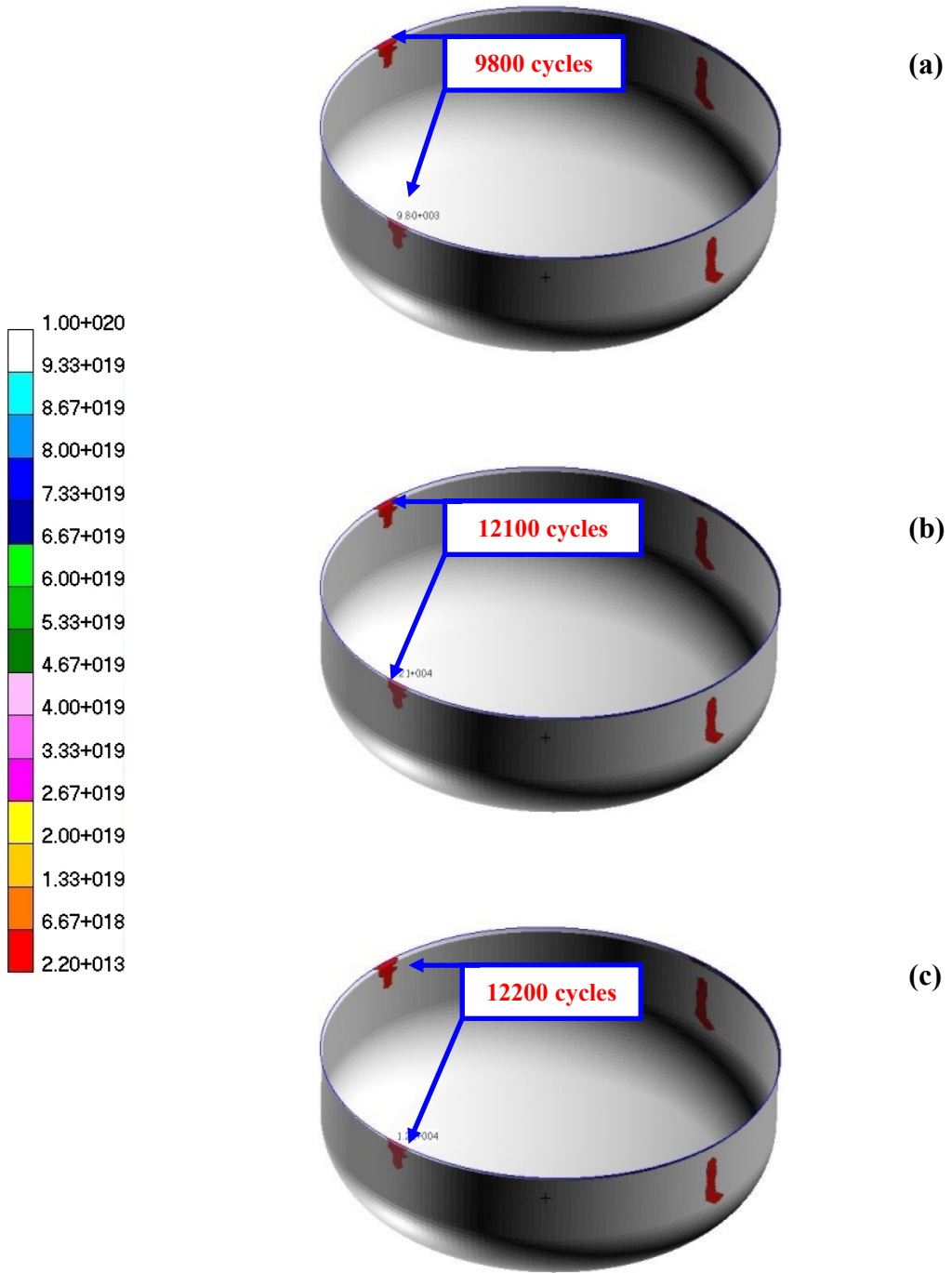


Figure B. 5

Case 1 (7 bars)

Model 3

Stress-Life

(a) Goodman (b) Gerber (c) none

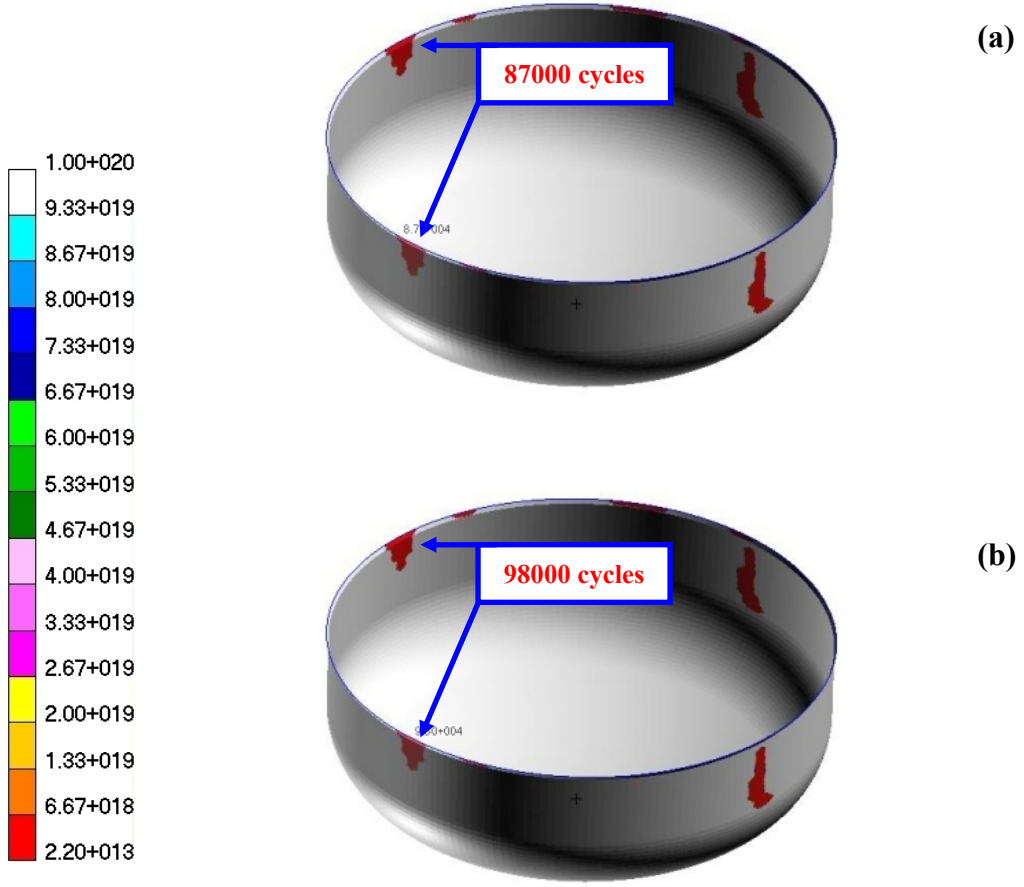


Figure B. 6 Case 1 (7 bars) Model 3 Strain-Life
 (a) S-W-T (b) Morrow

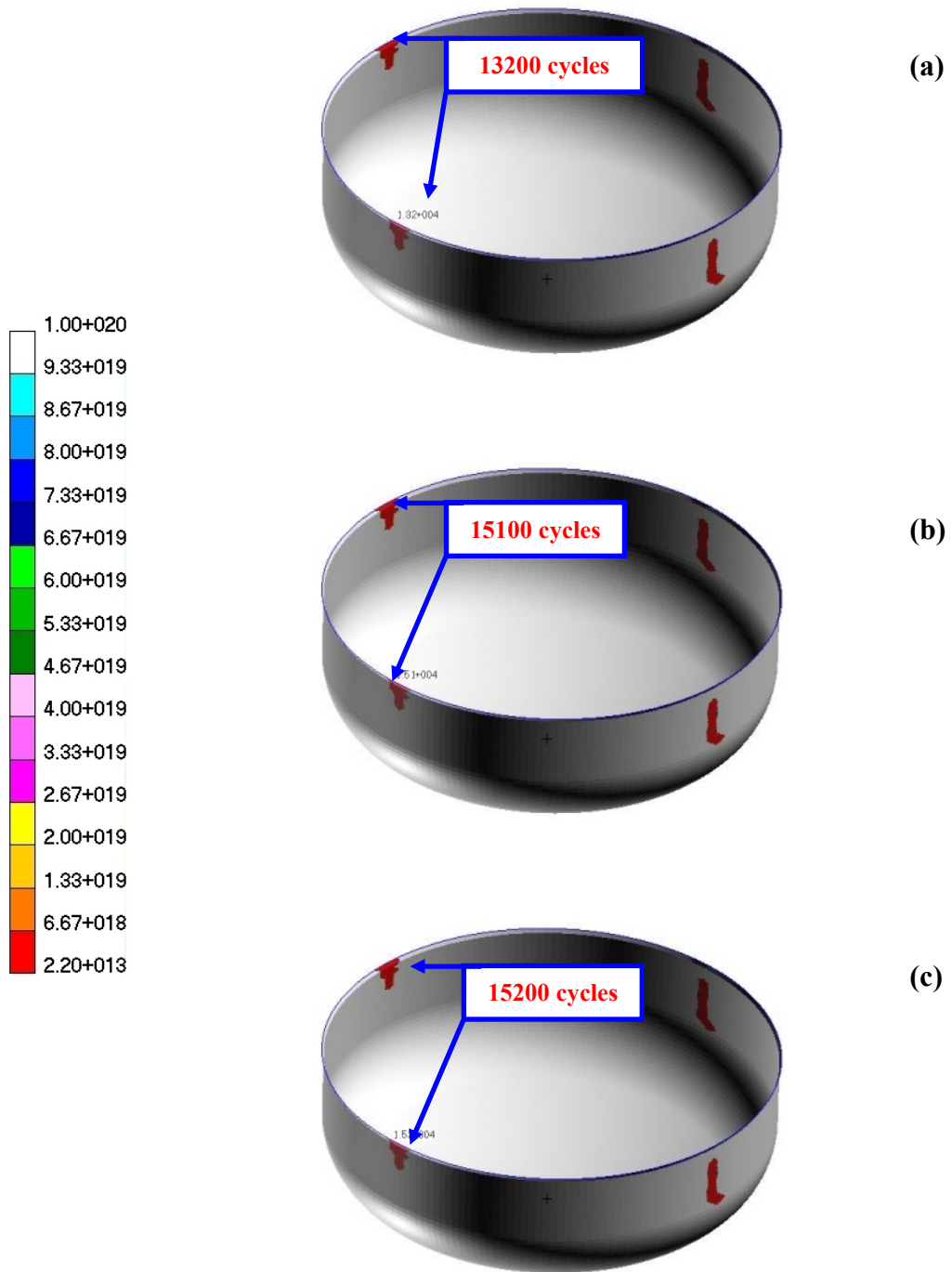


Figure B. 7

Case 1 (7 bars)

Model 4

Stress-Life

(a) Goodman (b) Gerber (c) none

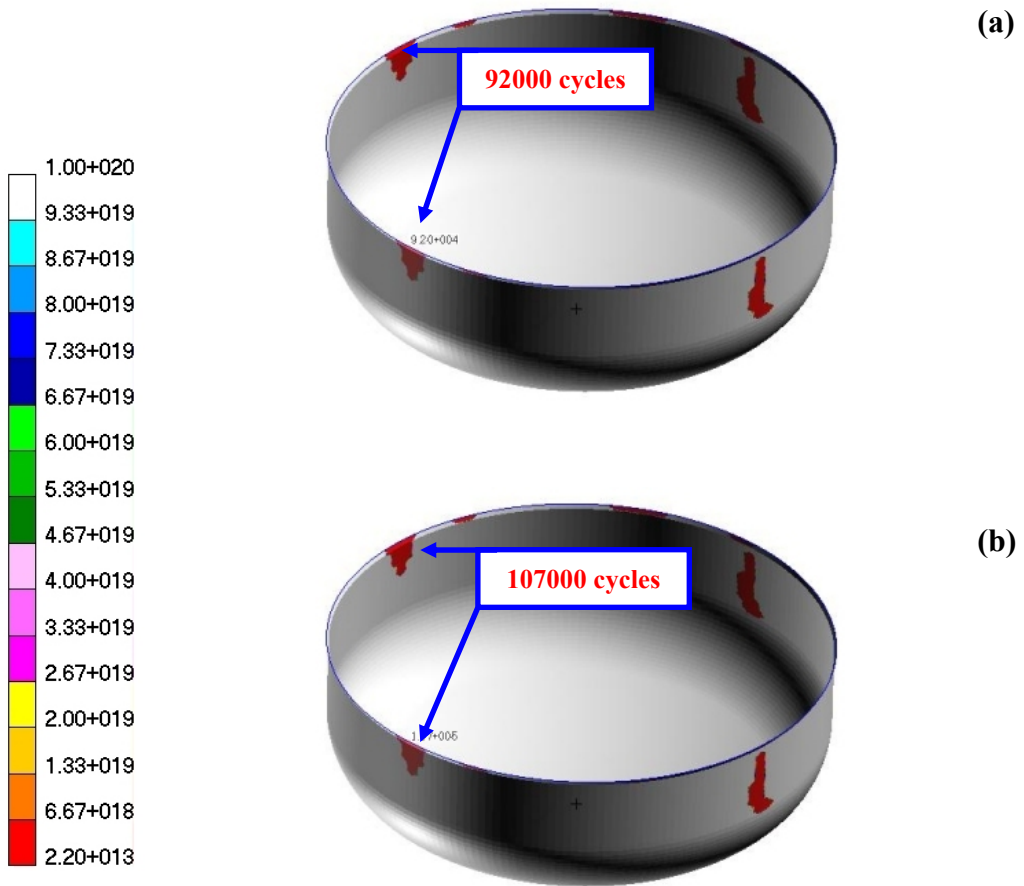


Figure B. 8 Case 1 (7 bars) Model 4 Strain-Life
 (a) S-W-T (b) Morrow

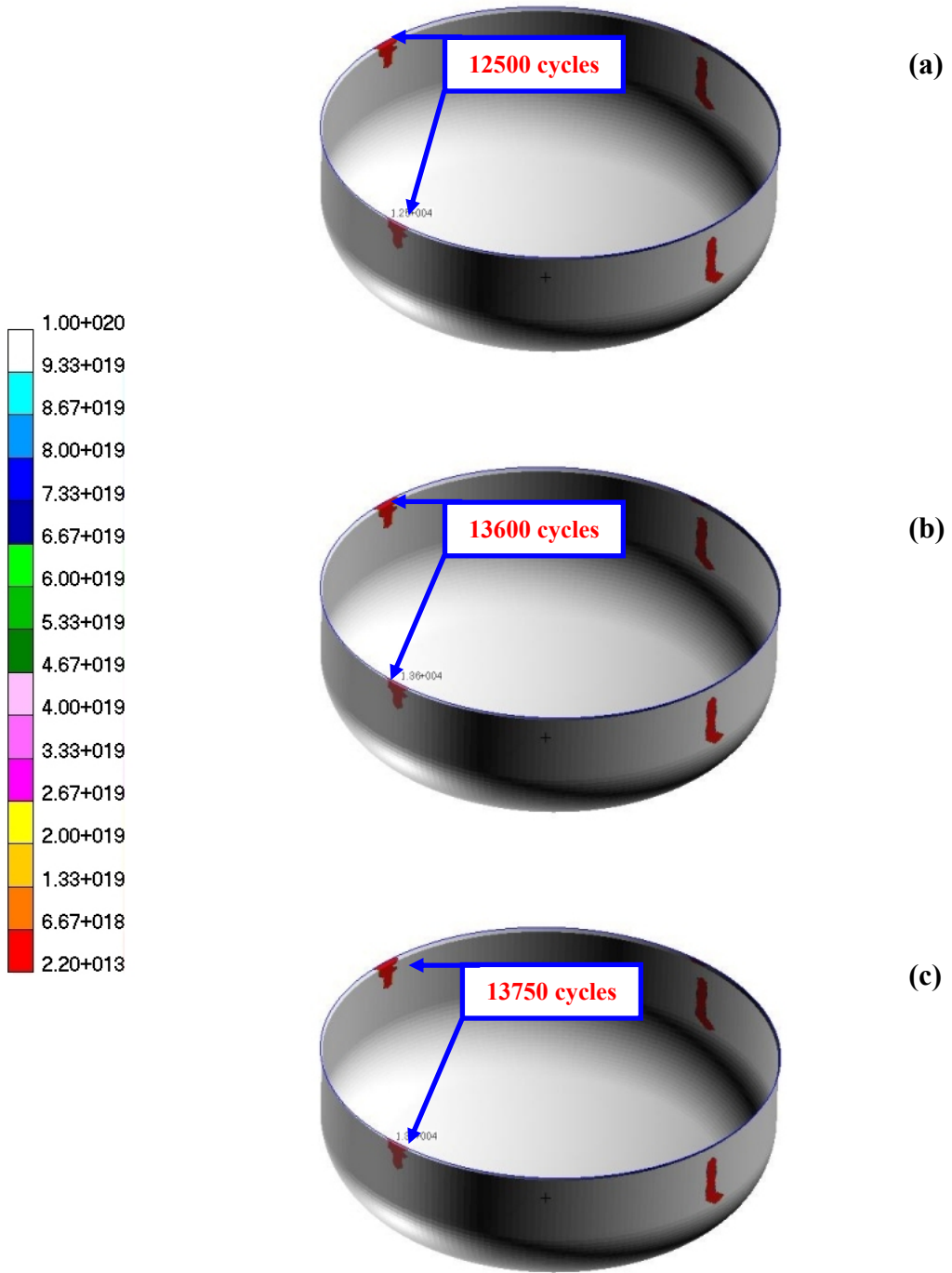


Figure B. 9

Case 1 (7 bars)

Model 5

Stress-Life

(a) Goodman (b) Gerber (c) none

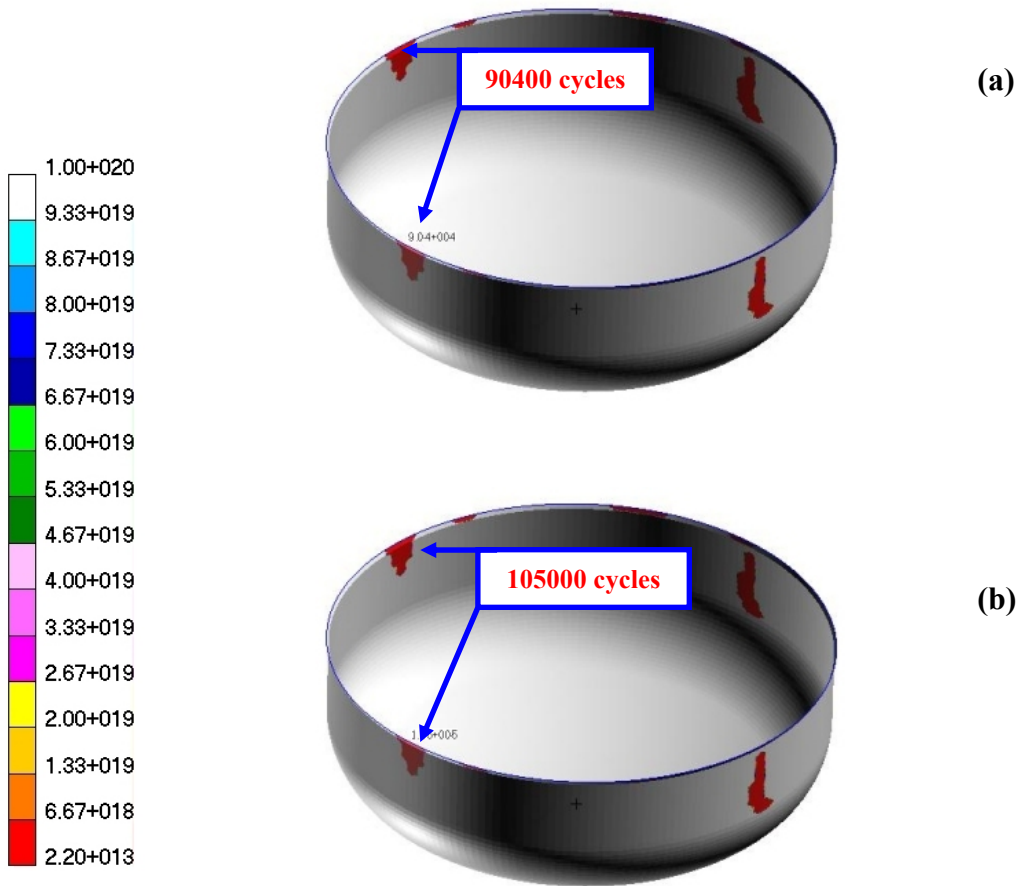


Figure B. 10 Case 1 (7 bars) Model 5 Strain-Life
 (a) S-W-T (b) Morrow